Chapter 6

Surface Morphology

We start, in this chapter, by treating surface morphology. At the outset, it is important to distinguish between two aspects of surface morphology: *structure*, the crystallography of defect-free surfaces, and *microstructure*, the distribution of point and line defects that interrupt that perfect crystallography. In this chapter we will be mainly concerned with microstructure and, to a much lesser extent, structure.

It is also important to distinguish between two kinds of surfaces: high-symmetry *singular* surfaces, at whose orientations surface free energies are cusped and have discontinuous first derivatives; and *vicinal* surfaces miscut slightly from singular orientations, composed of singular terraces separated by steps. In this chapter we will be concerned with both of these kinds of surfaces.

We first ask, in Section 6.1: what are the statistics of defects on singular and vicinal surfaces in equilibrium with their vapor, i.e., in the absence of net growth? We will find, not surprisingly, that those statistics depend both on temperature as well as on the average orientation of the surface. Moreover, those statistics are themselves a major determinant of the orientation dependences of surface free energies.

We then ask, in Section 6.2: *given* full knowledge of surface free energies, what is the equilibrium morphology of crystals, surfaces, and thin films? On the one hand, in one-material systems, e.g., "homoepitaxial" films of one material on substrates of the same material, morphology is determined by the orientation dependence of the surface free energy. On the other hand, in two-material systems, e.g., for "heteroepitaxial" films of one material on substrates of a different material, morphology is also determined by interface and volume free energies.

We finally ask, in Section 6.3: what is the defect microstructure of

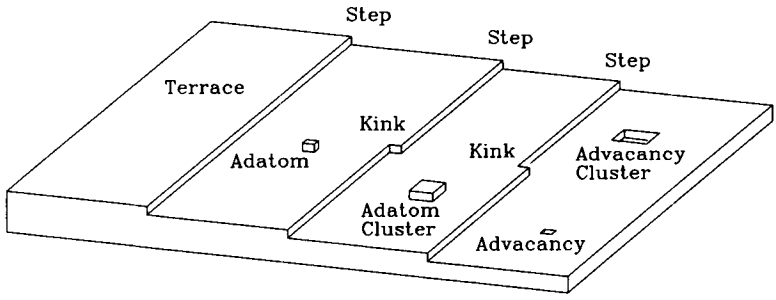

Figure 6.1: Terraces, ledges, kinks, adatoms, adatom clusters, advacancies, and advacancy clusters on a Kossel crystal.

surfaces *not* in equilibrium with their vapor, i.e., in the presence of net growth? We will find that growth is essentially a competition between surface defects of various kinds for adatoms arriving from the vapor. This competition results in a rich and often oscillatory time evolution to the overall microstructure of the surface.

6.1 Statistics of Adatoms, Kinks, and Steps

Let us start, in this section, by discussing defects on surfaces. Consider the idealized (001) surface of a cubic elemental crystal. For simplicity, we suppose it to be "unreconstructed," in that bonds dangling into free space do not rehybridize into pairs or higher order atom arrangements. The important microstructural features of the idealized surface of such a "Kossel" crystal[1] are illustrated in Figure 6.1.

At low to medium temperatures, the dominant microstructural features are terraces, steps and kinks. The terraces can be considered planar defects in a bulk three-dimensional crystal. Separating terraces of different heights are ledges, or steps, which are line defects on a two-dimensional surface. Finally, along these steps there may also be kinks, which are point defects on one-dimensional steps.

[1]W. Kossel, *Nachr. Ges. Wiss. Gottingen*, p. 135 (1927); I.N. Stranski, *Z. Phys. Chem.* **136**, 259 (1928).

At higher temperatures, or away from equilibrium, microstructural features such as adatoms and advacancies, either isolated or clustered into two-dimensional islands, become important. We will begin, in Subsection 6.1.1, by treating adatoms on singular surfaces. Then, in Subsection 6.1.2, we treat kinks in isolated steps. Finally, in Subsection 6.1.3, we treat interacting steps on vicinal surfaces.

6.1.1 Adatoms on Singular Surfaces

Let us start, in this subsection, by considering adatoms, which we imagine adding one by one to a flat, singular surface. There are two extreme ways in which the adatoms can be distributed on this surface. First, they can cluster together predominantly into a half sheet, as illustrated at the bottom of Figure 6.2, so as to maximize the number of lateral in-plane bonds and hence minimize energy. Second, they can distribute randomly, as illustrated at the top of Figure 6.2, so as to maximize configurational entropy.

To describe qualitatively the competition between these two kinds of distributions,[2] consider the number of bonds formed as a new adatom arrives on the surface. The new adatom has four dangling lateral bonds and one dangling vertical bond, but has also "annihilated" the dangling vertical bond of the atom underneath it. Therefore, the adatom has associated with it four "missing" bonds. If each bond has an energy w, then the adatom has associated with it an energy $4w$.

Note, though, that as the adatom coverage, θ, on the surface builds up, adatoms will occasionally find themselves next to other adatoms. If the adatoms are distributed randomly, then the sites adjacent to a given adatom have a probability θ of being occupied. Since there are four such sites, the energy associated with that adatom decreases by $4w\theta$. The energy per adatom is therefore $4w - 4w\theta$, or $4w(1-\theta)$. Altogether, the energy per surface site is the adatom coverage times the energy per adatom, or

$$u_{\text{adat}} = 4w\theta(1-\theta). \tag{6.1}$$

This energy is exactly that (see Table 3.1 on page 50) associated with a two-component strictly regular solution in which the two components are considered to be adatoms and "missing" adatoms. Viewed in this way, the

[2]See, e.g., K.A. Jackson, "Theory of crystal growth," in *Treatise on Solid State Chemistry, Vol. 5*, N.B. Hannay, Ed. (Plenum Press, New York, 1975), pp. 233-282; and D.E. Temkin, "O molekulyarnoi sherokhovatosti granitsy kristall-rasplav (On molecular roughness of the crystal-melt interface)," in *Mekhanizm i kinetika kristallizatsii (Mechanism and Kinetics of Crystallization)*, N.N. Sirota, Ed. (Nauka i Tekhnika, Minsk, 1964), p. 86.

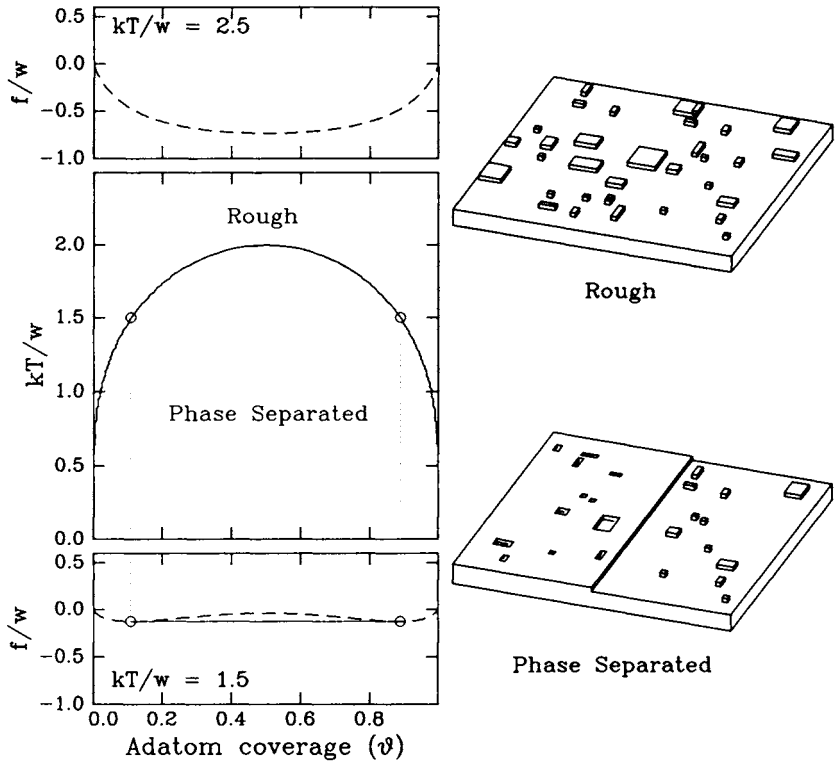

Figure 6.2: x-T phase diagrams for surface roughening. Above and below each phase diagram are also shown the normalized molar free energies of the adlayer phases at $kT/w = 2.5$ and $kT/w = 1.5$, their common tangents, and the critical compositions (open circles) determined by those common tangents.

ideal configurational entropy of mixing per surface site is, by analogy to Equation 3.24,

$$-\frac{s_{\text{adat}}}{k} = \theta \ln \theta + (1-\theta)\ln(1-\theta). \tag{6.2}$$

The free energy per surface site, normalized to the bond strength, is then

$$\begin{aligned} \frac{f_{\text{adat}}}{w} &= \frac{u_{\text{adat}} - T s_{\text{adat}}}{w} \\ &= 4\theta(1-\theta) + \frac{kT}{w}\left[\theta \ln \theta + (1-\theta)\ln(1-\theta)\right]. \end{aligned} \tag{6.3}$$

This normalized free energy is shown in Figure 6.2 for two different normalized temperatures.

At low temperatures, the bond energy contribution dominates, and the free energy curve is basically concave down. Hence, an adlayer having an average coverage of 1/2 can minimize its free energy by "phase-separating" into regions having near-zero coverage and other regions having near-unity coverage. Note that, just as in the discussion of Section 3.1, the $\theta = 0$ and $\theta = 1$ intercepts of the tangents to the free energy curve are the chemical potentials of the missing adatoms and adatoms, respectively. Therefore, the two phases can only be in equilibrium on the surface if the chemical potentials of their two components are equal. In other words, again following the discussion of Section 3.1, the "compositions" of the two phases are determined by the familiar common tangent construction. Physically, the adlayer minimizes its free energy if most of the adatoms condense into a smooth sheet having a large number of lateral in-plane bonds, with a few stray adatoms to increase configurational entropy.

At high temperatures, the entropy contribution dominates, and the free energy is everywhere concave up. Then, adlayers of *any* composition are stable against phase separation into clusters of adatoms and clusters of missing adatoms. The adatoms are distributed randomly and the surface appears microscopically "rough."

The critical temperature separating smooth, phase-separated adlayers from microscopically rough adlayers is the so-called roughening temperature. It is essentially the critical temperature above which the miscibility gap in this two-component solution vanishes. Since the miscibility gap vanishes when the free energy curve at $\theta = 0.5$ just becomes concave up, the critical temperature is that temperature at which $[\partial^2 f/\partial\theta^2]_{\theta=0.5} = 0$, or $T_{\mathrm{r,adat}} = 2w/k$. Note that the enthalpy of sublimation for this Kossel crystal is the bond energy (w) times the number of bonds per atom (6), divided by the number of atoms per bond (2). Therefore, $\Delta h_{\mathrm{sub}} = 3w$, and we have

$$T_{\mathrm{r,adat}} \approx \frac{2}{3}\Delta h_{\mathrm{sub}}. \tag{6.4}$$

We emphasize that this equation can only give a crude indication of the actual roughening temperature of real crystal surfaces. Its derivation neglected, among other things, multilayer roughness, next-nearest-neighbor and longer-range adatom-adatom interactions, and possible dependences of adatom energies on cluster sizes due to surface reconstruction effects, all of which will tend to decrease $T_{\mathrm{r,adat}}$. Nevertheless, the main idea is that a critical temperature exists above which the equilibrium surface is rough. In some cases, though, this temperature may be above the melting temperature of the crystal, and hence will be unobservable.

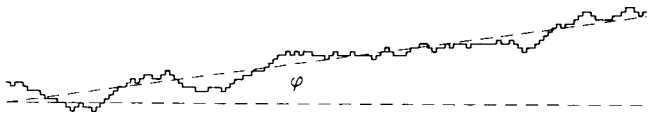

Figure 6.3: A step wandering on the surface of a Kossel crystal due to randomly distributed kinks.

6.1.2 Kinks in Isolated Steps

In Subsection 6.1.1, we considered adatom "excitations" on a singular surface. In practice, real surfaces nearly always contain steps. If the steps are far enough apart not to interact, then their energetics are determined by kink "excitations" along their length. In this subsection, we consider such kink excitations in isolated steps.

Consider the isolated step shown in Figure 6.3. Along this step there may be positive or negative kinks that cause the step to wander randomly.[3] On the one hand, this kink-induced step wandering is favorable, in that it increases the entropy of the step. On the other hand, the kinks themselves are unfavorable, because they cost energy. Indeed, for a simple Kossel crystal, the energy of a single-kink can be calculated, as shown in Fig. 6.4, to be $\epsilon_{\text{kink}} = w/2$, where w is the bond strength. For real crystals, however, the energy of a single kink may be considerably different, due to the reconstructed bonds on the surface.

To quantify the statistics of kinks in steps, let us suppose, for simplicity, that kinks that move steps laterally one lattice unit are much more numerous than those which move steps laterally more than one lattice unit. Note, though, that this approximation breaks down when kink energies are low relative to kT (see e.g., Figure 6.5).

If we nevertheless make this approximation, then we are interested in the probabilities, p_+, p_- and p_o, that an arbitrarily chosen position along a step contains either plus or minus single kinks, or no kink, respectively.[4] Since we have excluded all other possibilities, these must sum to unity:

$$p_+ + p_- + p_o = 0. \tag{6.5}$$

[3] J. Frenkel, "On the surface motion of particles in crystals and the natural roughness of crystalline faces," *J. Phys. U.S.S.R.* **9**, 392 (1945).

[4] W.K. Burton, N. Cabrera, and F.C. Frank, "The growth of crystals and the equilibrium structure of their surfaces," *Philos. Trans. R. Soc. London Ser. A* **243**, 299 (1951).

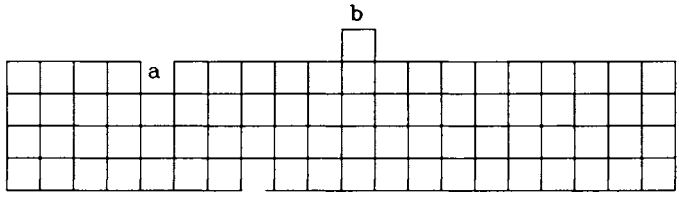

Figure 6.4: In moving an atom from position a to position b, two net bonds are broken, but four kinks are formed. If the bond energy is w, then the energy per kink is $\epsilon_{\text{kink}} = 2w/4 = w/2$.

If we also allow for the step to make a nonzero average angle, ϕ, with the underlying lattice, then the difference between the plus and minus kink probabilities is determined by

$$p_+ - p_- = \tan\phi \equiv p_{\text{ext}}. \tag{6.6}$$

In a sense, p_{ext} defines an "extrinsic" kink probability imposed by the miscut of the step. Then, $p_{\text{int}} = 2p_-$ may be thought of as an "intrinsic" kink probability. Their sum, $p_{\text{int}} + p_{\text{ext}} = p_+ + p_-$, is the total kink probability. If we also assume that the kinks do not interact with each other, then the additional energy of the step due to kinks, per lattice unit along the step, is the total kink probability, times the kink energy, ϵ_{kink}. Hence, the total energy of the step is

$$u_{\text{step}} = \epsilon_{\text{kink}}(p_+ + p_-) + \epsilon_{\text{step}}, \tag{6.7}$$

where ϵ_{step} is the energy per lattice unit of a straight step without kinks.

Since we have assumed the kinks to be independent of each other, the configurational entropy associated with the kinks is determined by the number of ways they may be distinguishably distributed along the length of the step. Following a simple extension of Equation 3.24 to a three-component alloy, the ideal entropy of mixing is

$$-\frac{s_{\text{step}}}{k} = p_+ \ln p_+ + p_- \ln p_- + p_o \ln p_o. \tag{6.8}$$

Altogether, the step free energy is $f_{\text{step}} = u_{\text{step}} - Ts_{\text{step}}$, which we can rewrite in terms of the extrinsic and intrinsic kink probabilities as

$$\begin{aligned} f_{\text{step}} \;=\; & \epsilon_{\text{step}} + \epsilon_{\text{kink}}(p_+ + p_-) \\ & + kT[(p_{\text{ext}} + p_{\text{int}}/2)\ln(p_{\text{ext}} + p_{\text{int}}/2) + (p_{\text{int}}/2)\ln(p_{\text{int}}/2) \\ & + (1 - p_{\text{ext}} - p_{\text{int}})\ln(1 - p_{\text{ext}} - p_{\text{int}})]. \end{aligned} \tag{6.9}$$

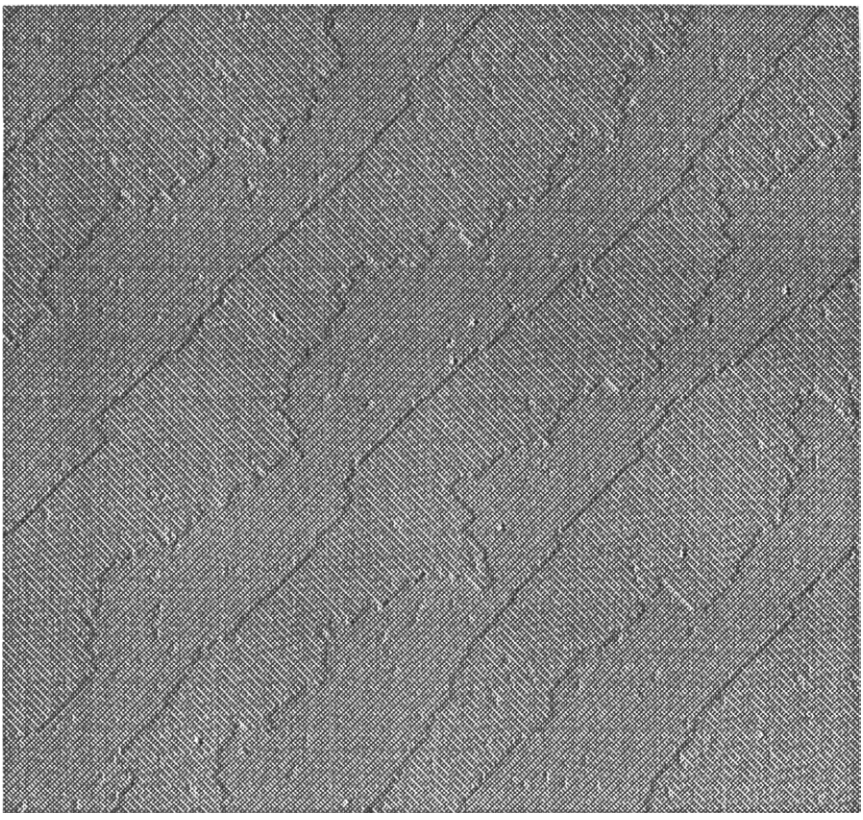

Figure 6.5: Scanning tunneling micrograph of a Si surface misoriented 0.5° from (001) toward [110]. The surface height decreases from upper left to lower right.[a] On this surface, alternate single-height steps are referred to as type SA and SB, and are smooth and rough, respectively, reflecting the relative energies of kink formation.

[a]B.S. Swartzentruber, *Steps on Si(001): Energetics and Statistical Mechanics* (Ph.D Thesis, U. Wisconsin-Madison, 1992).

For a given extrinsic kink probability, the equilibrium intrinsic kink probability is that which minimizes f_{step}, or

$$\begin{aligned} \frac{\partial f_{\text{step}}}{\partial p_{\text{int}}} &= \epsilon_{\text{kink}} + kT[(1/2)\ln(p_{\text{ext}} + p_{\text{int}}/2) + (1/2)\ln(p_{\text{int}}/2) \\ &\quad - (1/2)\ln(1 - p_{\text{ext}} - p_{\text{int}})] \\ &= 0. \end{aligned} \tag{6.10}$$

Rewriting this in terms of the positive, negative, and missing kink probabilities then gives

$$p_+ p_- = p_o^2 e^{-2\epsilon_{\text{kink}}/kT}. \tag{6.11}$$

Note that this equation reproduces exactly the "quasi-chemical" expression of Equation 4.44. The reason is that equilibrium between kinks on a step can be thought of as a balance between forward and backward chemical reactions, with positive and negative kinks annihilating to form missing kinks, and missing kinks thermally unbinding to form positive and negative kinks.

Equations 6.5, 6.6, and 6.11 are sufficient to determine the three equilibrium kink probabilities, and give, after some algebra,

$$\begin{aligned} p_o^{\text{equ}} &= \frac{1 - \sqrt{1 - (1 - 4e^{-2\epsilon_{\text{kink}}/kT})(1 - \tan^2\phi)}}{1 - 4e^{-\epsilon_{\text{kink}}/kT}} \\ p_+^{\text{equ}} &= \frac{\tan\phi}{2} + \sqrt{p_o^2 e^{-2\epsilon_{\text{kink}}/kT} + \frac{1}{4}\tan^2\phi} \\ p_-^{\text{equ}} &= -\frac{\tan\phi}{2} + \sqrt{p_o^2 e^{-2\epsilon_{\text{kink}}/kT} + \frac{1}{4}\tan^2\phi}. \end{aligned} \tag{6.12}$$

For the special case of perfectly cut step for which $\tan\phi = 0$, the energy, entropy, and free energy of an isolated step simplify to

$$\begin{aligned} u_{\text{step}} &= \epsilon_{\text{step}} + 2\epsilon_{\text{kink}} p_- \\ -\frac{s_{\text{step}}}{k} &= 2p_- \ln p_- + (1 - 2p_-)\ln(1 - 2p_-) \\ f_{\text{step}} &= u_{\text{step}} - T s_{\text{step}}. \end{aligned} \tag{6.13}$$

These energies, entropies, and free energies, normalized to the energy of a straight step, are plotted in Figure 6.6 as a function of $p_- = p_+$. For concreteness, we have assumed that kinks add an additional energy equal to the energy of the step itself, $\epsilon_{\text{kink}} = \epsilon_{\text{step}} = w/s$, as they would in a Kossel crystal. At all nonzero temperatures, the free energy initially decreases with increasing p_-, due to entropy, and then increases, due to energy. The kink probabilities at which the free energies minimize are given by Equations 6.12, which, in the limit $\tan\phi = 0$, simplify to

$$\begin{aligned} p_o^{\text{equ}} &= \frac{1}{1 + 2e^{-\epsilon_{\text{kink}}/kT}} \\ p_+^{\text{equ}} = p_-^{\text{equ}} &= \frac{e^{-\epsilon_{\text{kink}}/kT}}{1 + 2e^{-\epsilon_{\text{kink}}/kT}}. \end{aligned} \tag{6.14}$$

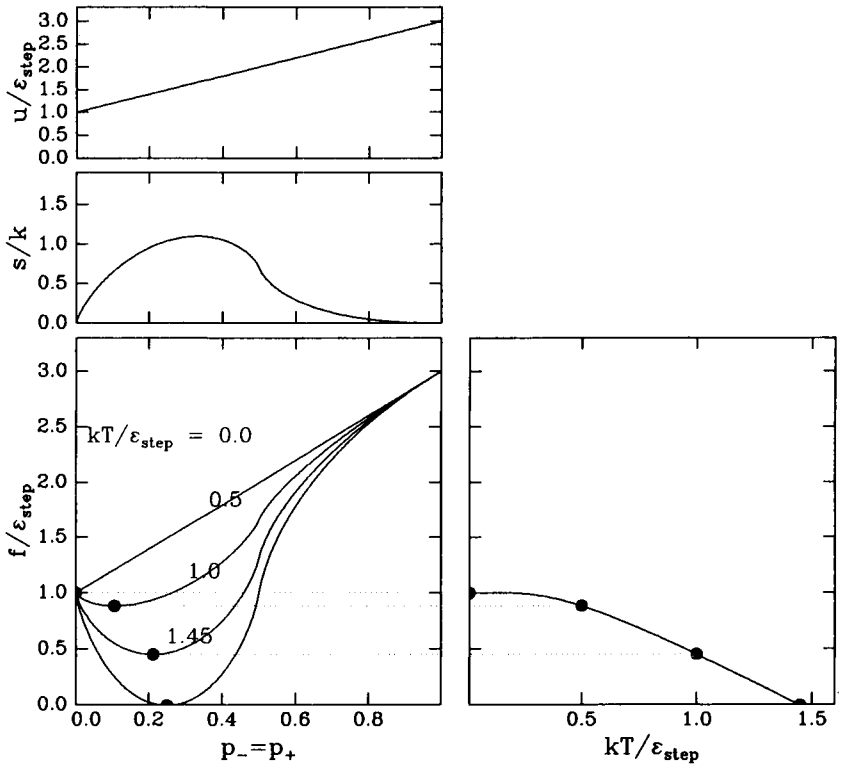

Figure 6.6: Dependences of the energy, entropy, and free energy of a step on the probability of intrinsic kinks. The step is assumed to have no extrinsic kinks, and a kink is assumed to add an additional energy equal to half the energy of a straight step. The energies and free energies are normalized to the energy of a straight step. As the temperature increases, the intrinsic kink probability that minimizes the free energy of the step increases, and the minimum free energy decreases.

At a critical temperature, $T_{r,step}$, the step free energy vanishes at its minimum. Above this temperature, steps will form spontaneously on the surface, and the surface is said to be above its roughening temperature.[5] For a Kossel crystal, this critical temperature is $T_{r,step} \approx \Delta h_{sub}/4$.

Note that this temperature is considerably below that given in the previous subsection by Equation 6.4. Physically, the reason is that, per lattice

[5]An alternative way of calculating the roughening temperature is to calculate the temperature at which the free energies of closed step loops vanishes; see, e.g., A. Zangwill, *Physics at Surfaces* (Cambridge University Press, Cambridge, 1988), pp. 16-17.

site, step excitations on terraces are energetically less costly than adatom and missing adatom excitations. Note also that even this temperature is only a crude indication of the actual roughening temperature of real crystal surfaces. Its derivation neglected, among other things, the possibility that kinks may move steps laterally more than one lattice unit, and the solid-on-solid constraint that prevents steps from crossing each other.

More advanced treatments take both of these effects into account, and are based on an analogy between noncrossing wandering steps on a surface and 1D spinless fermion gases,[6] where the Pauli principle automatically prohibits crossing.[7] These treatments also borrow heavily from studies of domain walls in 2D commensurate adsorbate phases,[8] which are also analogous to 1D spinless fermion gases.[9] The result is that step free energies approach zero at $T_{\mathrm{r,step}}$ according to[10]

$$f_{\mathrm{step}} \sim e^{-c/\sqrt{|T-T_{\mathrm{r}}|}}, \tag{6.15}$$

and represent a second-order phase transition from smooth to rough.

6.1.3 Steps on Vicinal Surfaces

In Subsection 6.1.2, we calculated the free energy of an isolated step wandering on a surface. The free energy was decreased below that of a perfectly straight step due to the configurational entropy associated with the mixing of positive, negative, and missing kinks. In the absence of step-step interactions, the free energy of a surface depends only on the free energy of the terraces plus those of the steps. For a surface miscut by an angle θ away from the orientation of a singular surface, and hence having a step density per lattice site of $s \equiv \tan\theta$, the free energy, per lattice site, would then be

$$f_{\mathrm{surf}} = f_{\mathrm{terr}} + f_{\mathrm{step}} \tan\theta, \tag{6.16}$$

where f_{terr} is the free energy of the singular, unstepped surface, and f_{step} is given by Equation 6.13.

In this subsection, we consider the possibility that the steps interact, and that those interactions give rise to nonlinear dependences of the surface

[6] C. Jayaprakash, C. Rottman and W.F. Saam, "Simple model for crystal shapes: step-step interactions and facet edges," *Phys. Rev.* **B30**, 6549 (1984).

[7] P.G. de Gennes, "Soluble model for fibrous structures with steric constraints," *J. Chem. Phys.* **48**, 2257 (1968).

[8] J.M. Kosterlitz and D.J. Thouless, "Ordering, metastability and phase transitions in two-dimensional systems," *J. Phys.* **C6**, 1181 (1973).

[9] H.J. Schulz, B.I. Halperin, and C.L. Henley, "Dislocation interaction in an adsorbate solid near the commensurate-incommensurate transition," *Phys. Rev.* **B26**, 3797 (1982).

[10] H.J. Schulz, "Equilibrium shape of crystals," *J. Physique* **46**, 257 (1985).

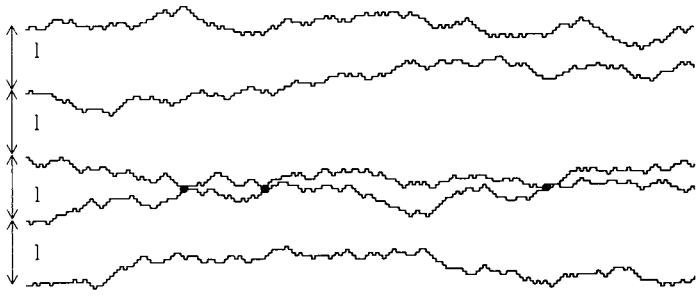

Figure 6.7: Five wandering steps of average spacing l. Two of the steps intersect, by chance, three times.

free energy on $\tan\theta$. Consider the array of steps illustrated in Figure 6.7. On average, they are parallel to each other, but as they wander they occassionally touch. If we do not allow "overhangs" on the surface, then, as mentioned above, the steps are not free to cross each other. Each step is confined by the random wanderings of its immediate neighbors, and its entropy is reduced.[11]

To quantify this entropy reduction, consider again the step intersections shown in Figure 6.7. On the one hand, if the steps were truly independent, then each step intersection point would have two equally likely interpretations: either the steps actually cross, or they bounce back from each other. On the other hand, if the steps cannot cross, then each step intersection can have only the second interpretation. Each step intersection, therefore, has associated with it an entropy decrease of $k \ln 2$.

How often, on average, do the steps intersect? Let $b^2 \equiv p_+ a^2 + p_- a^2$ be the mean square lateral displacement of the step per lattice unit. Then, after n lattice units, the step will have wandered laterally on the average $\sqrt{n}b$ lattice units. Therefore, we expect a collision whenever $\sqrt{n}b$ exceeds the mean spacing between steps, l, or every $n = l^2/b^2$ lattice units.[12]

Altogether, the entropy decrease, per lattice unit, is roughly $(1/n)\ln 2 = (b^2/l^2)\ln 2$. More precise calculations, taking into account the simultaneous

[11] E.E. Gruber and W.W. Mullins, "On the theory of anisotropy of crystal surface tension," *J. Phys. Chem. Solids* **28**, 875 (1967); and G.H. Gilmer and J.D. Weeks, "Statistical properties of steps on crystal surfaces," *J. Chem. Phys.* **68**, 950 (1978).

[12] M.E. Fisher and D.S. Fisher, "Wall wandering and the dimensionality dependence of the commensurate-incommensurate transition," *Phys. Rev.* **B25**, 3192 (1982).

wandering of all the steps, give an entropy decrease of[13]

$$\frac{\Delta s_{\text{step}}}{k} = \frac{\pi^2}{6}\frac{b^2/2}{l^2} = \frac{\pi^2}{12}\frac{b^2}{a^2}\tan^2\phi. \tag{6.17}$$

The surface free energy is therefore

$$f_{\text{surf}} = f_{\text{terr}} + f_{\text{step}}\tan\phi + kT\frac{\pi^2}{12}\frac{b^2}{a^2}\tan^3\phi, \tag{6.18}$$

and contains a cubic dependence on step density.

Suppose, now, that in addition to a short-range repulsion preventing step-step crossings, there is also longer range repulsion.[14] Such a repulsion might be generated, e.g., by strain fields in the substrate surrounding each step.[15] For simplicity, suppose the repulsion takes the quadratic form

$$\Delta u_{\text{step}} = A\left[\frac{1}{(l+x)^2} + \frac{1}{(l-x)^2}\right] \approx \frac{2A}{l^2}\left(1 + x^2/l^2\right), \tag{6.19}$$

where $x = \pm l$ are, as illustrated in Figure 6.8, the positions of rigid steps surrounding (and confining) a center, wandering step.

In the presence of this repulsion, the potential energy of the step decreases the less it wanders away from $x = 0$. However, the entropy of the step also decreases, by $\Delta s_{\text{step}} \approx (\pi^2/12)(b^2/x^2)$. The actual wandering will be determined by a balance between the two, or

$$\frac{d(\Delta u_{\text{step}} - T\Delta s_{\text{step}})}{dx} = \frac{d}{dx}\left[\frac{2A}{l^2}\left(1 + \frac{x^2}{l^2}\right) + kT\frac{\pi^2}{12}\frac{b^2}{x^2}\right] = 0. \tag{6.20}$$

Solving Equation 6.20 then gives the equilibrium alley width within which the step will wander:

$$d = \left(\frac{\pi^2}{24}\frac{kTb^2}{A}\right)^{1/4} l. \tag{6.21}$$

[13]C. Jayaprakash, C. Rottman, and W.F. Saam, "Simple model for crystal shapes: step-step interactions and facet edges," *Phys. Rev.* **B30**, 6549 (1984); and V.V. Voronkov, "Free energy of a stepped surface," in *Growth of Crystals*, Vol. 15, E.I. Givargizov and S.A. Grinberg, Eds. (Consultants Bureau, New York, 1988).

[14]Our treatment follows closely that of N.C. Bartelt, T.L. Einstein, and E.D. Williams, "The influence of step-step interactions on step wandering," *Surf. Sci. Lett.* **240**, L591 (1990).

[15]J.M. Blakely and R.L. Schwoebel, "Capillarity and step interactions on solid surfaces," *Surf. Sci.* **26**, 321 (1971); V.I. Marchenko and A. Ya. Parshin, "Elastic properties of crystal surfaces," *Sov. Phys. JETP* **52**, 129 (1980); F.K. Men, W.E. Packard, and M.B. Webb, "Si (100) surface under an externally applied stress," *Phys. Rev. Lett.* **61**, 2469 (1988); and O.L. Alerhand, A.N. Berker, J.D. Joannopoulos, D. Vanderbilt, R.J. Hamers, and J.E. Demuth, "Finite-temperature phase diagram of vicinal Si(100) surfaces," *Phys. Rev. Lett.* **64**, 2406 (1990).

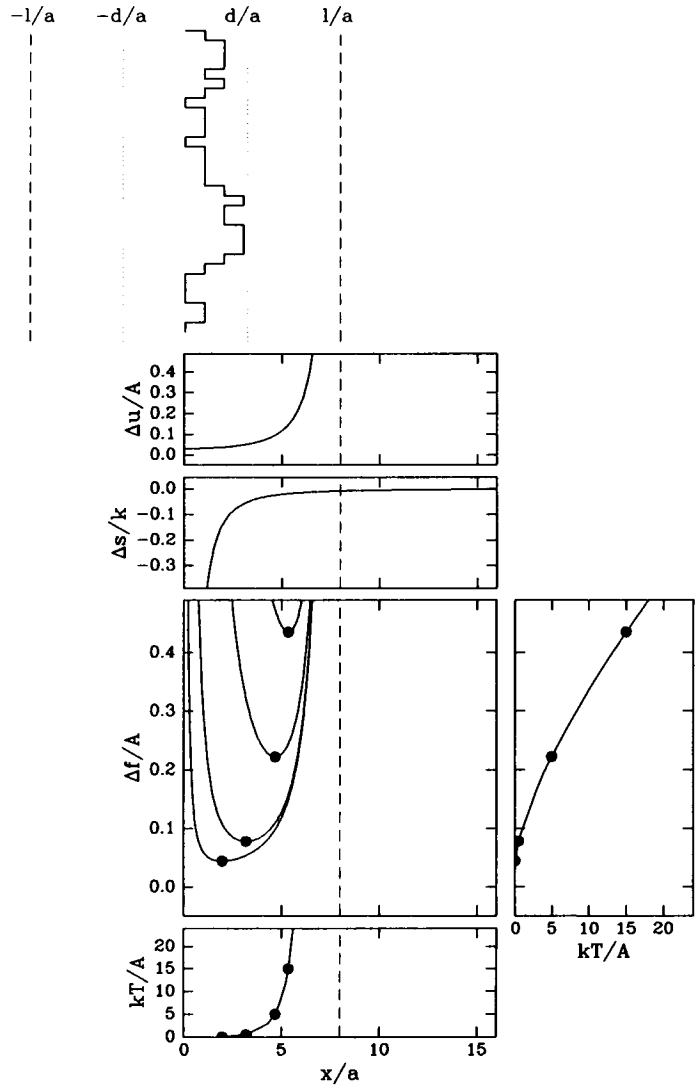

Figure 6.8: Changes in energy, entropy, and free energy as the width of the alley (x/a, in units of lattice constants) within which a step is allowed to wander increases. Both the energy and entropy increase as the width of the alley increases and approaches the mean step spacing (l/a, in units of lattice constants). The equilibrium alley width (d/a, in units of lattice constants) is that which minimizes the free energy. As the ratio between the temperature and the strength of the interaction between steps (kT/A) increases, both the equilibrium alley width and the free energy at that equilibrium alley width increase.

As illustrated in Figure 6.8, this balance will depend on temperature, though only weakly, because of the 1/4 power.

Altogether, the change in free energy, per step, due to step-step interactions, is

$$\Delta f_{\text{step}} = \frac{2A}{l^2}\left(1 + \sqrt{\frac{\pi^2 kTb^2}{6A}}\right). \tag{6.22}$$

As expected, the free energy change increases with the step-step interaction strength, A. It also increases with the root-mean-square kink amplitude, b, since the larger b is, the more "difficult" it is to confine the step.

Finally, we can write the surface free energy, per lattice site, as

$$\begin{aligned} f_{\text{surf}} &= f_{\text{terr}} + (f_{\text{step}} + \Delta f_{\text{step}}) \tan\theta \\ &= f_{\text{terr}} + f_{\text{step}} \tan\theta + \frac{2A}{a^2}\left(1 + \sqrt{\frac{\pi^2 kTb^2}{6A}}\right) \tan^3\theta. \end{aligned} \tag{6.23}$$

Note that the first nonlinear term is cubic, rather than quadratic, in step density. This has consequences, as will be seen in the next section, on the shape of the equilibrium crystal near the $\tan\theta = 0$ orientation.

6.2 Equilibrium Morphology

In Section 6.1, we discussed the statistics of adatoms, kinks, and steps. These statistics are the primary determinants of the orientation dependence of the free energies of vicinal surfaces. In this section, we suppose that we have been *given* complete knowledge of surface free energies, and ask: how do those free energies determine equilibrium morphologies? For macroscopic crystals of constant volume, we will find, in Subsection 6.2.1, that the equilibrium shape is determined by the orientation dependence of the surface free energy through what is known as the Wulff construction. For "planar" surfaces of constant average orientation, we will find, in Subsection 6.2.2, that the equilibrium morphology can be deduced from the orientation dependence of the surface free energy using a common tangent construction. Some average orientations will be stable, while others will tend to break up into combinations of other orientations. Finally, for thin heteroepitaxial films of one material on substrates of another material, we will find, in Subsection 6.2.3, that equilibrium morphologies are determined not only by surface free energies, but by interface and volume free energies as well.

6.2.1 Shapes of Crystals: Wulff's Theorem

We start, in this subsection, by considering a macroscopic crystal of a single material whose overall volume is specified. What shape will this crystal have in equilibrium? We discuss, in turn, three related constructions for equilibrium crystal shapes. The most basic is known as Wulff's construction; from Wulff's construction may be derived what is known as Herring's construction; and from Herring's construction in turn may be derived what is known as Andreev's construction.

Wulff's Construction

Intuitively, we expect the equilibrium shape of a crystal of constant volume to be such that those surfaces whose orientations have less energy will have greater area, while those whose orientations have greater energy will have lesser area.

For example, consider the rectangular prism illustrated in Figure 6.9, bounded by rectangular faces of specific surface free energies γ_x, γ_y, and γ_z. If the distances of each face from the crystal center are h_x, h_y, and h_z, then the face areas are $h_y h_z$, $h_x h_z$, and $h_x h_t$, and the total surface free energy is

$$E = 2\gamma_x h_y h_z + 2\gamma_y h_x h_z + 2\gamma_z h_x h_y. \tag{6.24}$$

If we require the volume, $V = 8h_x h_y h_z$, to be constant, then we can write

$$E = \frac{\gamma_x V}{4h_x} + \frac{\gamma_y V}{4h_y} + 2\gamma_z h_x h_y. \tag{6.25}$$

To find the distances h_x and h_y that minimize the energy, we set $\partial E/\partial h_x = \partial E/\partial h_y = 0$, giving

$$\gamma_x h_y h_z = \gamma_y h_x h_z = \gamma_z h_x h_y = (\gamma_x \gamma_y \gamma_z)^{1/3} V^{2/3} = \text{constant}. \tag{6.26}$$

In other words, the free energies of all the faces of the equilibrium crystal are equal.

Note also that the areas of the faces are inversely proportional to their distances from the center of the crystal [e.g., $h_x h_y = V/(8h_z)$]. Therefore, those distances are in turn proportional to the specific surface free energies:

$$\frac{\gamma_x}{h_x} = \frac{\gamma_y}{h_y} = \frac{\gamma_z}{h_z} = \left(\frac{\gamma_x \gamma_y \gamma_z}{V}\right)^{1/3}. \tag{6.27}$$

In other words, faces of high specific surface free energy lie farther from the center of the crystal than those of low specific surface free energy, and therefore have lower relative surface areas.[16]

[16] P. Curie, "Sur la formation des cristaux et sur les constantes capillaires de leurs différentes faces," *Bull. Soc. Min. de France* **8**, 145 (1885).

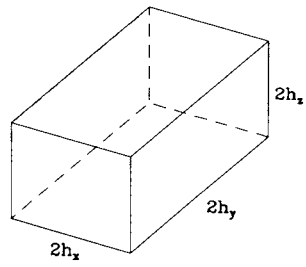

Figure 6.9: Curie's construction for a rectangular prism of fixed volume but minimum surface energy.

The generalization of this argument to all convex bodies is known as the Wulff construction[17]: the crystal shape that minimizes total surface free energy at constant volume is given by the inner envelope of "Wulff" planes perpendicular to and passing through the radius vectors of the orientation-dependent molar surface free energy $\gamma(\theta, \phi)$. This construction is illustrated in two dimensions in Figure 6.10, for a hypothetical $\gamma(\theta)$. As can be seen, this construction places low molar surface free energy orientations nearer to the center of the crystal, thereby increasing their relative surface areas, and places higher molar surface free energy orientations farther from the center of the crystal, thereby decreasing their relative surface areas. Indeed, as we shall see, orientations with very high molar surface free energies may by this construction be placed so far from the center of the crystal that their surface areas vanish entirely, and are no longer represented on the equilibrium crystal shape.

Herring's Construction

An equivalent construction, which may be called Herring's construction,[18] is illustrated in Figure 6.11. One draws spheres passing through the origin and tangent to the $\gamma(\theta, \phi)$ plot. The interior envelope of the points on the spheres diametral to the origin is the equilibrium crystal shape.

To see why, consider the three points labeled O, P, and A on the circumference of the two-dimensional projection of one such sphere. Point O

[17]G. Wulff, *Z. Kristallogr. Mineral.* **34**, 449 (1901); H. Hilton, *Mathematical Crystallography* (Oxford University Press, 1903).

[18]C. Herring, "Some theorems on the free energies of crystal surfaces," *Phys. Rev.* **82**, 87 (1951).

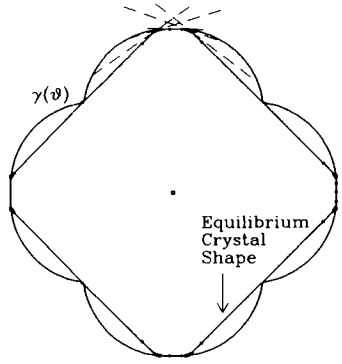

Figure 6.10: Wulff's construction for a two-dimensional crystal of fixed volume but minimum surface energy.

is the origin both of the $\gamma(\theta, \phi)$ plot as well as of the equilibrium crystal. Point A is the point *on* the $\gamma(\theta, \phi)$ plot that the sphere passes tangentially through. Point P is the point on the sphere diametral to the origin.

Because $\overline{OP}$ is a diameter of the sphere, it follows from elementary geometry that the angle $\angle OAP$ is a right angle, and that AP is a Wulff "plane" perpendicular to the $\gamma(\theta, \phi)$ plot at A. Consequently, P is a possible point bounding the equilibrium crystal. To see whether it is an actual such point, we consider two possibilities.

On the one hand, suppose, as illustrated in the left panel of Figure 6.11, that the $\gamma(\theta, \phi)$ plot passes within the tangent sphere at some other point B lying between the origin and another point C on the tangent sphere. Since, again from elementary geometry, $\angle OCP$ must be a right angle, the plane through C at right angles to $\overline{OC}$ must pass through P. Hence, the plane through B at a right angle to $\overline{OB}$ must intersect the line segment $\overline{OP}$ "interior" to the point P, precluding point P from bounding the equilibrium crystal.

On the other hand, suppose, as illustrated in the right panel of Figure 6.11, that the $\gamma(\theta, \phi)$ plot nowhere passes within the tangent sphere. Then, for every point E on the $\gamma(\theta, \phi)$ plot, there must exist some point D on the tangent sphere lying between E and the origin. Since, again, $\angle ODP$ must be a right angle, the plane through D at right angles to OD must pass through P. Hence, the plane through E at a right angle to $\overline{OE}$ must intersect the line through $\overline{OP}$ "exterior" to the point P, and cannot preclude point P from bounding the equilibrium crystal.

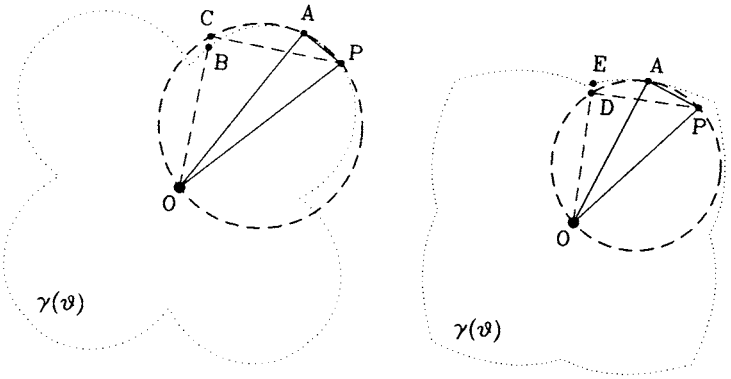

Figure 6.11: Herring's construction for deducing whether orientation A is represented on the equilibrium crystal shape at P. For the $\gamma(\theta)$ plot shown on the left, orientation A is *not* represented, because the $\gamma(\theta)$ plot at another orientation B lies within the tangent circle. For the $\gamma(\theta)$ plot shown on the right, orientation A *is* represented, because at every other orientation (e.g., E) the $\gamma(\theta)$ plot lies outside the tangent circle.

Altogether, the equilibrium crystal shape is the locus of diametral points P on all tangent spheres *not* intersected by other portions of the $\gamma(\theta, \phi)$ plot. Alternatively, one may find first the locus of diametral points P on all tangent spheres without regard to intersections with the $\gamma(\theta, \phi)$ plot, and then take the interior envelope of those points.

Andreev's Construction

In a sense, Herring's construction maps points like A in energy–orientation (θ, ϕ, γ) space onto points like P in real (x, y, z) space. In other words, it tells us where in real space a surface of a particular orientation will appear. To quantify this mapping, consider the circle shown in Figure 6.12 tangent to and passing through the $\gamma(\theta)$ plot at point A. We would like to deduce the (x, z) coordinates of the point P diametral to point O in terms of $\gamma(\theta)$ and $\gamma'(\theta)$ at point A.

First, let us deduce the x coordinates of point P. Denote the lengths of the line segments $\overline{AJ}$ and $\overline{AP}$ by l_1 and l_2, respectively. Then, the x-coordinate of the point P is

$$x = (l_1 + l_2) \cos\theta. \tag{6.28}$$

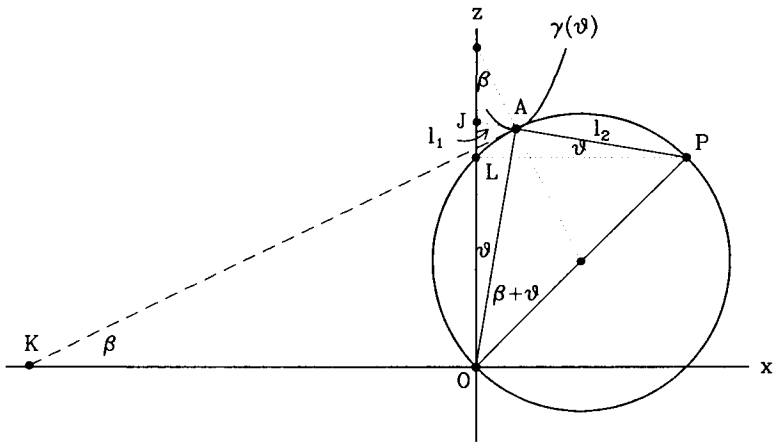

Figure 6.12: Andreev's construction for deducing the mapping between point A in energy–orientation space onto point P on the equilibrium crystal in real space.

Now we note that l_1 is $\gamma \tan\theta$, and if we let β be the angle $\angle AKO$, where the line through $\overline{AK}$ is tangent to $\gamma(\theta)$ at A, then l_2 is $\gamma \tan(\beta + \theta) = \gamma(\tan\beta + \tan\theta)/(1 - \tan\beta\tan\theta)$. Hence,

$$x = \gamma\cos\theta\left(\tan\theta + \frac{\tan\beta + \tan\theta}{1 - \tan\beta\tan\theta}\right). \tag{6.29}$$

Finally, since $\tan\beta$ is the slope of the $\gamma(\theta)$ plot, we can rewrite it as

$$\tan\beta = \frac{\partial(\gamma\cos\theta)}{\partial(\gamma\sin\theta)} = \frac{\partial(\gamma\cos\theta)/\partial\theta}{\partial(\gamma\sin\theta)/\partial\theta} = \frac{-\gamma\sin\theta + \gamma'\cos\theta}{\gamma\cos\theta + \gamma'\sin\theta}. \tag{6.30}$$

Inserting this expression for $\tan\beta$ into Equation 6.29 then gives, after some algebra,

$$x = \gamma'\cos\theta + \gamma\tan\theta\cos\theta = \frac{\partial(\gamma/\cos\theta)}{\partial(\tan\theta)}. \tag{6.31}$$

Second, let us deduce the z-coordinate of point P. By inspection of Figure 6.12, the z-coordinate is the difference between the lengths of the line segments $\overline{OJ}$ and $\overline{LJ}$. Since $\overline{OJ}$ is $\gamma/\cos\theta$ and $\overline{LJ}$ is $x\tan\theta$, we then have

$$z = \frac{\gamma}{\cos\theta} - x\tan\theta = \frac{\gamma}{\cos\theta} - \tan\theta\frac{\partial(\gamma/\cos\theta)}{\partial(\tan\theta)}. \tag{6.32}$$

Equations 6.31 and 6.32 are explicit algebraic expressions for the Herring construction. Note that both are expressed in terms of $f \equiv \gamma/\cos\theta$ and

$s \equiv \tan\theta$. The first is the surface free energy per unit area projected onto a reference surface of orientation $\theta = 0$ and the second is the slope of the misorientation from $\theta = 0$. In terms of f and s, Equations 6.31 and 6.32 can then be rewritten more conveniently as

$$\begin{aligned} x &= \frac{\partial f}{\partial s} \\ z &= f - s\frac{\partial f}{\partial s}. \end{aligned} \tag{6.33}$$

As illustrated in Figures 6.13 and 6.14, the x-coordinate of the surface of the equilibrium crystal having orientation $\theta = \tan^{-1} s$ is the slope $\partial f/\partial s$, and the z-coordinate is the intercept of the tangent to $f(s)$ with the $s = 0$ axis. This simple and elegant mapping, originally derived by Andreev,[19] may be called Andreev's construction.

Note that this mapping of $f(s)$ onto $z(x)$ is essentially a Legendre transformation analogous to those that map energies onto free energies.[20] For example, recall from Chapter 1 that temperature-dependent Helmholtz free energies can be written as $F(T) = U - S(\partial U/\partial S)$, where $T = \partial U/\partial S$. Hence, the equilibrium crystal shape may be regarded as a kind of free energy in which the "extensive" quantity, s, has been replaced by a conjugate "intensive" quantity, $\partial f/\partial s$.

Note also that for vicinal surfaces characterized by a terrace and step structure, s can be regarded as a step density, and $\partial f/\partial s$ can be regarded as a kind of chemical potential for steps. Viewed in this way, crystals evolve toward their equilibrium shape because their surfaces represent "open" systems with respect to interchange of "steps."

To illustrate the use of this powerful and convenient mapping, consider the $f(s)$ and corresponding $z(x)$ plots shown in Figures 6.13 and 6.14. In Figure 6.13, $f(s)$ near $s = 0$ has been assumed to take the cubic form derived in Section 6.1.3,

$$f(s) = a + bs + ds^3. \tag{6.34}$$

Then, the shape of the equilibrium crystal is given by

$$z(x) = f - s\frac{\partial f}{\partial s} = a - 2ds^3 = a - 2d\left(\frac{x-b}{3d}\right)^{3/2}, \tag{6.35}$$

where we have used the mapping $x = \partial f/\partial s = b + 3ds^2$. Hence, the rounded region of the equilibrium crystal joins the $s = 0$ facet at $x =$

[19] A.F. Andreev, "Faceting phase transitions of crystals," *Sov. Phys. JETP* **53**, 1063 (1982).

[20] C. Rottman and M. Wortis, "Statistical mechanics of equilibrium crystal shapes: interfacial phase diagrams and phase transitions," *Phys. Rep.* **103**, 59 (1984).

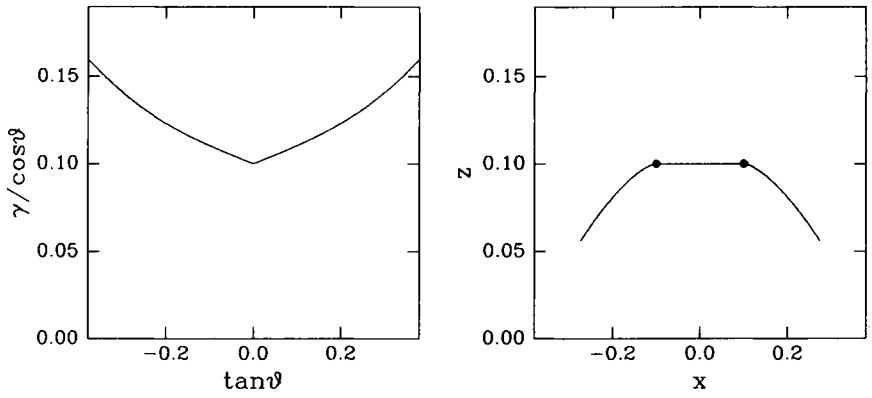

Figure 6.13: Andreev's construction near an orientation around which the projected surface free energy per unit area (left) is concave up in $\tan\theta$, and for which the $\tan\theta = 0$ facet joins the rest of the crystal (right) with a continuous first derivative.

b with a "critical exponent" of 3/2. Because the misorientation of the rounded region goes to zero continuously as the facet is approached [$z'(x)$ is continuous but $z''(x)$ is not], the junction can be thought of as a second-order phase transition.[21]

In Figure 6.14, $f(s)$ has been assumed to be concave down except for cusps at $s = 0$ and $s = \pm 1$. Then, the $z(x)$ mapping becomes "reentrant," and the $s = 0$ and $s = 1$ facets join directly. Because the orientation of the crystal changes discontinuously [$z'(x)$ is discontinuous], the junction can be thought of as a first-order phase transition.

6.2.2 Shapes of Surfaces: Facetting

In Subsection 6.2.1, we discussed various constructions and mappings for deducing the equilibrium shapes of crystals subject to the constraint of constant volume. Often, however, a different constraint is imposed, that of constant average surface orientation. In this subsection, we ask: under what conditions will such a surface be stable, and under what other conditions will it tend to "facet" into combinations of other orientations? An example of such facetting is shown in Figure 6.15.

To answer this question it will be convenient to use the quantities introduced in Subsection 6.2.1. These are the surface free energies per unit

[21] V.L. Pokrovsky and A.L. Talapov, "Ground state, spectrum, and phase diagram of two-dimensional incommensurate crystals," *Phys. Rev. Lett.* **42**, 65 (1979).

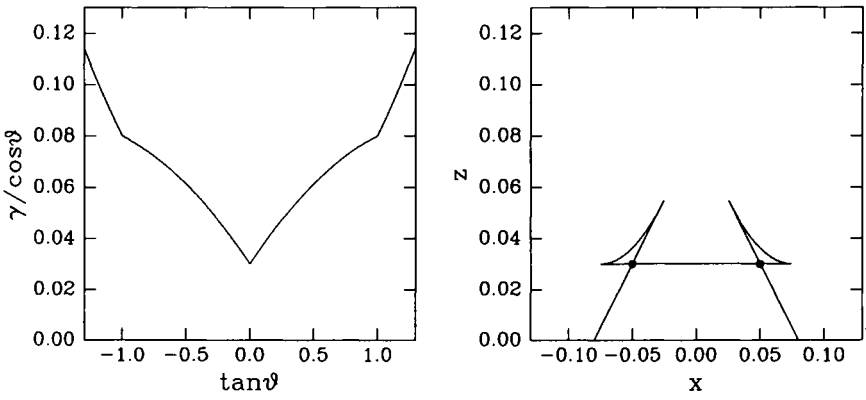

Figure 6.14: Andreev's construction for a crystal with $\tan\theta = 0$ and $\tan\theta = \pm 1$ facets, and between which the projected surface free energy per unit area (left) is concave down in $\tan\theta$. Then, the $\tan\theta = 0$ and $\tan\theta = \pm 1$ facets join (right) with discontinuous first derivatives.

area projected onto a reference surface of orientation $\theta = 0$, $f = \gamma/\cos\theta$; and the slope of the misorientation from $\theta = 0$, $s = \tan\theta$. In terms of these quantities, we will discuss, in turn, the following questions. First, under what conditions will a surface be stable against facetting? Second, if a surface is unstable against facetting, what will the misorientations of the new facetted surfaces be? Third, what is the analogous stability criterion in the more conventional $\gamma(\theta)$ representation? Fourth and finally, how can these ideas be used to generate phase diagrams on which coexistence of surfaces of differing orientations may be represented?

A Stability Criterion

Let us begin by deriving a criterion for the stability of a surface against facetting. Consider the surface depicted by the dotted lines in Figure 6.16, oriented at some angle θ with respect to the reference surface depicted by the dashed lines. Suppose that surface breaks up into the hill and valley structure depicted by the solid lines. If the two new orientations make angles θ_1 and θ_2 with respect to the reference surface, and have areas projected onto the reference surface of x_1 and x_2, then their projected vertical heights are $h_1 = x_1 \tan\theta_1$ and $h_2 = x_2 \tan\theta_2$, respectively.

Under what conditions will the original surface be stable against formation of this hill and valley structure? Since the projected free energy of the original surface is $f(\theta)(x_1 + x_2)$, and that of the two new surfaces is $f(\theta_1)x_1 + f(\theta_2)x_2$, the criterion is that there not exist straddling orienta-

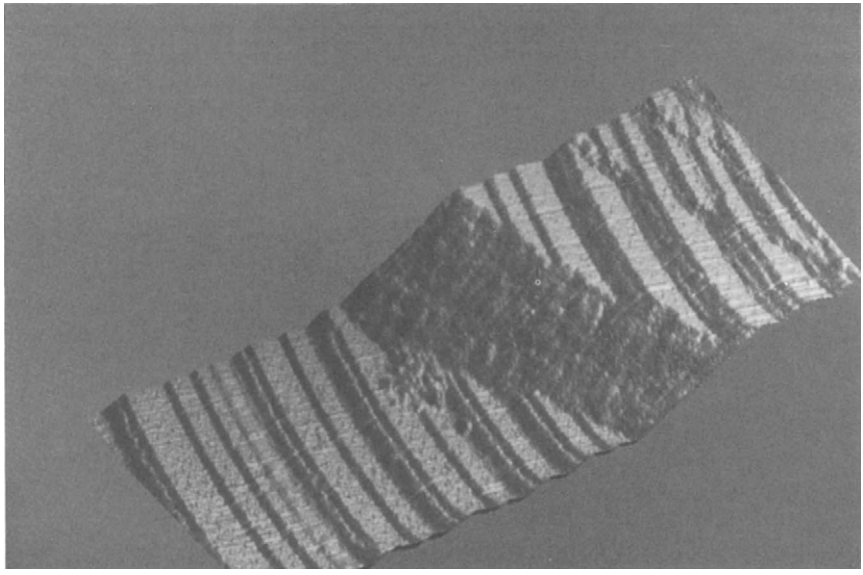

Figure 6.15: Scanning tunneling micrograph of a Si surface cut 6° from (111) along an azimuth rotated about 10° away from the high symmetry $[\bar{1}\bar{1}2]$ direction. The scan area is approximately 200 × 300 Å. The surface has phase separated into two facets of different orientations, one containing 7 × 7 reconstructed terraces separted by straight $[\bar{1}\bar{1}2]$ steps and one rotated azimuthally by approximately 40° from the $[\bar{1}\bar{1}2]$ direction.[a]

[a] J. Wei, X-S Wang, N.C. Bartelt, E.D. Williams, and R.T. Tung, "The precipitation of kinks on stepped Si(111) surfaces," *J. Chem. Phys.* **94**, 8384 (1991).

tions θ_1 and θ_2 such that

$$f(\theta) > f(\theta_1)\frac{x_1}{x_1 + x_2} + f(\theta_2)\frac{x_2}{x_1 + x_2}. \tag{6.36}$$

Note that from the relations $x_1 = h_1/\tan\theta_1$, $x_2 = h_2/\tan\theta_2$, and $x_1 + x_2 = (h_1 + h_2)/\tan\theta$, the fractions of the reference surface that have the two orientations can be deduced, after some algebra, to be

$$\begin{aligned} \frac{x_2}{x_1 + x_2} &= \frac{\tan\theta - \tan\theta_1}{\tan\theta_2 - \tan\theta_1} \\ \frac{x_1}{x_1 + x_2} &= 1 - \frac{\tan\theta - \tan\theta_1}{\tan\theta_2 - \tan\theta_1}. \end{aligned} \tag{6.37}$$

These equations are equivalent to a lever rule that determines, given an average orientation θ, the amounts of two other orientations required for a

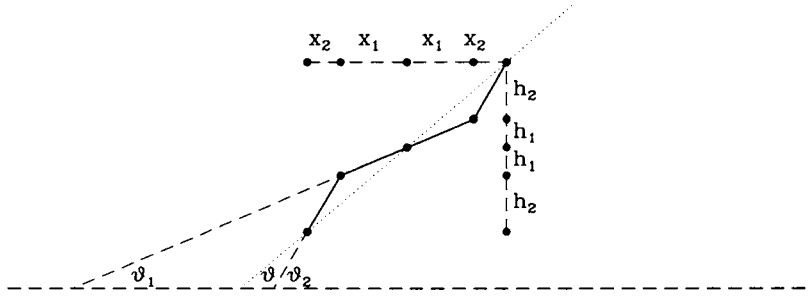

Figure 6.16: Geometry of a surface of average orientation θ that has facetted into two surfaces of orientations θ_1 and θ_2 relative to a reference surface. The projected horizontal widths and vertical heights of the two surfaces are $2x_1$, $2x_2$, $2h_1$, and $2h_2$, respectively.

continuous joining of surfaces. Altogether, the stability criterion is then

$$f(\tan(\theta) < f(\tan\theta_1)\left(1 - \frac{\tan\theta - \tan\theta_1}{\tan\theta_2 - \tan\theta_1}\right) + f(\tan\theta_2)\left(\frac{\tan\theta - \tan\theta_1}{\tan\theta_2 - \tan\theta_1}\right), \tag{6.38}$$

where we consider f to be a function of $\tan\theta$ rather than θ. In other words, a surface of orientation θ is stable if on an f vs. $\tan\theta$ plot, $f(\tan\theta)$ is less than all lever-rule-weighted sums of $f(\tan\theta_1)$ and $f(\tan\theta_2)$.

The Common Tangent Criterion

Now that we have derived a criterion for stability of a surface against facetting, let us ask the opposite question. Suppose that the original surface *is* unstable with respect to breakup? What will be the two straddling orientations, which can be considered two "phases," that will coexist stably in its stead? To answer this question, we imagine making two distinct concerted variations in the geometries of the two surfaces, and require the total free energy change to vanish.

First, we imagine varying the projected vertical height of surface 1 by dh_1, while at the same time varying the projected vertical height of surface 2 by $dh_2 = -dh_1$, so that the two surfaces continue to join perfectly. If each surface is thought of loosely as made up of steps and "missing steps," then

this variation can be thought of as moving steps from surface 2 to surface 1, and at the same time moving missing steps from surface 1 to surface 2.

Since x_1 and x_2 are unchanged during this variation, the free energy changes associated with surfaces 1 and 2 are

$$\frac{\partial(f_1 x_1)}{\partial h_1} = x_1 \frac{\partial f_1}{\partial(x_1 \tan\theta_1)} = \frac{\partial f_1}{\partial \tan\theta_1} \tag{6.39}$$

and

$$-\frac{\partial(f_2 x_2)}{\partial h_2} = -x_2 \frac{\partial f_2}{\partial(x_2 \tan\theta_2)} = -\frac{\partial f_2}{\partial \tan\theta_2}, \tag{6.40}$$

where f_1 and f_2 are the surface free energies per unit area projected onto the reference surface. If the sum of these changes is to vanish, then we must have

$$\frac{\partial f_1}{\partial \tan\theta_1} = \frac{\partial f_2}{\partial \tan\theta_2}. \tag{6.41}$$

In other words, the slopes of the $f(\tan\theta)$ plot at the two orientations θ_1 and θ_2 must be equal.

Second, we imagine varying the projected area of surface 1 by dx_1, while at the same time varying the projected area of surface 2 by $dx_2 = -dx_1$, again so that the two surfaces continue to join perfectly. If each surface is thought of loosely as composed of steps and "missing steps," then this variation can be thought of as moving missing steps from surface 1 to surface 2.

Since h_1 and h_2 are unchanged during this variation, the free energy changes associated with surfaces 1 and 2 are

$$\begin{aligned}
\frac{\partial(f_1 x_1)}{\partial x_1} &= f_1 + \left(\frac{h_1}{\tan\theta_1}\right) \frac{\partial f_1}{\partial(h_1/\tan\theta_1)} \\
&= f_1 - \tan\theta_1 \left(\frac{\partial f_1}{\partial \tan\theta_1}\right) \\
-\frac{\partial(f_2 x_2)}{\partial x_2} &= -f_2 - \left(\frac{h_2}{\tan\theta_2}\right) \frac{\partial f_2}{\partial(h_2/\tan\theta_2)} \\
&= -f_2 + \tan\theta_2 \left(\frac{\partial f_2}{\partial \tan\theta_2}\right).
\end{aligned} \tag{6.42}$$

If the sum of these changes is to vanish, then we must have

$$f_1 - \tan\theta_1 \left(\frac{\partial f_1}{\partial \tan\theta_1}\right) = f_2 - \tan\theta_2 \left(\frac{\partial f_2}{\partial \tan\theta_2}\right). \tag{6.43}$$

In other words, the $\tan\theta = 0$ intercepts of the tangents to the $f(\tan\theta)$ plot at the two orientations θ_1 and θ_2 must be equal.

Altogether, Equations 6.41 and 6.43 combined tell us that both the slopes and intercepts of the two tangents must be equal, and so the tangents themselves must coincide. Therefore, the condition for coexistence of two surfaces of different orientation is that their $f(\tan\theta)$ plots *share a common tangent.*[22] Another way of viewing the origin of this construction is to think of the steps as particles. Then, equilibrium between surfaces of different orientation is analogous to equilibrium with respect to interchange of particles, hence equality of chemical potentials.[23] In a sense, $s \equiv \tan\theta$ is an extensive, rather than an intensive, variable, and can vary inhomogeneously within an equilibrium system.[24]

Herring's Criterion

The common tangent criterion for orientational stability just derived is a powerful and useful one. It implies that conditions for stability and coexistence of surface orientations are formally equivalent to the conditions for stability and coexistence of binary alloy phases. Hence, the arguments and insights derived from Chapter 3 apply directly.

For example, if the $f(\tan\theta)$ plot is concave up as in the top of Figure 6.17, then all orientations are stable. If it is concave down, as in the bottom of Figure 6.17, then only the $\tan\theta = 0$ and $\tan\theta = \pm 1$ facets are stable; all other orientations decompose into a phase mixture of those facets, in proportions given by the lever rule.

This common tangent criterion in the $f(\tan\theta)$ representation can also be understood using the more conventional $\gamma(\theta)$ representation. To see how, note that the critical shape for the $f(\tan\theta)$ plot dividing these two extremes of behavior is a straight line:

$$f(\tan\theta) = A + B\tan\theta. \tag{6.44}$$

Note that on a $\gamma(\theta)$ plot, such straight lines become circles passing through the origin,

$$\gamma(\theta) = (\cos\theta) f(\tan\theta) = A\cos\theta + B\sin\theta, \tag{6.45}$$

with origin at $(A/2, B/2)$ and radius $(A/2)^2 + (B/2)^2$. Hence, $f(\tan\theta)$ plots that are concave up correspond to $\gamma(\theta)$ plots that "bulge" out between facets less than would a sphere passing through the origin, as in the top of Figure 6.17, and $f(\tan\theta)$ plots that are concave down correspond to

[22] A.A. Chernov, "The spiral growth of crystals," *Sov. Phys.–Usp.* **4**, 116 (1961); and N. Cabrera, "The equilibrium of crystal surfaces," *Surf. Sci.* **2**, 320 (1964).

[23] P. Nozières, "Surface melting and crystal shape," *J. Phys.* **50**, 2541 (1989).

[24] N.C. Bartelt, T.L. Einstein, and C. Rottman, "First-order transitions between surface phases with different step structures," *Phys. Rev. Lett.* **66**, 961 (1991).

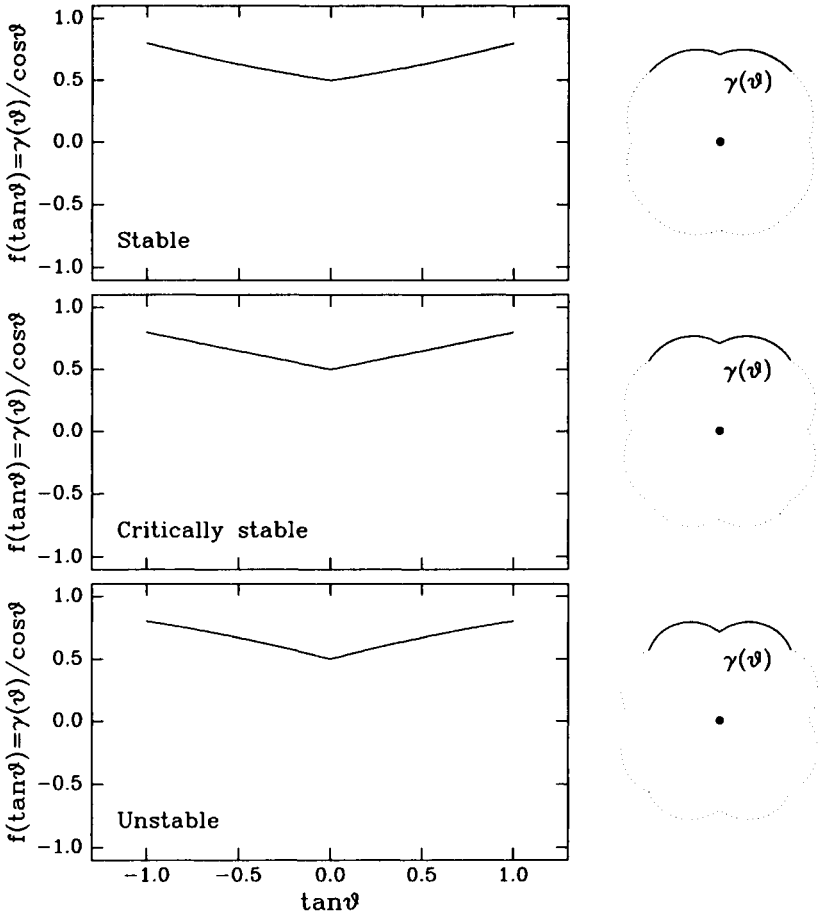

Figure 6.17: Common tangent criteria for orientational stability. The $f(\tan\theta) = \gamma/\cos\theta$ plot at top is concave up between $\tan\theta = 0$ and $\tan\theta = \pm 1$, hence surfaces whose orientations lie between those angles are stable against facetting into an inhomogeneous mix of $\theta = 0$ and $\theta = \pm\pi/4$ surfaces. The $f(\tan\theta) = \gamma/\cos\theta$ plot at bottom is concave down between $\tan\theta = 0$ and $\tan\theta = \pm 1$, hence surfaces whose orientations lie between those angles are unstable against facetting into an inhomogeneous mix of $\theta = 0$ and $\theta = \pm\pi/4$ surfaces. The $f(\tan\theta) = \gamma/\cos\theta$ plot in the middle are straight lines between $\tan\theta = 0$ and $\tan\theta = \pm 1$, hence surfaces whose orientations lie between those angles are critically stable against facetting into an inhomogeneous mix of $\theta = 0$ and $\theta = \pm\pi/4$ surfaces.

$\gamma(\theta)$ plots that bulge out between facets more than would a sphere passing through the origin, as in the bottom of Figure 6.17.[25]

Now, tangent spheres at orientations that bulge less than spherically must lie inside the $\gamma(\theta)$ plot, and hence lie on the equilibrium crystal shape, while tangent spheres at orientations that bulge more than spherically must lie outside the $\gamma(\theta)$ plot, and hence be absent from the equilibrium crystal shape. As a consequence, we also have Herring's criterion, originally proved in a different maner: those orientations are stable that are represented on the equilibrium crystal shape, and those orientations are unstable that are not represented on the equilibrium crystal shape.

Temperature-Dependent Phase Equilibria

Let us now illustrate the stability criterion and common tangent constructions just derived with a concrete example. Consider the cubic 2D crystal shown in Figure 6.18, whose lowest free energy surfaces are (11) and (01) facets. At low temperatures, we expect the $\gamma(\theta)$ plot to be deeply cusped at those orientations, leading to an equilibrium crystal bounded solely by these facets. As temperature increases, the $\gamma(\theta)$ plot becomes less and less cusped. In this case, the (01) facets are shown to roughen first, leading to an equilibrium crystal bounded by continuously curved surfaces joined to (11) facets. Then, the (11) facets roughen, leading to an equilibrium crystal bounded everywhere by continuously curved surfaces.

Another way of looking at the temperature evolution of this system is to plot, as illustrated in Figure 6.19, f vs $\tan\theta$ and $z = f - s(\partial f/\partial s)$ vs $x = \partial f/\partial s$ diagrams. At low temperatures, the $f(\tan\theta)$ plot is deeply cusped at $\tan\theta = 0$ and $\tan\theta = \pm 1$. Application of the common tangent construction then leads to the orientational gap shown in the bottom left of Figure 6.19, and to the first-order facet-facet joining shown in the bottom right of Figure 6.19. At higher temperatures, the $\gamma(\theta)$ plot becomes less and less cusped. As this happens, the orientational gap vanishes, and all orientations become stable. At the same time, the first-order facet-facet joining evolves to a second-order joining, and ultimately disappears entirely.

Finally, it is often convenient to plot these orientational gaps (in $\tan\theta$) and facet-facet phase transition positions (in $x = \partial f/\partial s$) as temperature-dependent phase diagrams. The resulting $T(\tan\theta)$ phase diagram is shown

[25] $\gamma(\theta)$ plots composed of *exactly* spherical bulges between facets, as in the middle of Figure 6.17, are also known as "raspberry" figures; see F.C. Frank, "The geometrical thermodynamics of surfaces," in W.D. Robertson and N.A. Gjostein, Eds., *Metal Surfaces: Structure, Energetics and Kinetics*, Proceedings of a joint seminar of the American Society for Metals and the Metallurgical Society of AIME, October 27-28, 1962 (American Society for Metals, Metals Park, Ohio, 1963), Chap. 1.

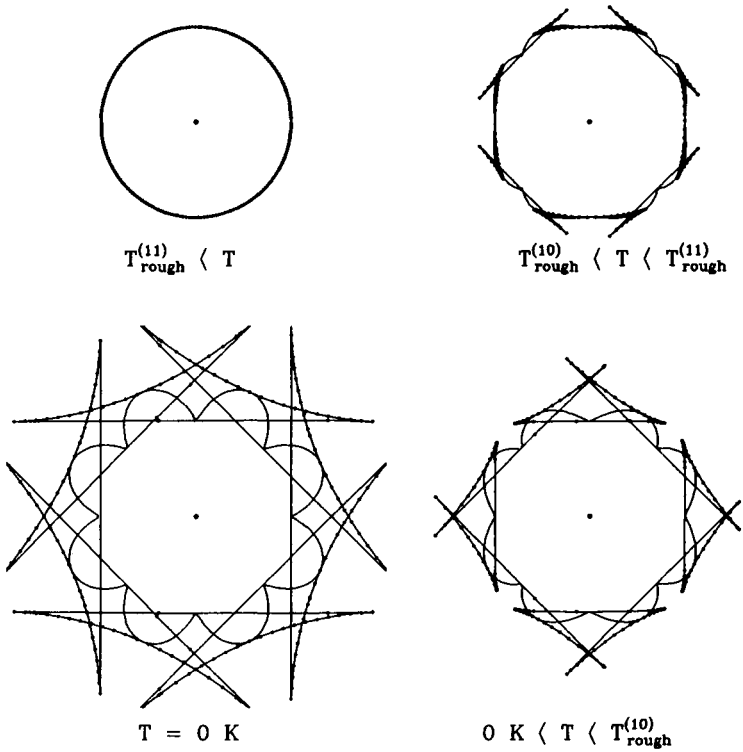

Figure 6.18: Equilibrium shapes for a hypothetical 2D crystal with both (11) and (01) facets. As temperature increases (counterclockwise from lower left), the $\gamma(\theta)$ plot becomes less and less cusped, and the equilibrium shape becomes less and less faceted.

in the middle left of Figure 6.19. It maps out the critical values of $\tan\theta$ for which surfaces of a specified average orientation will decompose into mixtures of orientations. At temperatures below 380 K, only (11) and (01) facets are stable; all other orientations decompose into lever-rule mixtures of those orientations. At temperatures above 380 K, orientations near (01) become stable; all other orientations now decompose into lever-rule mixtures of (11) facets and nonsingular orientations near (01). With increasing temperature above 380 K, orientations farther and farther from (01) become stable, until at 900 K, even orientations near (11) are stable. Above 900 K, surfaces of any average orientation will be stable against decomposition into inhomogeneous mixtures of surfaces of differing orientations.

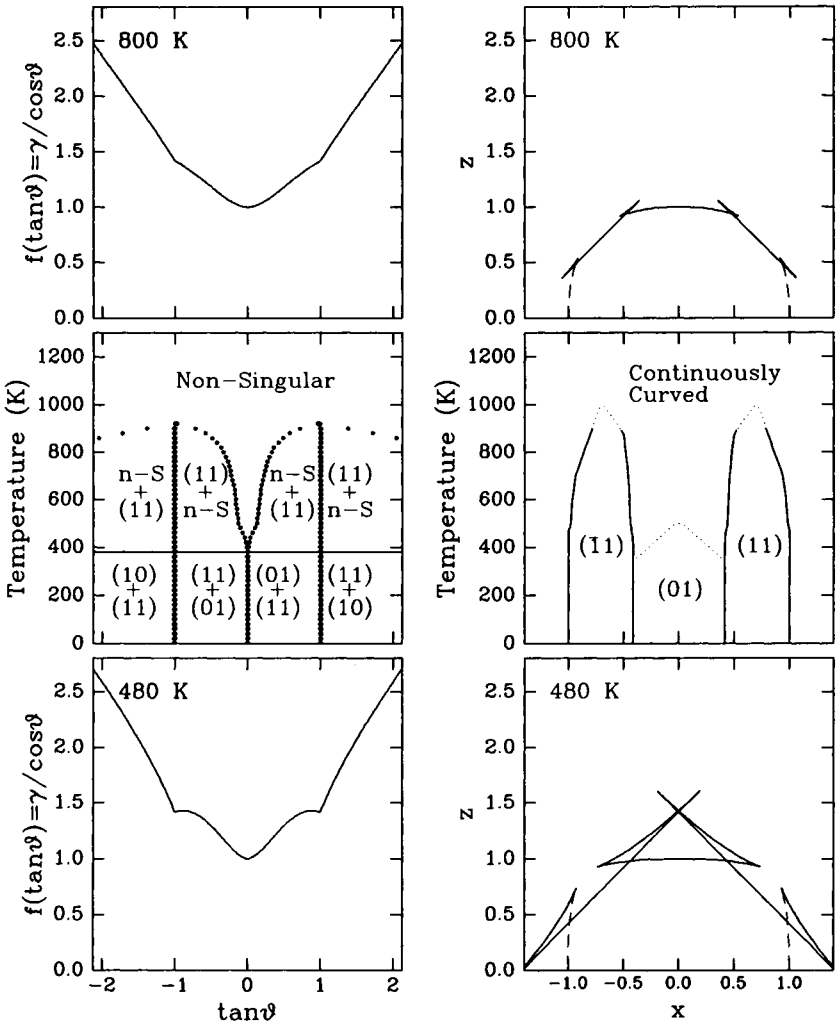

Figure 6.19: Orientational phase diagrams for the hypothetical 2D crystal illustrated in Figure 6.18. The left middle diagram shows the mixtures of orientations that a surface of a specifice average orientation will decompose into. The right middle diagram shows the horizontal positions at which different facets join on the equilibrium crystal; solid and dotted lines indicate first- and second-order phase transitions, respectively. Above and below the diagrams are examples of the $\gamma/\cos\theta$ vs $\tan\theta$ and $z = f - s(\partial f/\partial s)$ vs $x = \partial f/\partial s$ plots from which these diagrams were derived.

The corresponding $T(x)$ phase diagram is shown in the middle right of Figure 6.19. It maps out the critical horizontal positions at which different facets join on the equilibrium crystal. At temperatures below 380 K, (11) facets join (01) facets in first-order phase transitions. At temperatures above 380 K, orientations near (01) begin to appear. As a consequence, (11) facets join continuously curved orientations near (01) in first-order phase transitions, while the continuously curved orientations near (01) join (01) facets in second-order phase transitions. With increasing temperature above 380 K, these alternative orientations near (01) become increasingly stable, until at 500 K the (01) facets "roughen" and disappear entirely.

Above 500 K, (01) facets are absent from the equilibrium crystal, but (11) facets are present, and continue to join continuously curved orientations near (01) in first-order phase transitions. With increasing temperature above 500 K, though, these continuously curved orientations approach more and more closely (11) orientations, until at 900 K the (11) facets begin to join these continuously curved orientations in second-order phase transitions. Finally, at 1000 K, the (11) facet itself "roughens" and disappears entirely.

6.2.3 Shapes of Thin Films: Growth Modes

Thus far, in Subsections 6.2.1 and 6.2.2, we have been concerned with single-material systems, e.g., homoepitaxial films of one material on substrates of the same material. Then, the surface free energy and, in particular, its orientation dependence, plays the most important role in determining the equilibrium morphology. However, for two-material systems, e.g., heteroepitaxial films of one material on substrates of another material, interface and volume free energies also play important roles.[26]

In this subsection, we discuss how these energies determine the equilibrium morphology, or "growth mode," of the film. We discuss two approaches in turn. The first approach considers the shape of the thickness-dependent total free energy. The second approach considers the contact angles that the film islands make with the substrate, as determined by the surface and interface energies.

Free Energies

Consider the thickness-dependent total free energy curves shown in Figure 6.20. Note that these are the total free energies of the system relative

[26] E.G. Bauer, "Phänomenologische theorie der kristallabscheidung an oberflächen. I & II," *Z. Kristallogr.* **110**, 372, 395 (1958), *NASA Technical Translations* **TT F-11**, 888 and 889 (NASA, Washington, D.C., August, 1968).

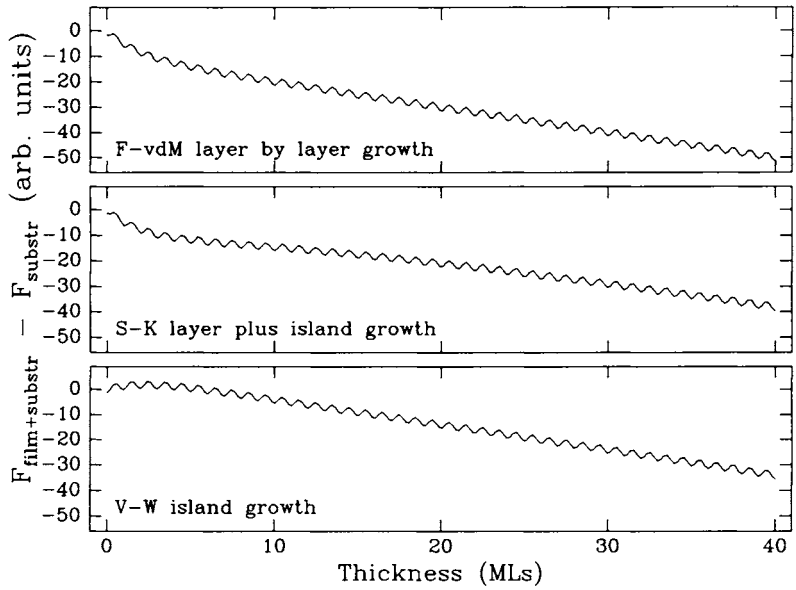

Figure 6.20: Thickness dependences of total free energies for the three classical heteroepitaxial growth modes.

to that of the bare substrate, and include both volume and surface contributions. We assume that there is a nonzero driving force for epitaxy, and so in each panel the overall trend is for the free energy to decrease with increasing thickness of the heteroepitaxial layer. We also assume that fully completed layers, with fully laterally coordinated atoms, have slightly lower energies than partially completed layers, and so in each panel the free energies are shown corrugated slightly with a monolayer periodicity.

There are three cases of interest.[27] In the top panel of Figure 6.20, the sum of the free energies associated with the free surface of the epitaxial film, $\gamma_{e/v}$, and with the interface between the substrate and the epitaxial film, $\gamma_{s/e}$, is less than or equal to that associated with the original substrate surface, $\gamma_{s/v}$:

$$\gamma_{e/v} + \gamma_{s/e} < \gamma_{s/v}. \tag{6.46}$$

Then, the overall free energy decreases faster over the first layer (or two), before settling down to a steady state slope for thicker films. The overall shape of the thickness-dependent free energy is then concave up. Therefore,

[27] M.H. Grabow and G.H. Gilmer, "Thin film growth modes, wetting and cluster nucleation," *Surf. Sci.* **194**, 333 (1988).

for every integral-monolayer thickness, the system is thermodynamically stable against breakup into inhomogeneous regions, some thicker and some thinner. This leads to what is known as the ideal Frank-van-der-Merwe layer-by-layer growth mode.[28]

In the bottom panel, the sum of $\gamma_{e/v}$ and $\gamma_{s/e}$ is greater than $\gamma_{s/v}$:

$$\gamma_{e/v} + \gamma_{s/e} > \gamma_{s/v}. \tag{6.47}$$

Then, the overall free energy *increases* at first as the first layer (or two) is deposited, before turning around and decreasing for thicker films. The overall shape of the thickness-dependent free energy is then concave down. Systems of uniform thickness are therefore thermodynamically unstable against breakup into inhomogeneous regions, some very thick and some completely uncovered. This leads to what is known as the Volmer-Weber island growth mode.[29] It is often observed in "dirty" systems in which impurities lower the free energy of the starting surface, but are buried shortly after heteroepitaxy begins.[30]

In the middle panel, the sum of $\gamma_{e/v}$ and $\gamma_{s/e}$ is, just as in the top panel, less than $\gamma_{s/v}$:

$$\gamma_{e/v} + \gamma_{s/e} > \gamma_{s/v}. \tag{6.48}$$

Therefore, the surface free energy decreases faster as the first layer (or two) is deposited. However, because of some constraint that the substrate imposes on the epilayer, the energy decreases less steeply as subsequent layers are deposited. Only for very thick films, when the epilayer decouples from the substrate, does the energy decrease as steeply as expected for a given driving force for homoepitaxy. The overall shape of the thickness-dependent free energy is therefore initially concave up, but then subsequently concave down. Films thicker than a few layers are therefore unstable to breakup into inhomogeneous regions, some very thick and some having only one (or two) layers. This leads to what is known as the Stranski-Krastanov layer plus island growth mode.[31]

[28]F.C. Frank and J.H. van der Merwe, "One-dimensional dislocations. I. Static theory," *Proc. R. Soc. London* **A198**, 205 (1949); F.C. Frank and J.H. van der Merwe, "One-dimensional dislocations. II. Misfitting monolayers and oriented overgrowth," *Proc. R. Soc. London* **A198**, 216 (1949); F.C. Frank and J.H. van der Merwe, "One-dimensional dislocations. III. Influence of the second harmonic term in the potential representation, on the properties of the model," *Proc. R. Soc. London* **A200**, 125 (1950); and F.C. Frank and J.H. van der Merwe, "One-dimensional dislocations. IV. Dynamics," *Proc. R. Soc. London* **A201**, 261 (1950).

[29]M. Volmer and A. Weber, "Keimbildung in übersättigten gebilden," *Z. Phys. Chem.* **119**, 277 (1926).

[30]B.A. Joyce, "The growth and structure of semiconducting thin films," *Rep. Prog. Phys.* **37**, 363 (1974).

[31]I.N. Stranski and L. Krastanow, "Zur theorie der orientierten ausscheidung von

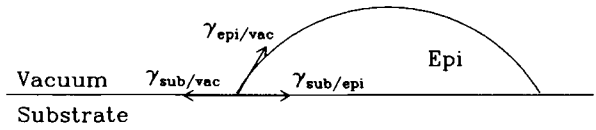

Figure 6.21: Surface tension forces acting on a heteroepitaxial nucleus on a substrate.

In practice, the growth mode that often applies to strained-layer heteroepitaxy is the Stranski-Krastanov growth mode. Films thinner than the critical thickness for strain relaxation are strained, and their free energies do not decrease with increasing thickness as steeply as the free energies of unstrained films. Films above the critical layer thickness, however, relax, and their free energies decrease at a rate approaching that for unstrained homoepitaxy.

Contact Angles

Another way of looking at these three classic growth modes is to consider the contact angle of a spherical heteroepitaxial cap on the surface.[32] If, as shown in Figure 6.21, the free energies of each interface are considered vector forces lying within their respective interfaces, then lateral force balance requires that

$$\gamma_{s/v} = \gamma_{s/e} + \gamma_{e/v} \cos\beta. \tag{6.49}$$

The contact angle will therefore be given by

$$\cos\beta = \frac{\gamma_{s/v} - \gamma_{s/e}}{\gamma_{e/v}}. \tag{6.50}$$

If $(\gamma_{s/v} - \gamma_{s/e})/\gamma_{e/v} > 1$, then there is no contact angle satisfying Equation 6.50, the cap is unstable, the heteroepitaxial layer wets the substrate, and Frank-van-der-Merwe layer-by-layer growth occurs. If $(\gamma_{s/v} - \gamma_{s/e})/\gamma_{e/v} < 1$ then there is a finite contact angle satisfying Equation 6.50, caps having that contact angle are stable, the heteroepitaxial layer does not wet the substrate, and Volmer-Weber island growth occurs.

ionenkristallen aufeinander," *Ber. Akademie der Wissenschaften und der Literatur, Mainz. Mathematisch-Naturwissenschaftliche Klasse*, **146**, 797 (1939).

[32]R. Kern, G. Le Lay and J.J. Metois, "Basic mechanisms in the early stages of epitaxy," in *Current Topics in Materials Science*, Vol. 3, E. Kaldis, Ed. (North-Holland, Amsterdam, 1979).

If $(\gamma_{s/v} - \gamma_{s/e})/\gamma_{e/v}$ depends on thickness, then it is possible for the first few layers to wet the substrate, for subsequent layers to island, and for the growth mode to be Stanski-Krastanov layer-plus-island. For example, for an island on a bare substrate, $(\gamma_{s/v} - \gamma_{s/e})/\gamma_{e/v}$ may be greater than unity, so that a wetting epilayer forms. Then, for an island on a wetting epilayer, $(\gamma_{w/v} - \gamma_{w/e})/\gamma_{e/v}$, where $\gamma_{w/v}$ is the surface free energy of the wetting layer and $\gamma_{w/e}$ is the interface free energy between the wetting layer and the epilayer, may be less than unity, so that islands form on the wetting epilayer.

This can come about in strained heteroepitaxy if the strain and dislocation energies of the epitaxial film are thought of as an effective interface free energy that is included as part of $\gamma_{w/e}$. Then, for very thin (monolayer) films, $\gamma_{s/v}$ may be so large that $(\gamma_{s/v} - \gamma_{s/e})/\gamma_{e/v}$ is greater than unity and the first epilayer wets the substrate. For very thick, unstrained films, the free energy of the interface between the first wetting epilayer and subsequent epilayers ($\gamma_{w/e}$) would normally vanish, and the surface free energies of the wetting epilayer ($\gamma_{w/v}$) and subsequent epilayers ($\gamma_{e/v}$) would be equal. Hence $(\gamma_{w/v} - \gamma_{w/e})/\gamma_{e/v} \to 1$, and islands would be unstable. For intermediate thickness strained films, however, with a finite $\gamma_{w/e}$, $(\gamma_{w/v} - \gamma_{w/e})/\gamma_{e/v} < 1$, and islands will be stable.

6.3 Nonequilibrium Morphology

In Section 6.2, we discussed equilibrium shapes of crystals and crystal surfaces in the *absence* of growth. In this section, we discuss nonequilibrium shapes in the *presence* of growth. We restrict our attention to homoepitaxy on simple starting surfaces at or near singular orientations, and composed of noninteracting arrays of steps. We do not treat the interesting but exceedingly complex cases of epitaxy on starting surfaces well away from singular orientations or of growth on inhomogeneous, "patterned" starting surfaces composed of multiple orientations.[33] We also do not treat the important but complex case of heteroepitaxy, in which surface morphology is often tightly coupled to the transition between coherency and semicoherency (see, e.g., Exercise 2 in Chapter 5), and in which Stranski-Krastonov layer-plus-island and Volmer-Weber island growth modes are often observed. Finally, we also neglect effects due to surface reconstructions in covalently bonded

[33] W.W. Mullins, "Flattening of a nearly plane solid surface due to capillarity," *J. Appl. Phys.* **30**, 77 (1959); W.T. Tsang and A.Y. Cho, "Growth of GaAs–$Ga_{1-x}Al_xAs$ over preferentially etched channels by molecular beam epitaxy: a technique for two-dimensional thin-film definition," *Appl. Phys. Lett.* **30**, 293 (1977); and E. Kapon, M.C. Tamargo, and D.M. Hwang, "Molecular beam epitaxy of GaAs/AlGaAs superlattice heterostructures on nonplanar substrates," *Appl. Phys. Lett.* **50**, 347 (1987).

semiconductors,[34] or due to the interplay between morphology and composition that can occur on the surfaces of binary alloys.[35]

In modeling nonequilibrium surface morphology, it is useful to distinguish between two approaches. In the first approach, surface morphology is modeled directly. At one extreme, molecular dynamics simulations track the exact positions $\{\vec{r_1}, \vec{r_2}, \ldots\}$ of all atoms as they move in response to forces between them.[36] At the other extreme, continuum models track the height h of a coarse-grained surface position (x, y). The time evolution of $h(x, y)$ is determined by various driving (e.g., growth with stochastic noise) and relaxation (e.g., diffusional) terms.[37] In between these two extremes, Monte Carlo simulations track the column heights n of discrete surface lattice sites (i, j). The time evolution of the $n(i, j)$ is determined by the probabilities of surmounting assumed energy barriers separating various configurations.[38]

In the second approach, surface morphology is not modeled directly. Instead, the surface is decomposed into defects of various kinds, such as steps, 2D islands, and adatoms. The time evolution of surface morphology is then determined by the dynamics of the motion and interactions of these defects.

In this section, we will take the second approach. Its disadvantage is

[34] See, e.g., S.A. Barnett and A. Rockett, "Monte Carlo simulations of Si(001) growth and reconstruction during molecular beam epitaxy," *Surf. Sci.* **198**, 133 (1988); and H.-J. Gossman and L.C. Feldman, "Initial stages of silicon molecular-beam epitaxy: effects of surface reconstruction," *Phys. Rev.* **B32**, 6 (1985).

[35] A. Madhukar and S.V. Ghaisas, "The nature of molecular beam epitaxial growth examined via computer simulations," *CRC Critical Reviews in Solid State and Materials Sciences* **14**, 1 (1988).

[36] M. Schneider, A. Rahman, and I.K. Schuller, "Role of relaxation in epitaxial growth: a molecular-dynamics study," *Phys. Rev. Lett.* **55**, 604 (1985); E.T. Gawlinski and J.D. Gunton, "Molecular-dynamics simulation of molecular-beam epitaxial growth of the silicon (100) surface," *Phys. Rev.* **B36**, 4774 (1987); S. Das Sarma, S.M. Paik, K.E. Khor, and A. Kobayashi, "Atomistic numerical simulation of epitaxial crystal growth," *J. Vac. Sci. Technol.* **B5**, 1179 (1987); and D. Srivastava and B.J. Garrison, "Growth mechanisms of Si and Ge epitaxial films on the dimer reconstructed Si (100) surface via molecular dynamics," *J. Vac. Sci. Technol.* **A8**, 3506 (1990).

[37] M. Kardar, G. Parisi, and Y-C Zhang, "Dynamic scaling of growing interfaces," *Phys. Rev. Lett.* **56**, 889 (1986); D.E. Wolf, "Kinetic roughening of vicinal surfaces," *Phys. Rev. Lett.* **67**, 1783 (1991); Z.-W. Lai and S. Das Sarma, "Kinetic growth with surface relaxation: continuum versus atomistic models," *Phys. Rev. Lett.* **66**, 2348 (1991).

[38] F.F. Abraham and G.H. White, "Computer simulation of vapor deposition on two-dimensional lattices," *J. Appl. Phys.* **41**, 1841 (1970); G.H. Gilmer and P. Bennema, "Simulation of crystal growth with surface diffusion," *J. Appl. Phys.* **43**, 1347 (1972); S. Clarke and D.D. Vvedensky, "Origin of reflection high-energy electron-diffraction intensity oscillations during molecular-beam epitaxy: a computational modeling approach," *Phys. Rev. Lett.* **58**, 2235 (1987); and P.A. Maksym, "Fast Monte Carlo simulation of MBE growth," *Semicond. Sci. Technol.* **3**, 594 (1988).

that it requires *a priori* knowledge of the important defect types and the ways in which they interact, knowledge that is currently far from complete. Its advantage, though, is that it simplifies and brings deeper physical understanding to a rich statistical behavior. The evolution of surface morphology is complex and highly nonlinear, often even oscillatory upon initiation of growth. Indeed, such oscillations, illustrated in Figure 3.14 have been observed by reflection high-energy electron diffraction (RHEED) and other *in situ* measurements in a variety of materials, including III-V,[39] IV-IV,[40] II-VI[41] and I-VII[42] compounds, as well as metals[43] and high-T_c superconductors.[44] Similar oscillations have also been observed during

[39]J.J. Harris, B.A. Joyce, and P.J. Dobson, "Oscillations in the surface structure of Sn-doped GaAs during growth by MBE," *Surf. Sci.* **103**, L90 (1981); C.E.C. Wood, "RED intensity oscillations during MBE of GaAs," *Surf. Sci.* **108**, L441 (1981); J.N. Eckstein, C. Webb, S.-L. Weng, and K.A. Bertness, "Photoemission oscillations during epitaxial growth," *Appl. Phys. Lett.* **51**, 1833 (1987); L.P. Erickson, M.D. Longerbone, R.C. Youngman, and B.E. Dies, "The observation of oscillations in secondary electron emission during the growth of GaAs by MBE," *J. Crystal Growth* **81**, 55 (1987); J.P. Harbison, D.E. Aspnes, A.A. Studna, L.T. Florez, and M.K. Kelly, "Oscillations in the optical response of (001) GaAs and AlGaAs surfaces during crystal growth by molecular beam epitaxy," *Appl. Phys. Lett.* **52**, 2046 (1988); and J.Y. Tsao, T.M. Brennan, and B.E. Hammons, "Oscillatory As_4 surface reaction rates during molecular beam epitaxy of AlAs, GaAs and InAs," *J. Crystal Growth* **111**, 125 (1991).

[40]T. Sakamoto, N.J. Kawai, T. Nakagawa, K. Ohta, and T. Kojima, "Intensity oscillations of reflection high-energy electron diffraction during silicon molecular beam epitaxial growth," *Appl. Phys. Lett.* **47**, 617 (1985).

[41]L.A. Kolodziejski, R.L. Gunshor, N. Otsuka, B.P. Gu, Y. Hefetz, and A.V. Nurmikko, "Use of RHEED oscillations for the growth of 2D magnetic semiconductor superlattices (MnSe/ZnSe)," *J. Cryst. Growth* **81**, 491 (1987).

[42]H. Dabringhaus and H.J. Meyer, "Untersuchung der kondensation und verdampfung von alkalihalogenid-kristallen mit molekularstrahlmethoden. II. Relaxationseffekte auf der (100)-oberfläche von KCl," *J. Cryst. Growth* **16**, 31 (1972); and H.J. Meyer and H. Dabringhaus, "Molecular processes of condensation and evaporation of alkali halides," in *Current Topics in Materials Science* Vol. 1, E. Kaldis, Ed. (North-Holland, Amsterdam, 1978), Chap. 2.

[43]Y. Namba, R.W. Vook, and S.S. Chao, "Thickness periodicity in the Auger line shape from epitaxial (111) Cu films," *Surf. Sci.* **109**, 320 (1981); T. Kaneko, M. Imafuku, C. Kokubu, R. Yamamoto, and M. Doyama, "The first observation of RHEED intensity oscillation during the growth of Cu/Mo multi-layered films," *J. Phys. Soc. Jpn.* **55**, 2903 (1986); S.T. Purcell, B. Heinrich, and A.S. Arrott, "Intensity oscillations for electron beams reflected during epitaxial growth of metals," *Phys. Rev.* **B35**, 6458 (1987); C. Koziol, G. Lilienkamp, and E. Bauer, "Intensity oscillations in reflection high-energy electron diffraction during molecular beam epitaxy of Ni on W (110)," *Appl. Phys. Lett.* **51**, 901 (1987); and D.A. Steigerwald and W.F. Egelhoff, Jr., "Observation of intensity oscillations in RHEED during the epitaxial growth of Cu and fcc Fe on Cu (100)," *Surf. Sci.* **192**, L887 (1987).

[44]T. Terashima, Y. Bando, K. Iijima, K. Yamamoto, K. Hirata, K. Hayashi, K. Kamigaki, and H. Terauchi, "Reflection high-energy electron diffraction oscillations during epitaxial growth of high-temperature superconducting oxides," *Phys. Rev. Lett.* **65**, 2684 (1990).

Péclet number	Growth Regime
$L^2 j/D \ll 1$	"Diffusional" Step Flow
$L^2 j/D \approx 1$	"Convective" Step Flow
$L^2 j/D > 1$	2D Nucleation and Growth
$L^2 j/D \gg 1$	Statistical Growth

Table 6.1: Magnitudes of Péclet numbers and the corresponding type of growth.

other kinds of crystal growth, such as electrocrystallization[45] and gas source or chemical beam epitaxy.[46]

To organize our treatment, we consider in the following Subsections the four regimes of behavior on vicinal (stepped) surfaces indicated in Table 6.1. These regimes are distinguished by the ratio between the velocity at which the steps move as they consume adatoms and the velocity at which adatoms diffuse to the steps. If j is the deposition rate in monolayers per second, and if L is the average spacing between the steps, then the velocity at which the steps move is roughly $v_{\text{step}} = jL$. If D is the adatom diffusivity, then the velocity of adatom diffusion to the steps is roughly $v_{\text{adat}} \approx D/L$. The ratio between the velocities is therefore $L^2 j/D$. This ratio is a kind of Péclet number, in that it is a dimensionless measure of the relative importance of convective over diffusional mass flow. Low Péclet numbers imply high temperatures and a dominance of diffusional mass flow; high Péclet numbers imply low temperatures and a dominance of convective mass flow. Another way of understanding the Péclet number is to note that it is also the ratio between the diffusion time across the terraces, L^2/D, and the adatom arrival time, $\tau_{\text{ML}} = 1/j$. Low ratios imply either low growth rates or high adatom diffusivities; high ratios imply either high growth rates or low adatom diffusivities.

6.3.1 Fast Adatoms and "Diffusive" Step Flow

In this subsection, we discuss how surface morphology evolves if Péclet numbers are much less than unity, so that adatom diffusion to nearby steps is fast relative both to step flow and to the rate at which adatoms arrive from the vapor. Then, adatom coverages will be low, adatom-adatom interactions can be neglected, and growth will proceed exclusively by the flow

[45] V. Bostanov, R. Roussinova, and E. Budevski, "Multinuclear growth of dislocation-free planes in electrocrystallization," *J. Electrochem. Soc.* **119**, 1346 (1972).

[46] W.T. Tsang, T.H. Chiu, J.E. Cunningham, and A. Robertson, "Observations on intensity oscillations in reflection high-energy electron diffraction during chemical beam epitaxy," *Appl. Phys. Lett.* **50**, 1376 (1987).

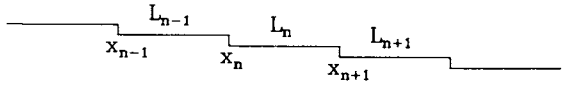

Figure 6.22: An array of steps at horizontal positions $\{x_n\}$ separated by terraces of widths $\{L_n\}$.

of steps across the surface. In other words, adatoms are fast, and it is their diffusion that mediates step flow.

To understand how the morphology of a surface evolves in this step flow regime, consider the array of steps illustrated in Figure 6.22. Suppose adatoms on terrace n have probability p^+ of attaching at the "up" step n on the left, and probability $p^- = 1 - p^+$ of attaching at the "down" step $n+1$ on the right. If L_n is the width of terrace n in monolayers, then jL_n adatoms land on that terrace each second, of which p^+ attach at step n and p^- attach at step $n+1$. Terrace n makes an "up" contribution to the velocity of step n of jL_np^+ and a "down" contribution to the velocity of step $n+1$ of jL_np^-. Alternatively, the velocity of step n can be viewed as containing an "up" contribution from terrace n of jL_np^+, and a "down" contribution from step $n-1$ of $jL_{n-1}p^-$. In other words,

$$\dot{x}_n = v_n = jL_n\left(\frac{p^+}{p^+ + p^-}\right) + jL_{n-1}\left(\frac{p^-}{p^+ + p^-}\right). \tag{6.51}$$

Since the width of the nth terrace is $L_n = x_{n+1} - x_n$, we can also write

$$\dot{x}_n = j(x_{n+1} - x_n)\left(\frac{p^+}{p^+ + p^-}\right) + j(x_n - x_{n-1})\left(\frac{p^-}{p^+ + p^-}\right), \tag{6.52}$$

which is a set of difference equations for the time evolution of the positions of the steps in the array.

If the incorporation probabilities are rewritten as

$$\begin{aligned} p^+ &= \frac{(p^+ + p^-)}{2} + \frac{(p^+ - p^-)}{2} \\ p^- &= \frac{(p^+ + p^-)}{2} - \frac{(p^+ - p^-)}{2}, \end{aligned} \tag{6.53}$$

then Equation 6.52 can be recast, after some algebra, into the form

$$\dot{x}_n = j\left(\frac{x_{n+1} - x_{n-1}}{2}\right) + j\left(\frac{p^+ - p^-}{p^+ + p^-}\right)\left(\frac{x_{n+1} - x_n}{2} - \frac{x_n - x_{n-1}}{2}\right). \tag{6.54}$$

The first term on the right-hand side of Equation 6.54 is a simple difference between step positions, while the second term is a difference between differences. Hence, the continuum equivalent of Equation 6.54 is

$$\dot{x}(n,t) = j\frac{\partial x}{\partial n} + j\left(\frac{p^+ - p^-}{p^+ + p^-}\right)\frac{\partial^2 x}{\partial n^2}, \tag{6.55}$$

which is a single differential equation for the evolution of the step positions. An identical equation may be derived for the evolution of the terrace widths by inserting Equation 6.51 into $\dot{L}_n = \dot{x}_{n+1} - \dot{x}_n$:

$$\dot{L}(n,t) = j\frac{\partial L}{\partial n} + j\left(\frac{p^+ - p^-}{p^+ + p^-}\right)\frac{\partial^2 L}{\partial n^2}. \tag{6.56}$$

The first derivative terms in both of these equations give rise to wave behavior such that, for a fixed horizontal coordinate x, the step index n decreases as time increases. In particular, as steps move to the right during growth, the indices of the steps seen by a stationary observer decrease as $\partial n/\partial t = -j$.

The second derivative terms in both of these equations are dispersion terms that tend to either damp or amplify fluctuations. Suppose, e.g., a surface at time $t = 0$ is composed of terraces having average widths of L_{avg}, but with an additional small sinusoidal variation of amplitude ΔL over step index changes of n_λ, i.e., $L(n) = L_{\text{avg}} + \Delta L \sin(n/n_\lambda)$. Then, its time evolution can be shown (see Exercise 8) to be given by

$$L(n,t) = L_{\text{avg}} + \Delta L \sin 2\pi\left(\frac{n + jt}{n_\lambda}\right) e^{-t/\tau_D}, \tag{6.57}$$

where the rate at which the sinusoidal variation decays is[47]

$$\frac{1}{\tau_D} = j\left(\frac{2\pi}{n_\lambda}\right)^2 \left(p^+ - p^-\right). \tag{6.58}$$

The decay rate depends inversely on the square of the wavelength of the perturbation. As a consequence, growth will tend to smoothen short-wavelength perturbations sooner than long-wavelength ones, and very long-wavelength perturbations will tend to smoothen exceedingly slowly.[48]

[47] R.L. Schwoebel, "Step motion on crystal surfaces. II," *J. Appl. Phys.* **40**, 614 (1969); and T. Fukui, H. Saito, and Y. Tokura, "Superlattice structure observation for $(AlAs)_{1/2}(GaAs)_{1/2}$ grown on (001) vicinal GaAs substrates," *Japan. J. Appl. Phys.* **27**, L1320 (1988).

[48] H.-J. Gossman, F.W. Sinden, and L.C. Feldman, "Evolution of terrace size distributions during thin-film growth by step-mediated epitaxy," *J. Appl. Phys.* **67**, 745 (1990).

Note that it is the *anisotropy* between the up and down step incorporation probabilities that determines whether the perturbation will grow or shrink. If $p^+ > p^-$, then the perturbation decays; if $p^+ < p^-$, then the perturbation grows. This can be understood by inspection of Figure 6.22. If L_n is at some instant wider than its neighbors, then if adatoms on that terrace preferentially attach at the "up" step, L_n will decrease and the perturbation will decay, while if they preferentially attach at the "down" step, L_n will increase and the perturbation will grow.

Note that although Equation 6.56 describes a wave moving backward in step index with increasing time, the horizontal position $x \approx L_{\text{avg}}(n + jt)$ of a given step index itself moves forward with time as steps flow to the right. Hence, Equation 6.57 can be rewritten approximately as

$$L(x,t) = L_{\text{avg}} + \Delta L \sin 2\pi \left(\frac{x}{L_{\text{avg}} n_\lambda} \right) e^{-t/\tau_D}. \tag{6.59}$$

In real space, terrace width perturbations propagate nearly vertically, even though the steps themselves propagate horizontally to the right. This behavior is illustrated in Figure 6.23, which shows the evolution of an array of steps having an initial Gaussian perturbation centered at $x_n = 80$.

Finally, we note that, in deriving Equation 6.56, adatoms were assumed to attach only at adjacent steps. If, instead, adatoms cross adjacent steps and ultimately attach at more distant steps, then higher order derivatives appear in Equations 6.55 and 6.56 that can cause perturbations to propagate to the right.[49]

6.3.2 Slow Adatoms and "Convective" Step Flow

In Subsection 6.3.1, we discussed how surface morphology evolves if Péclet numbers are much less than unity, so that adatom diffusion to nearby steps is fast. In this subsection, we discuss how surface morphology evolves if Péclet numbers are on the order of unity, so that adatom diffusion to nearby steps is comparable to the step flow velocity. Then, as we shall see, adatom annihilation occurs not only by adatom diffusion to steps, but by step flow over adatoms. As a consequence, there can arise an oscillatory interplay between accumulation of adatoms between the steps, and sweeping of adatoms by step flow.

To quantify this, consider the equi-spaced array of steps illustrated in Figure 6.24, with a space and time-dependent adatom coverage $\theta(x,t)$. On the terrace bounded by steps at x_{L} and x_{R}, the coverage increases with time

[49] S.A. Chalmers, J.Y. Tsao, and A.C. Gossard, "Lateral motion of terrace width distributions during step-flow growth," *Appl. Phys. Lett.* **61**, 645 (1992).

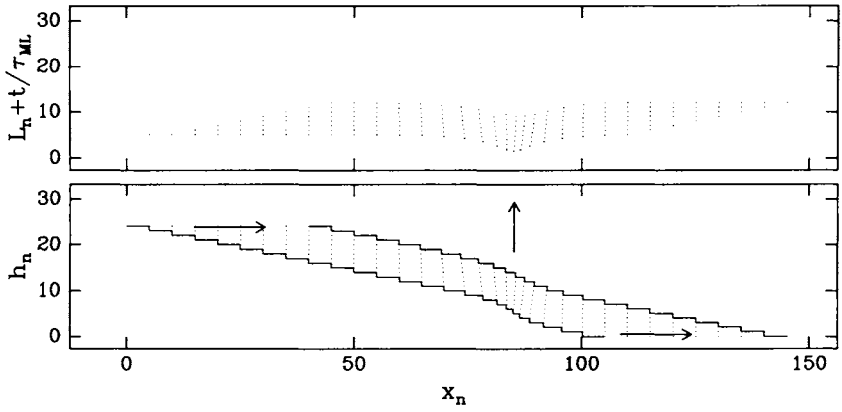

Figure 6.23: Snapshots in time of the terrace widths, $L_n(t)$, heights, $h_n(t)$ and lateral positions, $x_n(t)$, of an array of steps after successive monolayers have been deposited. The terraces are on average five lattice parameters wide, but with an initial Gaussian bunching centered at $x_n \approx 80$. Bottom: The heights h_n of the steps are constant, but their lateral positions x_n increase with time as the steps flow to the right. Top: Even though the steps flow to the right, the perturbation in the terrace widths propagates vertically up. For clarity, the terrace widths L_n are shown offset by successive monolayers $t/\tau_{\rm ML}$.

due to deposition at a rate j, and the spatial distribution of the coverage broadens in time due to diffusion at a rate $D\partial^2\theta/\partial x^2$. If evaporation back into the vapor is negligible, then the coverage evolves according to[50]

$$\dot{\theta}(x,t) = j + D\frac{\partial^2\theta}{\partial x^2}. \tag{6.60}$$

At the left step edge, the rate at which adatoms attach will be proportional to the adatom coverage, $k^+_{\rm att}\theta(x_{\rm L},t)$, where $k^+_{\rm att}$ is a kinetic rate constant for successful adatom attachment at an up step. If adatoms can also detach from steps, then there will be a competing rate, $k^+_{\rm det}$, where $k^+_{\rm det}$ is a kinetic rate constant for successful adatom detachment from an up step.

The difference between these two rates must be exactly balanced by the diffusive flow of adatoms into the step, $D[\partial\theta/\partial x]_{x_{\rm L}}$. Hence, we have at the left step

$$k^+_{\rm att}\theta(x_{\rm L},t) - k^+_{\rm det} = D\left[\frac{\partial\theta}{\partial x}\right]_{x_{\rm L}}. \tag{6.61}$$

[50]W.K. Burton, N. Cabrera, and F.C. Frank, "The growth of crystals and the equilibrium structure of their surfaces," *Philos. Trans. R. Soc. London Ser.* **A243**, 299 (1951).

Figure 6.24: Steady-state adatom coverages on an equi-spaced array of "fast" steps.

Using similar reasoning, we also have at the right step

$$k_{\rm att}^{-}\theta(x_{\rm R},t) - k_{\rm det}^{-} = -D\left[\frac{\partial\theta}{\partial x}\right]_{x_{\rm R}}, \tag{6.62}$$

where $k_{\rm att}^{-}$ and $k_{\rm det}^{-}$ are kinetic rate constants for successful adatom attachment and detachment from the down step. These two boundary conditions determine, along with Equation 6.60, the time evolution of the adatom coverage.[51]

Note, however, that these boundary conditions are complicated by the fact that, as adatoms attach at the steps, the steps themselves move, so that the positions in space at which the boundary conditions must be applied also move. Since the velocities at which the steps move is determined by the sum of the attachment rates of adatoms coming from the left and the right of each step, we have

$$\begin{aligned} v(t) &= [k_{\rm att}^{+}\theta(x_{\rm L},t) - k_{\rm det}^{+}] + [k_{\rm att}^{-}\theta(x_{\rm R},t) - k_{\rm det}^{-}] \\ &= D\left[\frac{\partial\theta}{\partial x}\right]_{x_{\rm L}} - D\left[\frac{\partial\theta}{\partial x}\right]_{x_{\rm R}}. \end{aligned} \tag{6.63}$$

To remove this complication, it is convenient to transform into a coordinate system, $x' = x + \int v dt$, that itself moves with the steps. Then, the boundary conditions given by Equations 6.61 and 6.62 may be applied at fixed $x'_{\rm L}$ and $x'_{\rm R}$, but the differential Equation 6.60 becomes

$$\dot{\theta}(x',t) = j + D\frac{\partial^2\theta}{\partial x'^2} + v\frac{\partial\theta}{\partial x'}. \tag{6.64}$$

The equation now contains both a "diffusive" term, $D\partial^2\theta/\partial x'^2$, as well as a "convective" term, $v\partial\theta/\partial x'$, due to the motion of the step.[52]

[51] R. Ghez and S.S. Iyer, "The kinetics of fast steps on crystal surfaces and its application to the molecular beam epitaxy of silicon," *IBM J. Res. Develop.* **32**, 804 (1988).

[52] K. Voigtlander, H. Risken, and E. Kasper, "Modified growth theory for high supersaturation," *Appl. Phys.* **A39**, 31 (1986); and V. Fuenzalida and I. Eisele, "High supersaturation layer-by-layer growth: application to Si MBE," *J. Crystal Growth* **74**, 597 (1986).

For simplicity, let us now assume that adatom detachment from steps is negligible, so that $k_{\text{det}}^{+} = k_{\text{det}}^{-} = 0$. Let us also assume that the local attachment rates are extremely fast, so that $k_{\text{att}}^{+} \to \infty$ and $k_{\text{att}}^{-} \to \infty$. Then, the boundary conditions given by Equations 6.61 and 6.62 simplify to

$$\theta(x'_{\text{L}}) = \theta(x'_{\text{R}}) = 0, \tag{6.65}$$

and the step velocity becomes

$$v(t) = D\left[\frac{\partial\theta}{\partial x'}\right]_{x'_{\text{L}}} - D\left[\frac{\partial\theta}{\partial x'}\right]_{x'_{\text{R}}}. \tag{6.66}$$

Equations 6.64, 6.65 and 6.66 together form a simplified set of equations for the time evolution of the adatom coverage in a reference frame moving at velocity $v(t)$.

The behavior of this set of equations is illustrated in Figure 6.25, which shows numerical simulations of the adatom coverage and step velocity at various times after the onset of growth. It can be seen that the step velocity *oscillates* in time during growth. The reason is that the adatom coverage initially builds up preferentially in the middle of the terrace, so the step moves slowly. As the step approaches the high-coverage region of the terrace, it accelerates and consumes the adatoms. Then, after most of the adatoms have been consumed, the step slows and the cycle continues.[53]

Also shown in Figure 6.25 is the time evolution of a simple measure of the smoothness of the terrace, $I = (1-2\theta_{\text{avg}})^2$, where $\theta_{\text{avg}} \equiv \int_{x'_{\text{L}}}^{x'_{\text{R}}} \theta(x',t)dx'/L$. This quantity is that which would be measured in a kinematic surface diffraction experiment under conditions for which diffraction from the uncovered terrace $(1-\theta_{\text{avg}})$ is out of phase with that from the adatoms (θ_{avg}):

$$I = [(1-\theta_{\text{avg}}) - (\theta_{\text{avg}})]^2 = (1-2\theta_{\text{avg}})^2. \tag{6.67}$$

The terrace smoothness also oscillates in time during growth, as the steps alternately accelerate and decelerate through high and low adatom coverage regions.

Ultimately, the oscillations damp out, and the adatom coverage approaches a steady-state distribution given by

$$\theta(x', t \to \infty) = \frac{1 - e^{-x'Lj/D}}{1 - e^{-L^2 j/D}} - \frac{x'}{L}. \tag{6.68}$$

This distribution is illustrated in the left half of Figure 6.26 for various values of the Péclet number, $L^2 j/D$.

[53] G.S. Petrich, P.R. Pukite, A.M. Wowchak, G.J. Whaley, P.I. Cohen, and A.S. Arrott, "On the origin of RHEED intensity oscillations," *J. Cryst. Growth* **95**, 23 (1989).

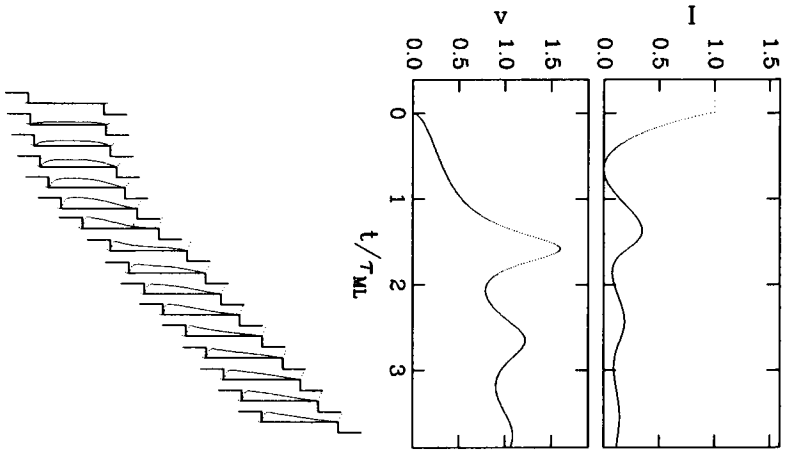

Figure 6.25: Non-steady-state adatom coverage (left), step velocity (middle), and terrace smoothness (right) during oscillatory flow of an equi-spaced array of "fast" steps. The adatom coverages are shown as snapshots taken every 0.25 monolayer.

For Péclet numbers less than unity, the step velocity is low relative to the adatom diffusive velocity. The adatom distribution becomes nearly symmetric, and approaches

$$\theta(x', t \to \infty) = \left[1 - \frac{(2x' - L)^2}{L^2}\right] \frac{jL^2}{8D}. \tag{6.69}$$

However, as the Péclet number increases beyond unity, the step velocity increases relative to the adatom diffusive velocity. The adatom distribution becomes more and more skewed, due to "pile-up" in front of the moving step.

The steady-state average adatom coverage on each terrace is

$$\begin{aligned} \theta_{\rm avg}(t \to \infty) &= \int_{x'_{\rm L}}^{x'_{\rm R}} \frac{\theta(x')}{L} dx' \\ &= \frac{1 + \left(e^{-L^2 j/D} - 1\right) D/(L^2 g)}{1 - e^{-L^2 j/D}} - \frac{1}{2} \\ &= \left(\frac{1}{2}\right) \frac{1 + e^{-L^2 j/D}}{1 - e^{-L^2 j/D}} - \frac{D}{jL^2}. \end{aligned} \tag{6.70}$$

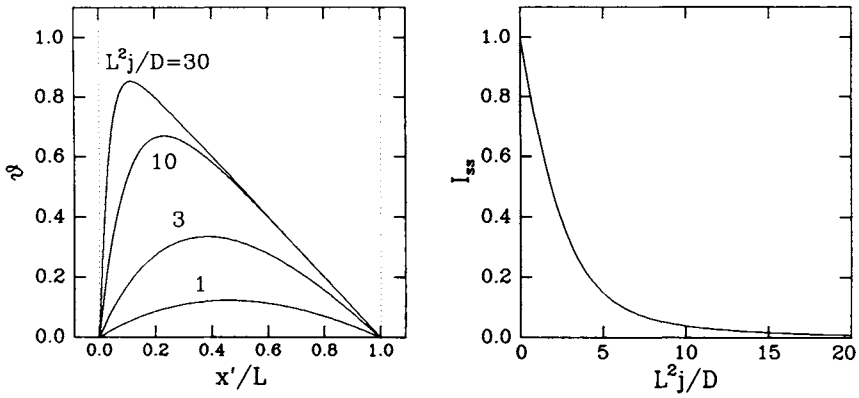

Figure 6.26: Left: Steady-state adatom coverages on an array of "fast" steps for various values of L^2j/D, the Péclet number. Right: Dependence of steady-state average terrace smoothness on the Péclet number.

The steady-state kinematic surface diffraction intensity corresponding to this average coverage is shown in the right half of Figure 6.26 as a function of the Péclet number. As can be seen, it decreases quickly as the step velocity increases relative to the adatom diffusivity, and hence as the average adatom coverage builds up on each terrace.[54]

6.3.3 2D Cluster Nucleation, Growth and Coalescence

In Subsection 6.3.2, we discussed how surface morphology evolves if Péclet numbers are on the order of unity, so that adatom diffusion to nearby steps is comparable to the step flow velocity. In this subsection, we discuss how surface morphology evolves if Péclet numbers are greater than unity, so that adatom diffusion to nearby steps is slow relative both to step flow and to the rate at which adatoms arrive from the vapor. Then, adatoms accumulate and interact on the terraces between the steps, and ultimately form 2D clusters.

If the clusters are transient, in that they break apart faster than they grow, then their main consequence will be to impede adatom diffusion. Adatoms diffusing toward steps will occasionally meet and merge with a

[54] J.H. Neave, P.J. Dobson, B.A. Joyce, and J. Zhang, "Reflection high-energy electron diffraction oscillations from vicinal surface – a new approach to surface diffusion measurements," *Appl. Phys. Lett.* **47**, 100 (1985); and T. Nishinaga and K-I Cho,"Theoretical study of mode transition between 2d-nucleation and step flow in MBE growth of GaAs," *Japan. J. Appl. Phys.* **27**, L12 (1988).

cluster or another adatom. Assuming the cluster itself is relatively immobile, the adatom will be unable to continue its journey until it breaks free from the cluster. Then, the effective adatom diffusivity decreases with increasing adatom coverage,[55] so that step flow becomes less and less "diffusive" and more and more "convective."

If the clusters are permanent, in that they form stable growing nuclei, then the kinetics of growth are altered drastically. In a sense, the clusters take on a life of their own. Their boundaries represent "extrinsic" steps that compete for adatoms with the intrinsic steps always present on a vicinal surface. As a consequence, the clusters grow and ultimately coalesce, often in a complex, oscillatory way.

To understand why, consider epitaxy on a singular surface, or on a vicinal surface whose terraces are very wide compared to the spacing of the clusters. Enumerate the layers by $n = 0, 1, 2, \ldots$, where $n = 0$ is the initially completely occupied substrate surface layer, $n = 1$ is the first, initially completely unoccupied epilayer, and so on. Associate with each of these layers three coverages: α_n, the total coverage of mobile adatoms created by impingement from the vapor; η_n, the total coverage of nuclei centers created by interaction between mobile adatoms; and θ_n, the total coverage of immobile atoms permanently incorporated into clusters. These coverages are represented in Figure 6.27 by the open circles, filled squares, and open squares, respectively.

Mobile Adatoms

For simplicity, assume that mobile adatoms are created exclusively by impingement from the vapor (rather than by detachment from clusters). Then, the rate at which the mobile adatom coverage in layer n increases is equal to the flux times the exposed coverage of layer $n-1$, or $(\theta_{n-1} - \theta_n)/\tau_{\mathrm{ML}}$.

Once mobile adatoms in layer n are created, they may diffuse to and attach at the edges of both layer $n-1$ and layer n clusters. The rates at which they do so will be proportional to the product of the mobile adatom coverage (α_n), the coverage of layer $n-1$ and layer n nuclei centers (η_{n-1} and η_n), and the capture numbers, or efficiencies, associated with those nuclei. These capture numbers are essentially the geometric cross sections that the clusters present to diffusing adatoms, and have been the subject of considerable study.[56] Here, we take them to be constant. The rate at which

[55] A.K. Myers-Beaghton and D.D. Vvedensky, "Nonlinear equation for diffusion and adatom interactions during epitaxial growth on vicinal surfaces," *Phys. Rev.* **B42**, 5544 (1990).

[56] G. Zinsmeister, "Theory of thin film condensation. Part D: Influence of a variable collision factor," *Thin Solid Films* **7**, 51 (1971); J.A. Venables, "Rate equation ap-

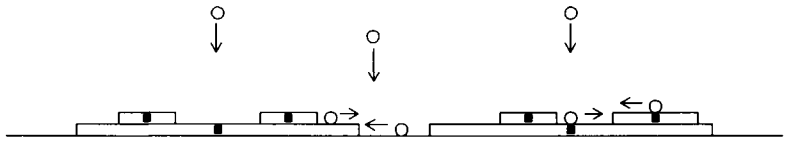

Figure 6.27: Adatom arrival, diffusion and attachment at step edges, accompanied by cluster nucleation, growth, and coalescence. The open circles on the surface represent mobile adatoms; the filled squares represent nuclei centers; and the open squares represent immobile atoms permanently incorporated into clusters.

adatoms in level n are captured by clusters in level $n-1$ is then $k^-_{\rm att}\alpha_n\eta_{n-1}$, where $k^-_{\rm att}$ is the kinetic rate constant for attachment at "down" steps; and the rate at which they are captured by clusters in level n is $k^+_{\rm att}\alpha_n\eta_n$, where $k^+_{\rm att}$ is the kinetic rate constant for attachment at "up" steps.

At the same time, mobile adatoms in layer n may also hop over steps into layers $n-1$ and $n+1$, while mobile adatoms in layers $n-1$ and $n+1$ may hop over steps into layer n. Here, we assume these adatom exchange rates to be proportional to the mobile adatom coverage in the layer the adatoms are jumping from and the exposed coverage of the layer the adatoms are jumping to. Hence, the exchange rate out of layer n is $k^+_{\rm exch}\alpha_n(\theta_n-\theta_{n+1})+k^-_{\rm exch}\alpha_n(\theta_{n-2}-\theta_{n-1})$, and the exchange rate into layer n is $k^+_{\rm exch}\alpha_{n-1}(\theta_{n-1}-\theta_n)+k^-_{\rm exch}\alpha_{n+1}(\theta_{n-1}-\theta_n)$, where $k^+_{\rm exch}$ and $k^-_{\rm exch}$ are the rates of hopping over "up" and "down" steps, respectively.

Altogether, the coverage of mobile adatoms evolves in time approximately as

$$\begin{aligned}\dot{\alpha}_n &= \frac{\theta_{n-1}-\theta_n}{\tau_{\rm ML}} - \alpha_n\left(k^-_{\rm att}\eta_{n-1}+k^+_{\rm att}\eta_n\right)\\ &\quad - k^+_{\rm exch}\alpha_n(\theta_n-\theta_{n+1}) - k^-_{\rm exch}\alpha_n(\theta_{n-2}-\theta_{n-1})\\ &\quad + k^+_{\rm exch}\alpha_{n-1}(\theta_{n-1}-\theta_n) + k^-_{\rm exch}\alpha_{n+1}(\theta_{n-1}-\theta_n). \quad (6.71)\end{aligned}$$

It increases due to deposition and to exchange from adjacent layers, but decreases due to incorporation into growing clusters and to exchange into adjacent layers.

proaches to thin film nucleation kinetics," *Phil. Mag.* **27**, 697 (1973); B. Lewis and G.J. Rees, "Adatom migration, capture and decay among competing nuclei on a substrate," *Phil. Mag.* **29**, 1253 (1974); and R. Kariotis and M.G. Lagally, "Rate equation modeling of epitaxial growth," *Surf. Sci.* **216**, 557 (1989).

Immobile Adatoms

As mobile adatoms attach at steps, the coverage of immobile atoms permanently incorporated into clusters must increase correspondingly. Since, as illustrated in Figure 6.27, the coverage of immobile atoms in layer n depends on the attachment of mobile adatoms in layers n and $n+1$, we can write

$$\dot{\theta}_n = k_{\text{att}}^{+}\alpha_n\eta_n + k_{\text{att}}^{-}\alpha_{n+1}\eta_n. \tag{6.72}$$

As in Equation 6.71, k_{att}^{+} and k_{att}^{-} are kinetic rate constants for attachment of mobile adatoms at up and down steps, respectively.

Note that in this simple treatment we neglected possible anisotropies in the shapes of the clusters. Such anisotropies can arise from anisotropic attachment or diffusion rates, and have been observed during growth of semiconductors having strong and anisotropic surface reconstructions.[57]

Nuclei Centers

Finally, the coverage of nuclei centers itself increases, as mobile adatoms collide to form 2D clusters, and then decreases as the clusters grow, impinge on each other, and ultimately coalesce. In general, nucleation is a complex process by which a distribution of clusters of various sizes evolves in time in response to kinetic adatom attachment and detachment rates and to highly nonlinear size and shape dependencies to cluster energetics.[58] Nucleation may also be "heterogeneous," in the sense of being catalyzed by defects on the surface.[59] In this simple treatment, we assume that two adatoms are sufficient to form a stable cluster, and that the nucleation rate is proportional to the collision rate between adatoms, $k_{\text{nuc}}\alpha_n^2$.

Coalescence of clusters is also a complex process that depends on the distribution of clusters in both size and space. At one extreme, if the nuclei centers are distributed randomly in space, then their initial coalescence rate can be shown to be proportional to both the coverage of cluster centers

[57] R.J. Hamers, "Nucleation and growth of epitaxial layers on Si(001) and Si(111) surfaces by scanning tunneling microscopy," *Ultramicroscopy* **31**, 10 (1989); J.Y. Tsao, E. Chason, U. Koehler, and R. Hamers, "Dimer strings, anistropic growth, and persistent layer-by-layer epitaxy," *Phys. Rev.* **B40**, 11951 (1989); and Y.-W. Mo, B.S. Swartzentruber, R. Kariotis, M.B. Webb, and M.G. Lagally, "Growth and equilibrium structures in the epitaxy of Si on Si (001)," *Phys. Rev. Lett.* **63**, 2393 (1989).

[58] See, e.g., D. Walton, "Nucleation of vapor deposits," *J. Chem. Phys.* **37**, 2182 (1962); K.F. Kelton, A.L. Greer, and C.V. Thompson, "Transient nucleation in condensed systems," *J. Chem. Phys.* **79**, 6261 (1983).

[59] Anti-phase boundaries between equivalent reconstruction domains on the surface are an example. See, e.g., R.J. Hamers, "Nucleation and growth of epitaxial silicon on Si(001) and Si(111) surfaces studied by scanning tunneling microscopy," *Ultramicroscopy* **31**, 10 (1989).

and the rate of change of the coverage of immobile adatoms incorporated into the clusters, or $2\eta_n\dot{\theta}_n$.[60] At the other extreme, if their centers are distributed equally in space, then the initial coalescence rate will be zero, increasing sharply when the clusters just begin to impinge on each other.[61] Here, we assume a coalescence rate between these two extremes: $\eta_n\dot{\theta}_n/(1-\theta_n)$. This form of the coalescence rate guarantees that the coverage of nuclei centers decreases smoothly to zero as the coverage of immobile adatoms incorporated into the clusters approaches unity, or that $\eta_n \to 0$ as $\theta_n \to 1$.

Altogether, the coverage of nuclei centers evolves in time approximately as

$$\dot{\eta}_n = k_{\text{nuc}}\alpha_n^2 - \left(\frac{\eta_n}{1-\theta_n}\right)\dot{\theta}_n. \tag{6.73}$$

Note that in deriving Equation 6.73, we have neglected, for simplicity, elimination of nuclei centers in the absence of growth. More comprehensive treatments must allow for such effects, which are due to surface tension. Small clusters, because of their large perimeter length to cluster area ratio, are thermodynamically less stable than, and will ultimately "ripen" into, increasingly larger clusters.[62]

Numerical Solutions

Equations 6.71, 6.72 and 6.73 form a set of coupled rate equations, three for each layer, describing the evolution of the coverages of mobile adatoms, immobile adatoms, and nuclei centers. They may be solved analytically in some simple limiting cases,[63] but in general require numerical integra-

[60] R. Vincent, "A theoretical analysis and computer simulation of the growth of epitaxial films," *Proc. Roy. Soc. Lond.* **A321**, 53 (1971); and M.J. Stowell, "Thin film nucleation kinetics," *Phil. Mag.* **26**, 361 (1972).

[61] J.A. Venables, "Rate equation approaches to thin film nucleation kinetics," *Phil. Mag.* **27**, 697 (1973).

[62] See, e.g., I.M. Lifschitz and V.V. Slyozov, "The kinetics of precipitation from supersaturated solid solutions," *J. Phys. Chem. Solids* **19**, 35 (1961); C. Wagner, "Theorie der alterung von niederschlägen durch umlösen," *Z. Electrochem.* **65**, 581 (1961); P.W. Voorhees and M.E. Glicksman, "Solution to the multi-particle diffusion problem with applications to Ostwald ripening – I. Theory," *Acta Met.* **32**, 2001 (1984); C.V. Thompson, "Coarsening of particles on a planar substrate: interface energy anisotropy and application to grain growth in thin films," *Acta Met.* **36**, 2929 (1988); and H.A. Atwater and C.M. Yang, "Island growth and coarsening in thin films – conservative and nonconservative systems," *J. Appl. Phys.* **67**, 6202 (1990).

[63] See, e.g., A.N. Kolmogoroff, *Bull. Acad. Sci. URSS* (Cl. Sci. Math. Nat.) **3**, 355 (1937); M. Avrami, "Kinetics of phase change I. General theory," *J. Chem. Phys.* **7**, 1103 (1939); M. Avrami, "Kinetics of phase change II. Transformation-time relations for random distribution of nuclei," *J. Chem. Phys.* **8**, 212 (1940); M. Avrami, "Kinetics of phase change III. Granulation, phase change and microstructure," *J. Chem. Phys.* **9**, 177 (1941); W.B. Hillig, "A derivation of classical two-dimensional nucleation kinetics

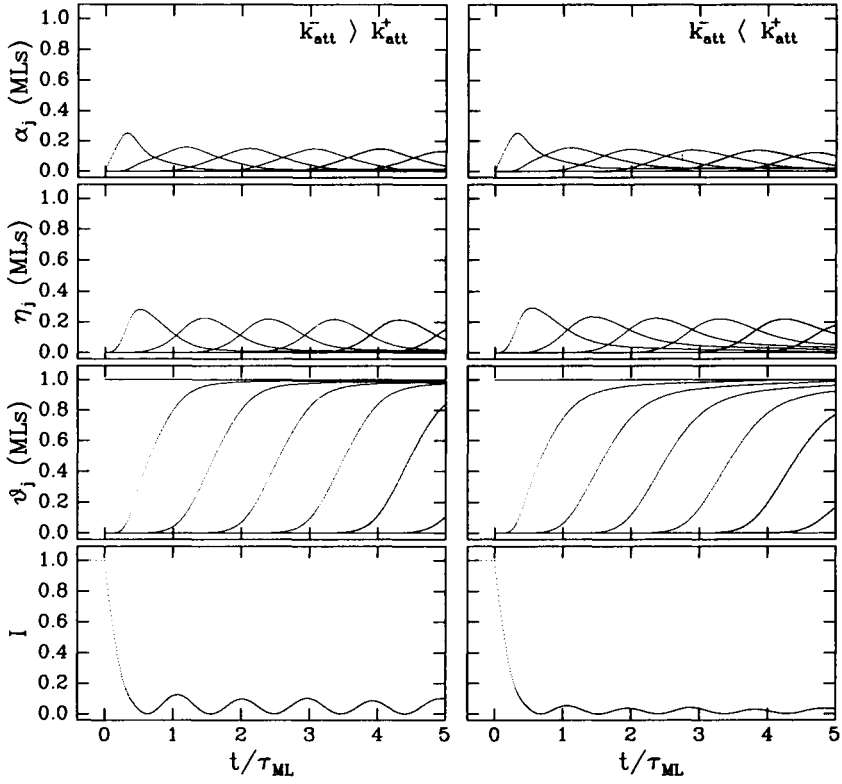

Figure 6.28: Time evolution, from top to bottom, of mobile adatom coverages (α_n), nuclei center coverages (η_n), immobile adatom coverages coverages (θ_n), and overall surface smoothness. The kinetic parameters were all taken to be $20/\tau_{\rm ML}$ except $k_{\rm att}^-$, which was slightly higher ($30/\tau_{\rm ML}$) in the left panels, and slightly lower ($15/\tau_{\rm ML}$) in the right panels.

tion. Two examples of time evolutions deduced by numerical integration are shown in Figure 6.28.

As growth commences, at $t/\tau_{\rm ML} = 0$, the mobile adatom coverage in layer 1 increases from zero at a rate $1/\tau_{\rm ML}$. At a critical coverage, clusters in layer 1 begin to nucleate and grow, and as they do so, the mobile adatom coverage in layer 1 begins to decrease while the immobile atom coverage in layer 1 begins to increase. Finally, the clusters begin to coalesce, the

and the associated crystal growth laws," *Acta Met.* **14**, 1868 (1966); and D. Kaschiev, "Growth kinetics of dislocation-free interfaces and growth mode of thin films," *J. Crystal Growth* **40**, 29 (1977).

nuclei center coverage decreases, and the rate at which mobile adatoms incorporate into permanent clusters also decreases.

In the meantime, as clusters in layer 1 form, mobile adatoms begin to be created in layer 2. In this way, successive layers are born by a burst of nucleation and growth of clusters, only to die by being covered by a burst of nucleation and growth of higher level clusters.[64] If these bursts are well separated in time, then growth is smooth, and successive layers are born only after previous layers have died. If the bursts overlap in time, then growth is rough, and successive layers are born even before previous layers have died.

Also shown is the time evolution of a generalization of Equation 6.67 for the smoothness of the surface,

$$I = \left\{ \sum_{n=0}^{\infty} (-1)^{n+1} [(\alpha_n + \theta_n) - (\alpha_{n+1} + \theta_{n+1})] \right\}^2 . \qquad (6.74)$$

Just as that defined by Equation 6.67, this quantity is that which would be measured in a kinematic surface diffraction experiment under conditions for which diffraction from adjacent exposed surface layers is out of phase.

In both cases shown in Figure 6.28, the smoothness of the surface oscillates in time with a monolayer periodicity. The strength of the oscillations is, however, very sensitive to the values of the kinetic parameters. For example, they are stronger when adatom attachment is faster at down steps than at up steps (left side of Figure 6.28), rather than vice-versa (right side of Figure 6.28). The reason is that if adatoms preferentially attach at down steps, then the mobile adatom coverage in higher layers will be lower, and cluster nucleation in these higher layers will tend to be suppressed until the lower layers are fully complete.

Note that the oscillations predicted by Equations 6.71, 6.72 and 6.73, even when weak, are relatively persistent. In practice, faster decays are nearly always observed, and are thought to be due to effects such as a small amount of step flow (see Figure 6.25) or slight nonuniformities in growth fluxes arriving at the surface (see Exercise 10).

As a final comment, note that this treatment neglected evaporation of mobile adatoms back into the vapor. At the low to medium temperatures typical of most MBE growth, this assumption is reasonable. At high temperatures, however, evaporation can become significant. Then, the os-

[64] S. Stoyanov, "Layer growth of epitaxial films and superlattices," *Surf. Sci.* **199**, 226 (1988); and P.I. Cohen, G.S. Petrich, P.R. Pukite, G.J. Whaley, and A.S. Arrott, "Birth-death models of epitaxy I. Diffraction oscillations from low index surfaces," *Surf. Sci.* **216**, 222 (1989).

cillations in surface smoothness and in mobile adatom coverages can also manifest themselves as oscillations in the growth rate itself.[65]

6.3.4 Statistical Roughening

In Subsection 6.3.3, we discussed how surface morphology evolves if Péclet numbers are greater than unity, so that adatom diffusion to nearby steps is slow relative to the step flow velocity. In this subsection, we discuss how surface morphology evolves if Péclet numbers are *much* greater than unity, so that the rate at which adatoms diffuse, even to adjacent lattice sites, becomes slower than the rate at which they arrive from the vapor. In other words, suppose adatoms "stick" wherever they happen to land. If they arrive randomly, then they will be uncorrelated in space, and it is sufficient to know the probability p that any particular column on the surface will have a height n. If they arrive randomly in time according to Poisson statistics, then this probability will be

$$p(n) = \frac{\theta_{\text{tot}}^n}{n!} e^{-\theta_{\text{tot}}}. \tag{6.75}$$

In this equation, θ_{tot} is the total coverage of deposited atoms, so that $\sum_{n=0}^{\infty} p(n) = 1$ and $\sum_{n=0}^{\infty} np(n) = \theta_{\text{tot}}$. As illustrated in the left half of Figure 6.29, the column height probabilities are roughly centered at $n = \theta_{\text{tot}}$, but become more and more dispersed as θ_{tot} increases. Ultimately, for large θ_{tot}, the asymmetric Poissonian distribution approaches a symmetric Gaussian distribution.[66]

If we again generalize Equation 6.67 to calculate the smoothness of the surface, then we can write

$$I = \left[\sum_{n=0}^{\infty} (-1)^n p(n)\right]^2 = \left[\sum_{n=0}^{\infty} \frac{(-\theta_{\text{tot}})^n}{n!} e^{-\theta_{\text{tot}}}\right]^2 = e^{-4\theta_{\text{tot}}}. \tag{6.76}$$

As illustrated in the right half of Figure 6.29, the surface smoothness decreases exponentially with increasing total coverage, at a rate four times faster than the simple deposition rate.

Suggested Reading

1. A.A. Chernov, *Modern Crystallography III. Crystal Growth* (Springer-Verlag, Berlin, 1984).

[65] G.H. Gilmer, "Transients in the rate of crystal growth," *J. Cryst. Growth* **49**, 465 (1980).

[66] E. Chason and J.Y. Tsao, "Adatoms, strings and epitaxy on singular surfaces," *Surf. Sci.* **234**, 361 (1990).

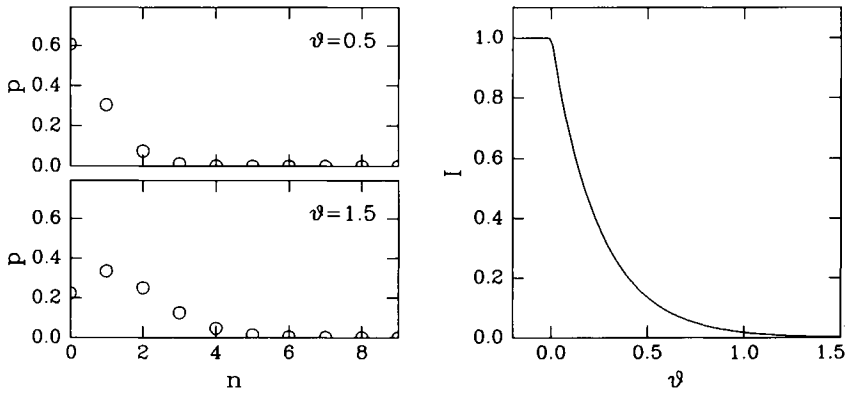

Figure 6.29: Probability p that a particular column will have height n (left) and decay of kinematic out-of-phase diffraction intensity (right) after statistical deposition of various average numbers of monolayers θ_{tot}.

2. R. Kern, G. Le Lay, and J.J. Metois, "Basic Mechanisms in the Early Stages of Epitaxy," in *Current Topics in Materials Science*, Vol. 3, E. Kaldis, Ed. (North-Holland, Amsterdam, 1979).

3. P.K. Larsen and P.J. Dobson, Eds., *Reflection High-Energy Electron Diffraction and Reflection Electron Imaging of Surfaces* (Plenum Press, New York, 1988).

4. B. Lewis and J.C. Anderson, *Nucleation and Growth of Thin Films* (Academic Press, New York, 1978).

5. J.W. Matthews, Ed., *Epitaxial Growth* Parts A and B, (Academic Press, New York, 1975).

6. W.D. Robertson and N.A. Gjostein, Eds., *Metal Surfaces: Structure, Energetics and Kinetics*, Proceedings of a joint seminar of the American Society for Metals and the Metallurgical Society of AIME, October 27-28, 1962 (American Society for Metals, Metals Park, Ohio, 1963).

7. J.A. Venables, G.D.T. Spiller, and M. Hanbucken, "Nucleation and growth of thin films," *Rep. Prog. Phys.* **47**, 399 (1984).

8. E.D. Williams and N.C. Bartelt, "Thermodynamics of surface morphology," *Science* **251**, 393 (1991).

9. A. Zangwill, *Physics at Surfaces* (Cambridge University Press, Cambridge, 1988).

Exercises

1. Derive Equation 6.12, the equilibrium probabilities of plus, minus and missing kinks.

2. Show that angles such as $\angle OAP$ in Figure 6.11, with origin on the circumference of a circle and with legs passing through the ends of a diameter of the circle, are right angles.

3. Consider the facetted 2D crystal illustrated in Figure 6.30 bounded by four faces of surface energy γ_o oriented perpendicular to rays along $\theta = 0, \pi/2, \pi, 3\pi/2$, and four faces of surface energy γ_1, oriented perpendicular to rays along $\theta = \pi/4, 3\pi/4, 5\pi/4, 7\pi/4$. Show that the pyramids that make up this polyhedra obey the "common vertex" relations

$$\begin{aligned} h_o &= b_o/2 + b_1/\sqrt{2} \\ h_1 &= b_o/\sqrt{2} + b_1/2. \end{aligned} \tag{6.77}$$

Using these relations, show that the pyramidal heights of the polyhedron with minimum surface energy, $E = 4(\gamma_o b_o + \gamma_1 b_1)$, at constant area, $A = 4(h_o b_o/2 + h_1 b_1/2)$, are proportional to the surface energies of the bases, $\gamma_o/h_o = \gamma_1/h_1$, in agreement with the Wulff construction.

4. Derive Equations 6.31 for the relationship between the fractional surface areas, $x_1/(x_1 + x_2)$ and $x_2/(x_1 + x_2)$, and the tangents of the orientation angles of those surfaces, $\tan\theta_1$ and $\tan\theta_2$.

5. Suppose $f(s)$ in Equation 6.34 were quadratic rather than cubic. What would be the shape of the equilibrium crystal near the $s = 0$ facet?

6. What is the functional form of $f(s)$, where $f \equiv \gamma/\cos\theta$ and $s \equiv \tan\theta$, for an orientation-independent molar surface free energy $\gamma(\theta) =$ constant? Is it concave up or down?

7. Is there an equilbrium island size for Volmer-Weber island growth, or will larger islands continuously grow in time at the expense of smaller islands?

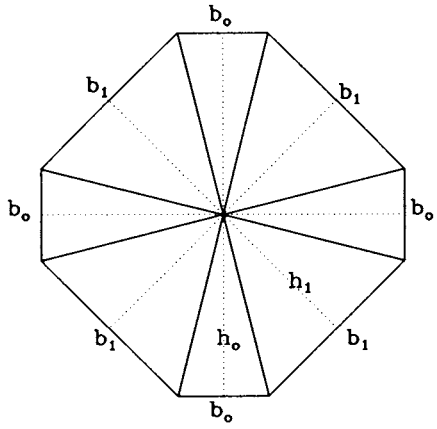

Figure 6.30: Decomposition of a facetted 2D crystal into pyramids.

8. Show that $1/\tau_D$ in Equation 6.57 is given by Equation 6.58.

9. Consider a surface whose layer coverages obey a power law, $\theta_n = [\theta_{\text{tot}}/(1+\theta_{\text{tot}})]^n$. Show that the total coverage of deposited atoms is $\theta_{\text{tot}} = \sum_{n=1}^{\infty} \theta_n$. Justify the equation

$$I = \left[\sum_{n=0}^{\infty} (-1)^n (\theta_{n-1} - \theta_n)\right]^2 \tag{6.78}$$

for the kinematic surface diffraction intensity in an out-of-phase condition, and use it to calculate the smoothness of this surface. Does it decrease more or less quickly with θ_{tot} than if the layer distribution were distributed according to Poissonian statistics? What if the layer coverages were distributed according to Gaussian statistics?

10. Suppose adatoms arrive at a surface with a nonuniformity of 10%. How might this cause an "artificial" decay in the amplitude of observed growth oscillations and what would be the decay rate?

Chapter 7

Surface Composition

In Chapter 6, we discussed the equilibrium and nonequilibrium morphology of a surface assuming that the *composition* of the surface was unimportant. In this chapter, we discuss the equilibrium and nonequilibrium composition of a surface assuming that the *morphology* of the surface is unimportant. In both of these chapters, therefore, we neglect possible interdependencies between morphology and composition, interdependencies that are clearly present but thus far poorly understood. For example, we do not discuss, except casually, the various reconstructions of the surfaces of III/V semiconductors, and how they might depend on the ratio between the column III and column V atom coverages on the surface.[1] Instead, we discuss those interesting and important aspects of surface composition that are to first order independent of surface morphology.

We begin, in Section 7.1, by describing a thermodynamic framework

[1] A.Y. Cho, "GaAs epitaxy by a molecular beam method: observations of surface structure on the (001) face," *J. Appl. Phys.* **42**, 2074 (1971); J.R. Arthur, "Surface stoichiometry and structure of GaAs," *Surf. Sci.* **43**, 449 (1974); M.D. Pashley, K.W. Haberern, W. Friday, J.M. Woodall, and P.D. Kirchner, "Structure of GaAs (001) (2x4)-c(2x8) determined by scanning tunneling microscopy," *Phys. Rev. Lett.* **60**, 2176, (1988); D.K. Biegelsen, R.D. Bringans, J.E. Northrup, and L.-E. Swartz, "Surface reconstructions of GaAs (100) observed by scanning tunneling microscopy," *Phys. Rev.* **B41**, 5701 (1990); C. Deparis and J. Massies, "Surface stoichiometry variation associated with GaAs (001) reconstruction transitions," *J. Cryst. Growth* **108**, 157 (1991); R. Ludeke, R.M. King, and E.H.C. Parker, "MBE surface and interface studies," in E.H.C. Parker, ed., *The Technology and Physics of Molecular Beam Epitaxy* (Plenum Press, New York, 1985), pp. 555-628; H.H. Farrell and C.J. Palmstrøm, "Reflection high energy electron diffraction characteristic absences in GaAs (100) (2x4)-As: a tool for determining surface stoichiometry," *J. Vac. Sci. Technol.* **B8**, 903 (1990); and J.Y. Tsao, T.M. Brennan, J.F. Klem, and B.E. Hammons, "Surface-stoichiometry dependence of As_2 desorption and As_4 'reflection' from GaAs (001)," *J. Vac. Sci. Techn.* **A7**, 2138 (1989).

for understanding surface alloys. For simplicity, we develop the framework within the approximation that the surface is exactly one monolayer thick. As a consequence, the framework, like those of other monolayer models, cannot be used to understand phenomena that depend on surface effects greater than one monolayer deep.[2] Nevertheless, the framework is intuitive, leads to a deep physical understanding of the relationship between bulk and surface alloy phases, and can be easily used in semi-empirical modeling.

Then, in Section 7.2, we apply the framework to equilibria and nonequilibria between vapor and monolayer adsorbate phases, treating the adsorbate phase as a surface alloy of adsorbates and "missing" adsorbates. In doing so, we will derive familiar equilibrium constructs, such as adsorption isotherms and adsorption isobars, as well as discuss less familiar nonequilibrium phenomena, such as transient and coverage-dependent adsorption and desorption.

Finally, in Section 7.3, we will apply the framework to the technologically important phenomena of segregation and trapping of dopants or other impurities at surfaces during MBE. This phenomenon is especially complex, in that it involves equilibria and nonequilibria between vapor, surface, *and* bulk crystalline phases.

7.1 Monolayer Thermodynamics

In this section, we discuss the equilibrium thermodynamics of the surface of a bulk alloy. We begin, in Subsection 7.1.1, by establishing a nomenclature consistent with that introduced in Chapter 3. We then ask, in the first half of Subsection 7.1.2: given a composition of the bulk alloy, what is the composition of the surface alloy that is in equilibrium with that bulk alloy? In general, the surface and bulk compositions will not be the same in equilibrium, in that one component of the alloy will tend to segregate to the surface, displacing the other component back into the bulk. We finally ask, in the second half of Subsection 7.1.2: given the compositions of the surface and bulk alloys, what is the free energy required to create new surface at that composition? This free energy is the surface work (also often called the surface tension), and is minimum if the surface composition is such that the surface alloy phase is in equilibrium with the bulk alloy phase.

[2] See, e.g., J.K. Strohl and T.S. King, "A multicomponent, multilayer model of surface segregation in alloy catalysts," *J. Catal.* **118**, 53 (1989).

7.1.1 Surface Free Energies and Chemical Potentials

Let us begin, in this subsection, by establishing our nomenclature. Consider a binary crystalline alloy phase, β, containing N_a moles (or atoms) of component a and N_b moles (or atoms) of component b. As in Chapter 3, we write the molar Gibbs free energy of this bulk phase as

$$g^\beta \equiv \frac{G^\beta}{N_a + N_b}, \tag{7.1}$$

where G^β is the total Gibbs free energy. Again, as in Chapter 3, the chemical potentials of the two components a and b in β are the intercepts with the $x = 0$ and $x = 1$ axes of the tangents to g^β:

$$\begin{aligned} \mu_a^\beta &= g^\beta - x^\beta \frac{\partial g^\beta}{\partial x^\beta} \\ \mu_b^\beta &= g^\beta + (1 - x^\beta)\frac{\partial g^\beta}{\partial x^\beta}, \end{aligned} \tag{7.2}$$

where $x^\beta \equiv N_b/(N_a + N_b)$ is the composition of β.

Consider second a surface of the bulk crystal, σ, characterized by N_a^σ exposed atoms of component a and N_b^σ exposed atoms of component b. Associate with the exposed atoms on this surface a Gibbs free energy equal to the difference between the total Gibbs free energy and the Gibbs free energy of the *nonsurface* atoms still in the bulk crystal:

$$G^\sigma(N_a^\sigma, N_b^\sigma) = G^{\text{tot}}(N_a^\sigma, N_b^\sigma, N_a^\beta, N_b^\beta) - G^\beta(N_a^\beta, N_b^\beta). \tag{7.3}$$

In general, G^σ depends not only on N_a^σ and N_b^σ, but on N_a^β and N_b^β as well. Here, we neglect this dependence, and note that such a dependence is nontrivial to include in a way that self-consistently treats bonding within the surface layer and bonding between the surface layer and the bulk layers below.[3]

Let us therefore consider this surface to be a 2D monolayer phase having its own thermodynamic properties apart from those of the bulk. In this way, we can adopt the nomenclature and definitions developed originally for bulk phases. For example, by analogy to Equation 7.1, the molar Gibbs free energy of the exposed surface atoms can be defined as

$$g^\sigma \equiv \frac{G^\sigma}{N_a^\sigma + N_b^\sigma}, \tag{7.4}$$

[3] J.W. Belton and M.G. Evans, "Studies in the molecular forces involved in surface formation. II. The surface free energies of simple liquid mixtures," *Trans. Faraday Soc.* **41**, 1 (1945); A. Schuchowitzky, *Acta Physicochim. URSS* **19** (2-3), 176 (1944); R. Defay and I. Prigogine, "Surface tension of regular solutions," *Trans. Faraday Soc.* **46**, 199 (1950); and S. Ono and S. Kondo, *Handb. Physik* **10**, 134 (1960).

and, by analogy to Equations 7.2, the chemical potentials of a and b in σ are the intercepts with the $x = 0$ and $x = 1$ axes of the tangents to g^σ:

$$\begin{aligned} \mu_{\mathrm{a}}^\sigma &= g^\sigma - x^\sigma \frac{\partial g^\sigma}{\partial x^\sigma} \\ \mu_{\mathrm{b}}^\sigma &= g^\sigma + (1 - x^\sigma)\frac{\partial g^\sigma}{\partial x^\sigma}. \end{aligned} \tag{7.5}$$

where $x^\sigma \equiv N_{\mathrm{b}}^\sigma/(N_{\mathrm{a}}^\sigma + N_{\mathrm{b}}^\sigma)$ is the composition of σ.

Furthermore, the composition dependence of the molar Gibbs free energy of surface phases may be semi-empirically modeled in the same way that the molar Gibbs free energy of bulk phases is often modeled, as ideal solutions, or as one of a heirarchy of regular solutions (see Table 3.1). Examples of such composition-dependent surface and bulk molar Gibbs free energies for the Ag–Au system are shown in Figure 7.1. In this system, the molar Gibbs free energies are thought to be characterized by the sub-regular forms

$$\begin{aligned} g^{\langle \mathrm{Ag}_{1-x^\beta}\mathrm{Au}_{x^\beta}\rangle} &= (1-x^\beta)g^{\langle \mathrm{Ag}\rangle} + x^\beta g^{\langle \mathrm{Au}\rangle} - s_{\mathrm{mix,ideal}}T + \Omega^\beta(1-x^\beta)x^\beta \\ g^{\rangle \mathrm{Ag}_{1-x^\sigma}\mathrm{Au}_{x^\sigma}(} &= (1-x^\sigma)g^{\rangle \mathrm{Ag}(} + x^\sigma g^{\rangle \mathrm{Au}(} - s_{\mathrm{mix,ideal}}T + \Omega^\sigma(1-x^\sigma)x^\sigma, \end{aligned} \tag{7.6}$$

and are linear interpolations between the molar Gibbs free energies of the pure-component phases, plus entropic and enthalpic "mixing" terms.

Note that in writing these equations, we have extended the notation of Section 2.4 so that interface phases are represented by *mismatched* pairs of brackets, braces, and parentheses to denote the bulk phases the interface is sandwiched between. In this notation, the two phases of interest, the crystalline bulk and surface phases, are denoted $\langle \mathrm{Ag}_{1-x^\beta}\mathrm{Au}_{x^\beta}\rangle$ and $\rangle \mathrm{Ag}_{1-x^\sigma}\mathrm{Au}_{x^\sigma}($, and their compositions are denoted x^β and x^σ.

For the crystalline solid, $g^{\langle \mathrm{Ag}\rangle}$ and $g^{\langle \mathrm{Au}\rangle}$ are the known molar Gibbs free energies of the pure-component phases Ag and Au,[4] and

$$\Omega^{\langle \mathrm{Ag}_{1-x^\beta}\mathrm{Au}_{x^\beta}\rangle} = A + Bx^\beta + CT \tag{7.7}$$

is a known composition and temperature-dependent interaction parameter.[5]

[4]The molar Gibbs free energies of the pure crystals were calculated according to the prescription described in Chapter 2, using the heat capacity expression $c_p = (c_o + c_1 T)T^2/(T^2 + \Theta_T^2)$. The heat capacity parameters for $\langle \mathrm{Ag}\rangle$ were $c_o = 0.253$ meV/(atomK), $c_1 = 0.0553$ μeV/atom/(atomK^2), $\Theta_T = 55.4$ K; the parameters for $\langle \mathrm{Au}\rangle$ were $c_o = 0.248$ meV/(atomK), $c_1 = 0.563$ μeV/atom/(atomK^2) and $\Theta_T = 43.5$ K.

[5]Following J.L. White, R.L. Orr, and R. Hultgren, "The thermodynamic properties

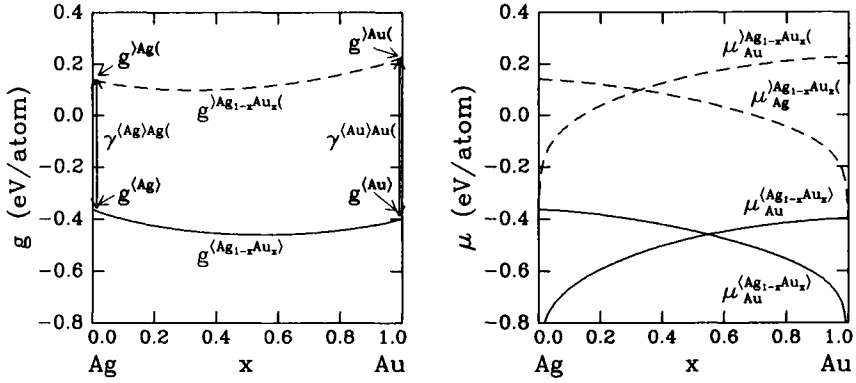

Figure 7.1: Left: Molar Gibbs free energies of the crystalline bulk and surface phases of the Ag–Au system at 700 K. Right: Chemical potentials of Ag and Au in these phases. As in Figure 3.1, the intercepts of the tangents to the molar Gibbs free energies with the $x = 0$ and $x = 1$ axes are the chemical potentials. As the tangents sweep around the arc of the molar Gibbs free energy curves, the intercepts of those tangents trace out the chemical potentials at the various compositions.

For the crystalline surface *at* the endpoint compositions, the molar Gibbs free energies are those for pure crystalline ⟨Ag⟩ and ⟨Au⟩, but offset upward by their known surface tensions. In other words,

$$\begin{aligned} g^{\rangle \mathrm{Ag}(} &= g^{\langle \mathrm{Ag} \rangle} + \gamma^{\langle \mathrm{Ag} \rangle \mathrm{Ag}(} \\ g^{\rangle \mathrm{Au}(} &= g^{\langle \mathrm{Au} \rangle} + \gamma^{\langle \mathrm{Au} \rangle \mathrm{Au}(}, \end{aligned} \tag{7.8}$$

where the experimentally measured values[6] for $\gamma^{\langle \mathrm{Ag} \rangle}$ and $\gamma^{\langle \mathrm{Au} \rangle}$, the work per unit area required to form new surfaces of pure crystalline Ag and Au, have been normalized by the number of atoms per unit area on close-packed (111) planes.

For the crystalline surface *away* from the endpoint compositions, the molar Gibbs free energy has been found to be consistent with a sub-regular solution behavior that mimics that of the crystalline bulk phase.[7] In other

of silver-gold alloys," *Acta Metall.* **5**, 747 (1957) and H. Okamoto and T.B. Massalski, in *Phase Diagrams of Binary Gold Alloys*, H. Okamoto and T.B. Massalski, Eds. (ASM International, Metals Park, Ohio, 1987), pp. 4-12, the sub-regular solution parameters were taken to be $A = -0.210$ eV/atom, $B = 0.0347$eV/atom and $C = 0.0000596$ eV/(atomK).

[6]We use the values $\gamma^{\langle \mathrm{Ag} \rangle \mathrm{Ag}(} = 0.50$ eV/atom and $\gamma^{\langle \mathrm{Au} \rangle \mathrm{Au}(} = 0.63$ eV/atom [H. Jones, "The surface energy of solid metals," *Met. Sci. J.* **5**, 15 (1971)].

[7]J.Y. Tsao, "Graphical representation of Ag–Au surface segregation," *Surf. Sci.* **262**, 382 (1992).

words,

$$\Omega^{\sigma} = \Omega^{\beta}. \tag{7.9}$$

As drawn in the left panel of Figure 7.1, the shape of the molar Gibbs free energy of the surface alloy is the same as that of the bulk alloy, but is offset upward by amounts that vary linearly from $\gamma^{\langle \mathrm{Ag} \rangle \mathrm{Ag}(}$ on one end to $\gamma^{\langle \mathrm{Au} \rangle \mathrm{Au}(}$ on the other end.

7.1.2 Atom Transfers between Surface and Bulk

Having defined, in Subsection 7.1.1, the thermodynamic functions for the crystalline bulk and surface phases, let us consider, in this subsection, *transferring* atoms between the two phases. Such transfers can take place in two ways, and are discussed separately in the following two subsubsections.

Parallel Tangents and Equilibrium Segregation

In the first way of transferring atoms between the two phases, the overall number of surface sites is preserved. Then, if we move, e.g., a Au atom from the bulk to the surface, we must at the same time move a Ag atom from the surface to the bulk: atom transfers between bulk and surface must be atom *exchanges*. Hence, they are accompanied by free energy changes equal to the *difference* between (a) the "excess" chemical potentials required to move a Au atom from the bulk to the surface, or

$$\mu_{\mathrm{Au}}^{\mathrm{exc}} \equiv \mu_{\mathrm{Au}}^{\rangle \mathrm{Ag}_{1-x^{\sigma}} \mathrm{Au}_{x^{\sigma}} (} - \mu_{\mathrm{Au}}^{\langle \mathrm{Ag}_{1-x^{\beta}} \mathrm{Au}_{x^{\beta}} \rangle}, \tag{7.10}$$

and (b) the "excess" chemical potentials required to move a Ag atom from the bulk to the surface, or

$$\mu_{\mathrm{Ag}}^{\mathrm{exc}} \equiv \mu_{\mathrm{Ag}}^{\rangle \mathrm{Ag}_{1-x^{\sigma}} \mathrm{Au}_{x^{\sigma}} (} - \mu_{\mathrm{Ag}}^{\langle \mathrm{Ag}_{1-x^{\beta}} \mathrm{Au}_{x^{\beta}} \rangle}. \tag{7.11}$$

In other words, they are accompanied by a free energy change of

$$\begin{aligned} \mu_{\mathrm{Au}}^{\mathrm{exc}} - \mu_{\mathrm{Ag}}^{\mathrm{exc}} \equiv & \left(\mu_{\mathrm{Au}}^{\rangle \mathrm{Ag}_{1-x^{\sigma}} \mathrm{Au}_{x^{\sigma}} (} - \mu_{\mathrm{Au}}^{\langle \mathrm{Ag}_{1-x^{\beta}} \mathrm{Au}_{x^{\beta}} \rangle} \right) \\ & - \left(\mu_{\mathrm{Ag}}^{\rangle \mathrm{Ag}_{1-x^{\sigma}} \mathrm{Au}_{x^{\sigma}} (} - \mu_{\mathrm{Ag}}^{\langle \mathrm{Ag}_{1-x^{\beta}} \mathrm{Au}_{x^{\beta}} \rangle} \right). \end{aligned} \tag{7.12}$$

This free energy change can be rewritten as

$$\begin{aligned} \mu_{\mathrm{Au}}^{\mathrm{exc}} - \mu_{\mathrm{Ag}}^{\mathrm{exc}} \equiv & \left(\mu_{\mathrm{Au}}^{\rangle \mathrm{Ag}_{1-x^{\sigma}} \mathrm{Au}_{x^{\sigma}} (} - \mu_{\mathrm{Ag}}^{\rangle \mathrm{Ag}_{1-x^{\sigma}} \mathrm{Au}_{x^{\sigma}} (} \right) \\ & - \left(\mu_{\mathrm{Au}}^{\langle \mathrm{Ag}_{1-x^{\beta}} \mathrm{Au}_{x^{\beta}} \rangle} - \mu_{\mathrm{Ag}}^{\langle \mathrm{Ag}_{1-x^{\beta}} \mathrm{Au}_{x^{\beta}} \rangle} \right), \end{aligned} \tag{7.13}$$

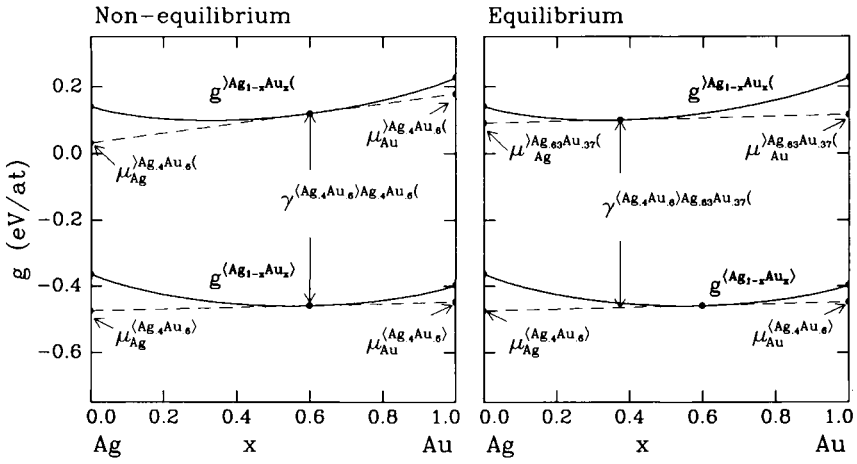

Figure 7.2: Surface and bulk phase equilibria in the Ag–Au system at 700 K. Left: The two tangents to the molar Gibbs free energies have different slopes and there is a driving force for Ag or Au atoms to segregate to the surface. Center: the two tangents are parallel and the surface is in equilibrium with the bulk.

and can be seen to be the difference between the slope of the tangent to $\mu^{\rangle \mathrm{Ag}_{1-x^\sigma}\mathrm{Au}_{x^\sigma}\langle}$ at x^σ and the slope of the tangent to $\mu^{\langle \mathrm{Ag}_{1-x^\beta}\mathrm{Au}_{x^\beta}\rangle}$ at x^β. When $\mu_{\mathrm{Au}}^{\mathrm{exc}} - \mu_{\mathrm{Ag}}^{\mathrm{exc}}$ is positive, as in the left panel of Figure 7.2, Au surface atoms will tend to exchange with Ag bulk atoms, and the surface will become enriched in Ag. When it is negative, then Ag surface atoms will tend to exchange with Au bulk atoms. When it is zero, as in the right panel of Figure 7.2, then the surface is in equilibrium with the bulk. In other words, the crystal and surface phases are in equilibrium with each other when the tangents to their molar Gibbs free energies have the same slopes, or, equivalently, when the tangents are parallel.[8]

Now, according to this parallel tangent criterion, to find the composition of a surface in equilibrium with a bulk crystal of a particular composition, we must solve $\partial g^{\rangle \mathrm{Ag}_{1-x^\sigma}\mathrm{Au}_{x^\sigma}\langle}/\partial x^\sigma = \partial g^{\langle \mathrm{Ag}_{1-x^\beta}\mathrm{Au}_{x^\beta}\rangle}/\partial x^\beta$ by varying x^σ for fixed x^β. Equivalently, and sometimes more conveniently, one can (see

[8]M. Hillert, "The role of interfaces in phase transformations," in *The Mechanism of Phase Transformations in Crystalline Solids*, Monograph and Report Series No. 33 (The Institute of Metals, London, 1969), pp. 231-247; and M. Guttmann, "Grain boundary segregation, two dimensional compound formation, and precipitation," *Met. Trans.* **8A**, 1383 (1977).

Exercise 1) minimize the function

$$\eta(x^\sigma, x^\beta) \equiv g^{\rangle \mathrm{Ag}_{1-x^\sigma}\mathrm{Au}_{x^\sigma}(} - x^\sigma \frac{\partial g^{\langle \mathrm{Ag}_{1-x^\beta}\mathrm{Au}_{x^\beta}\rangle}}{\partial x^\beta}, \tag{7.14}$$

by varying x^σ for fixed x^β. Both numerical prescriptions are general, and can be used even if the molar Gibbs free energies of the surface and bulk are represented by very complicated semi-empirical forms.

For example, consider the relationship between the equilibrium surface and bulk compositions of strictly regular bulk and surface phases β and σ. In the limit of small x^β and x^σ, this relationship can be shown (see Exercise 4) to be given by

$$\kappa_{\mathrm{equ}} \equiv \frac{x^\beta}{x^\sigma} = e^{-[\gamma^{\langle \mathrm{b}\rangle \mathrm{b}(} - \gamma^{\langle \mathrm{a}\rangle \mathrm{a}(} + \Omega^\sigma - \Omega^\beta]/kT}, \tag{7.15}$$

where $\gamma^{\langle \mathrm{a}\rangle \mathrm{a}(}$ and $\gamma^{\langle \mathrm{b}\rangle \mathrm{b}(}$ are the surface tensions of the pure a and pure b phases. The quantity κ_{equ}, the ratio between the equilibrium bulk and surface compositions, can be thought of as an equilibrium "partition" coefficient, in that it describes the physical partitioning of a dilute impurity between two adjacent phases.

More generally, Equation 7.14 must be solved numerically. For the Ag–Au system, the resulting dependence of the surface composition on bulk composition is shown as the segregation isotherm in Figure 7.3. Note that at all compositions, the surface tends to be enriched in Ag relative to the bulk. The reason is that, even though $g^{\rangle \mathrm{Ag}_{1-x^\sigma}\mathrm{Au}_{x^\sigma}(}$ has the same *shape* as $g^{\langle \mathrm{Ag}_{1-x^\beta}\mathrm{Au}_{x^\beta}\rangle}$, its *offset* relative to $g^{\langle \mathrm{Ag}_{1-x^\beta}\mathrm{Au}_{x^\beta}\rangle}$ increases linearly with composition because pure Au has a higher surface tension than does pure Ag. As a consequence, at the same composition, the slope of the tangent to $g^{\rangle \mathrm{Ag}_{1-x^\sigma}\mathrm{Au}_{x^\sigma}(}$ will be greater than the slope of the tangent to $g^{\langle \mathrm{Ag}_{1-x^\beta}\mathrm{Au}_{x^\beta}\rangle}$, and is compensated for by a decrease in the composition of $g^{\rangle \mathrm{Ag}_{1-x^\sigma}\mathrm{Au}_{x^\sigma}(}$.

Surface Work

In the second way of transferring atoms between the crystalline bulk and surface phases, the overall number of surface sites is not preserved. Instead, as Ag or Au are transferred from the bulk to the surface, new surface sites are created to accommodate them. The work per atom required to create new surface of composition x^σ from bulk crystal of composition x^β is now the *sum* of the changes in the chemical potentials of the two components, weighted by their mole fractions on the surface:

$$\gamma^{\langle \mathrm{Ag}_{1-x^\beta}\mathrm{Au}_{x^\beta}\rangle \mathrm{Ag}_{1-x^\sigma}\mathrm{Au}_{x^\sigma}(} \equiv (1-x^\sigma)\mu_{\mathrm{Ag}}^{\mathrm{exc}} + x^\sigma \mu_{\mathrm{Au}}^{\mathrm{exc}}. \tag{7.16}$$

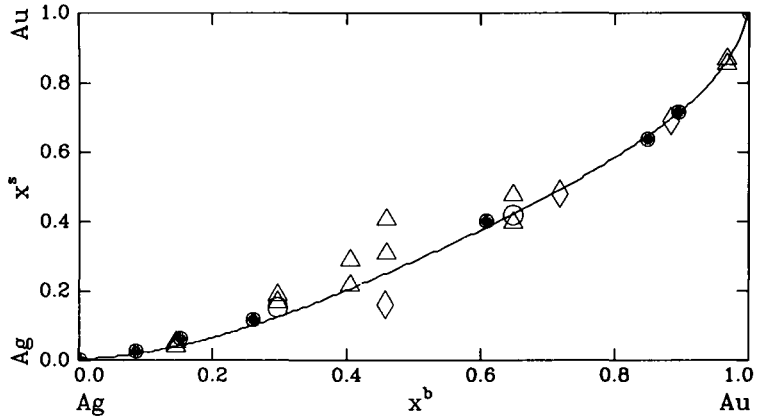

Figure 7.3: Surface segregation isotherm for the Ag–Au system at 700 K, deduced from the parallel tangent construction illustrated in Figure 7.2. Measured data are represented by open circles,[a] triangles,[b] diamonds,[c] and filled circles.[d]

[a]G.C. Nelson, "Determination of the surface versus bulk composition of silver–gold alloys by low energy ion scattering spectroscopy," *Surf. Sci.* **59**, 310 (1976).

[b]S.H. Overbury and G.A. Somorjai, "The surface composition of the silver–gold system by Auger electron spectroscopy," *Surf. Sci.* **55**, 209 (1976).

[c]M.J. Kelley, D.G. Swartzfager, and V.S. Sundaram, "Surface segregation in the Ag–Au and Pt–Cu systems," *J. Vac. Sci. Technol.* **16**, 664 (1979).

[d]K. Meinel, M. Klaua, and H. Bethge, "Segregation and sputter effects on perfectly smooth (111) and (100) surfaces of Au–Ag alloys studied by AES," *Phys. Stat. Sol.* **A106**, 133 (1988).

This equation defines the surface work, $\gamma^{\langle \mathrm{Ag}_{1-x^\beta}\mathrm{Au}_{x^\beta}\rangle \mathrm{Ag}_{1-x^\sigma}\mathrm{Au}_{x^\sigma}(}$, in terms of the surface and bulk compositions and chemical potentials.

Let us now expand $\mu_{\mathrm{Au}}^{\mathrm{exc}}$ and $\mu_{\mathrm{Ag}}^{\mathrm{exc}}$ using Equations 7.10 and 7.11, and apply the identities

$$\begin{aligned} g^{\langle \mathrm{Ag}_{1-x^\beta}\mathrm{Au}_{x^\beta}\rangle} &= (1-x^\beta)\mu_{\mathrm{Ag}}^{\langle \mathrm{Ag}_{1-x^\beta}\mathrm{Au}_{x^\beta}\rangle} + x^\beta \mu_{\mathrm{Au}}^{\langle \mathrm{Ag}_{1-x^\beta}\mathrm{Au}_{x^\beta}\rangle} \\ g^{\rangle \mathrm{Ag}_{1-x^\sigma}\mathrm{Au}_{x^\sigma}(} &= (1-x^\sigma)\mu_{\mathrm{Ag}}^{\rangle \mathrm{Ag}_{1-x^\sigma}\mathrm{Au}_{x^\sigma}(} + x^\sigma \mu_{\mathrm{Au}}^{\rangle \mathrm{Ag}_{1-x^\sigma}\mathrm{Au}_{x^\sigma}(}, \end{aligned} \tag{7.17}$$

which can be derived from Equations 7.2 and 7.5. Then, the surface work can be written as

$$\begin{aligned} &\gamma^{\langle \mathrm{Ag}_{1-x^\beta}\mathrm{Au}_{x^\beta}\rangle \mathrm{Ag}_{1-x^\sigma}\mathrm{Au}_{x^\sigma}(} = \\ &\quad \left(g^{\rangle \mathrm{Ag}_{1-x^\sigma}\mathrm{Au}_{x^\sigma}(} - g^{\langle \mathrm{Ag}_{1-x^\beta}\mathrm{Au}_{x^\beta}\rangle}\right) \\ &\quad - (x^\sigma - x^\beta)\left(\mu_{\mathrm{Au}}^{\langle \mathrm{Ag}_{1-x^\beta}\mathrm{Au}_{x^\beta}\rangle} - \mu_{\mathrm{Ag}}^{\langle \mathrm{Ag}_{1-x^\beta}\mathrm{Au}_{x^\beta}\rangle}\right). \end{aligned} \tag{7.18}$$

If we define the "excess" molar Gibbs free energy to be $g^{\text{exc}} \equiv g^{\langle \text{Ag}_{1-x^\sigma}\text{Au}_{x^\sigma}(} - g^{\langle \text{Ag}_{1-x^\beta}\text{Au}_{x^\beta}\rangle}$, then we also have

$$g^{\text{exc}} = \gamma^{\langle \text{Ag}_{1-x^\beta}\text{Au}_{x^\beta}\rangle \text{Ag}_{1-x^\sigma}\text{Au}_{x^\sigma}(} + (x^\sigma - x^\beta)\left(\mu_{\text{Au}}^{\langle \text{Ag}_{1-x^\beta}\text{Au}_{x^\beta}\rangle} - \mu_{\text{Ag}}^{\langle \text{Ag}_{1-x^\beta}\text{Au}_{x^\beta}\rangle}\right). \quad (7.19)$$

This last expression for the relationship between the excess molar Gibbs free energy and the surface work can be understood graphically by inspection of Figure 7.2. If the surface and bulk compositions are the same, as in the left panel, then $x^\sigma = x^\beta$ and $g^{\text{exc}} = \gamma^{\langle \text{Ag}_{1-x^\beta}\text{Au}_{x^\beta}\rangle \text{Ag}_{1-x^\sigma}\text{Au}_{x^\sigma}(}$ itself. Otherwise, as in the right panel, we must add a correction term equal to the slope of the tangent to $g^{\langle \text{Ag}_{1-x^\beta}\text{Au}_{x^\beta}\rangle}$ times the difference between the surface and bulk compositions. The surface work can thus be seen to be the vertical distance between the tangent to the molar Gibbs free energy of the surface at composition x^σ, evaluated at x^σ, and the tangent to the molar Gibbs free energy of the bulk at composition x^β, also evaluated at x^σ. Importantly, this graphical interpretation of the surface work holds whether or not the tangents are parallel, hence *whether or not the surface and bulk are in equilibrium with each other.*

To make contact with standard treatments of surface thermodynamics, note that Equation 7.19 can be rewritten in yet another equivalent form:

$$g^{\text{exc}} = \gamma^{\langle \text{Ag}_{1-x^\beta}\text{Au}_{x^\beta}\rangle \text{Ag}_{1-x^\sigma}\text{Au}_{x^\sigma}(} + x_{\text{Ag}}^{\text{exc}}\mu_{\text{Ag}}^{\langle \text{Ag}_{1-x^\beta}\text{Au}_{x^\beta}\rangle} + x_{\text{Au}}^{\text{exc}}\mu_{\text{Au}}^{\langle \text{Ag}_{1-x^\beta}\text{Au}_{x^\beta}\rangle}. \quad (7.20)$$

This equation reproduces the well-established relation[9] (at constant temperature) between the excess molar Gibbs free energy of the surface, the surface work, and the excess Ag and Au at the surface, $x_{\text{Ag}}^{\text{exc}} \equiv x^\beta - x^\sigma$ and $x_{\text{Au}}^{\text{exc}} \equiv x^\sigma - x^\beta$.

Finally, let us return to Equation 7.16, to understand more clearly the difference between the work required to transfer atoms to the surface in the two different ways. In the first way, we form new surface area at fixed composition. The work required is then $\gamma^{\langle \text{Ag}_{1-x^\beta}\text{Au}_{x^\beta}\rangle \text{Ag}_{1-x^\sigma}\text{Au}_{x^\sigma}(}$. In the second way, we change the composition of the surface at fixed surface area. The work required is then $\partial\gamma^{\langle \text{Ag}_{1-x^\beta}\text{Au}_{x^\beta}\rangle \text{Ag}_{1-x^\sigma}\text{Au}_{x^\sigma}(}/\partial x^\sigma = \mu_{\text{Au}}^{\text{exc}} - \mu_{\text{Ag}}^{\text{exc}}$ (see Exercise 3). In equilibrium, that work must be zero, as in the discussion following Equations 7.12 and 7.13.

[9] A.W. Adamson, *Physical Chemistry of Surfaces*, 4th Ed. (John Wiley and Sons, New York, 1982).

7.2 Adsorption and Desorption

In Section 7.1, we outlined a simple semi-empirical framework for understanding surface thermodynamics. The framework hinged on approximating the outermost exposed atomic monolayer as a phase whose composition and thermodynamic properties are distinct from those of the bulk. In fact, this approximation is most inaccurate for the surfaces of condensed alloy phases, whose composition and thermodynamic properties vary gradually over more than one atomic layer into the bulk.

In this section, we apply the framework to monolayer adsorbate phases on one-component bulk solids. We assume, as is often the case, that the adsorbate component does not indiffuse into the bulk and hence remains on the surface. Then, the composition of the system does change abruptly between the outermost surface monolayer and the bulk, and our approximate treatment is much more realistic. We will begin, in Subsection 7.2.1, by deriving two important equilibrium constructs: adsorption isotherms and adsorption isobars. Then, in Subsection 7.2.2, we discuss nonequilibrium adsorption and desorption.

7.2.1 Adsorption Isotherms and Isobars

Let us start, in this subsection, by deriving the equilibrium adsorbate coverages associated with an ambient vapor at a particular pressure and temperature. Consider a low-vapor-pressure bulk crystal composed of a single component, "m," bathed in a vapor composed of a single component, "a." As indicated in the left panel of Figure 7.4, the molar Gibbs free energy of the crystal is denoted $g^{\langle \mathrm{m} \rangle}$, and the molar Gibbs free energy of the vapor is denoted $g^{(\mathrm{a})}$.

In the absence of atoms of component a on the surface, the molar Gibbs free energy of the surface, $g^{\rangle \mathrm{m} (}$, is just offset upward from $g^{\langle \mathrm{m} \rangle}$ by the surface tension, $\gamma^{\langle \mathrm{m} \rangle \mathrm{m} (}$. In the presence of a full monolayer of atoms of component a on the surface, the molar Gibbs free energy of the surface is denoted $g^{\rangle \mathrm{a} (}$.

At intermediate compositions, as discussed in the previous section, the molar Gibbs free energy is a linearly weighted interpolation between $g^{\rangle \mathrm{m} (}$ and $g^{\rangle \mathrm{a} (}$, plus entropy and enthalpy of mixing terms. For example, a strictly regular solution would be written

$$\begin{aligned} g^{\rangle \mathrm{m}_{1-\theta}\mathrm{a}_{\theta} (} &= (1-\theta) g^{\rangle \mathrm{m} (} + \theta g^{\rangle \mathrm{a} (} + kT[\theta \ln \theta + (1-\theta)\ln(1-\theta)] \\ &\quad + \Omega\theta(1-\theta), \end{aligned} \tag{7.21}$$

where θ is the "composition" of the surface phase. In a sense, the surface phase can be considered a mixture of surface sites covered by adatoms and

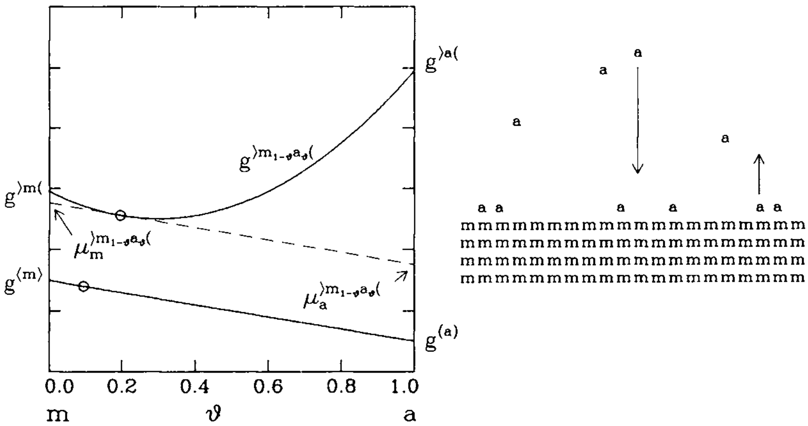

Figure 7.4: Vapor and surface adsorbate phase equilibria. Left: The two tangents to the molar Gibbs free energies are parallel, hence there is no driving force for the coverage of a atoms on the surface to change. Right: Schematic of adsorption and desorption of a atoms from the vapor onto a surface and from the surface back into the vapor.

surface sites not covered by adatoms, so that θ is also the average adatom coverage on the surface.

To find, given these molar Gibbs free energies, the equilibrium adatom coverage, we can apply the same arguments we applied in Section 7.1. Suppose, as illustrated in the left half of Figure 7.4, the surface coverage is θ_o, so that the chemical potential of atoms a is the intercept of the tangent to $g^{)\mathrm{m}_{1-\theta}\mathrm{a}_\theta(}(\theta_o)$ with the $\theta = 1$ axis,

$$\mu_{\mathrm{a}}^{)\mathrm{m}_{1-\theta}\mathrm{a}_\theta(} = g^{)\mathrm{m}_{1-\theta}\mathrm{a}_\theta(} + (1-\theta)\frac{\partial g^{)\mathrm{m}_{1-\theta}\mathrm{a}_\theta(}}{\partial\theta}. \tag{7.22}$$

and the chemical potential of atoms m is the intercept with the $\theta = 0$ axis,

$$\mu_{\mathrm{m}}^{)\mathrm{m}_{1-\theta}\mathrm{a}_\theta(} = g^{)\mathrm{m}_{1-\theta}\mathrm{a}_\theta(} - \theta\frac{\partial g^{)\mathrm{m}_{1-\theta}\mathrm{a}_\theta(}}{\partial\theta}, \tag{7.23}$$

If we adsorb an atom a from the vapor, then the free energy of the system increases by $\mu_{\mathrm{a}}^{)\mathrm{m}_{1-\theta}\mathrm{a}_\theta(} - g^{(\mathrm{a})}$ due to the movement of atom a from the vapor to the surface phase, but it decreases by $g^{\langle\mathrm{m}\rangle} - \mu_{\mathrm{m}}^{)\mathrm{m}_{1-\theta}\mathrm{a}_\theta(}$ because the m atom that was covered has moved from the surface phase into the bulk. The equilibrium condition is therefore

$$\mu_{\mathrm{a}}^{)\mathrm{m}_{1-\theta}\mathrm{a}_\theta(} - \mu_{\mathrm{m}}^{)\mathrm{m}_{1-\theta}\mathrm{a}_\theta(} = g^{(\mathrm{a})} - g^{\langle\mathrm{m}\rangle}, \tag{7.24}$$

which is equivalent to the parallel tangent construction derived in Section 7.1.

Now, recall from Equation 2.47 that the molar Gibbs free energy of an elemental vapor is

$$g^{(a)}(p,T) = g^{(a)}(p_o,T) + kT \ln\left(\frac{p}{p_o}\right), \tag{7.25}$$

where p_o is a reference pressure. Hence, as the pressure of (a) increases, the molar Gibbs free energy of (a) also increases. As a consequence, the slope of $g^{(a)} - g^{\rangle m(}$ increases, causing the parallel tangent to pivot around the $g^{\rangle m_{1-\theta} a_\theta(}$ curve, and ultimately causing the equilibrium coverage θ_{equ} itself to increase. For a strictly regular adsorbate phase, this parallel tangent condition is expressed by combining Equations 7.21, 7.22, 7.23, 7.24 and 7.25, giving

$$\frac{\theta_{equ}}{1-\theta_{equ}} e^{\Omega(1-\theta_{equ})/kT} = \frac{p}{p_o} e^{\Delta g_{des}/kT}, \tag{7.26}$$

where $\Delta g_{des} = (g^{(a)}(p_o,T) - g^{\rangle a(}) - (g^{(m)} - g^{\rangle m(})$ is the "activation" free energy of desorption at the reference pressure p_o. This equation defines the coverage of the surface phase in equilibrium with a vapor at pressure p and temperature T, and can be used to construct both adsorption isotherms (the pressure dependence of the coverage at constant temperature) and adsorption isobars (the temperature dependence of the coverage at constant pressure).

For example, if $\Omega = 0$, so that the solution is ideal, then

$$\theta_{equ} = \frac{p}{p + p_o e^{-\Delta g_{des}/kT}}, \tag{7.27}$$

which reproduces what is known as Langmuir's isotherm. The adatom coverage increases linearly at first with increasing pressure, then saturates beyond a critical temperature-dependent pressure, $p_o e^{-\Delta g_{des}/kT}$.

If $\Omega \neq 0$, then the solution is nonideal. On the one hand, if $\Omega > 0$, then adatoms and "missing" adatoms repel each other, which is equivalent physically to adatoms attracting each other. The adatom coverage increases more rapidly at first with increasing pressure, before again saturating beyond a critical temperature-dependent pressure. On the other hand, if $\Omega < 0$, then adatoms and "missing" adatoms attract each other, which is equivalent physically to adatoms repelling each other. The adatom coverage increases less rapidly at first with increasing pressure, before again saturating beyond a critical temperature-dependent pressure.

7.2.2 Sticking Coefficients and Desorption

In Subsection 7.2.1, we discussed the composition, or coverage, of an adsorbate surface phase in equilibrium with its vapor. Physically, that equilibrium can also be viewed as the balancing of a dynamic competition between adsorption of atoms or molecules from the vapor and desorption of atoms or molecules back into the vapor. As a consequence, if we know the adsorption rate, then, at equilibrium, we know the desorption rate as well. In this subsection, we derive expressions for this desorption rate, as well as for the rates at which coverages, perturbed away from their equilibrium values, will return to those equilibrium values.

From the kinetic theory of gases, the rate at which atoms or molecules in a vapor impinge upon a surface, per lattice site, is $p\lambda^2/\sqrt{2\pi mkT}$, where p and T are the pressure and temperature of the vapor, m is the atomic or molecular mass, and λ^2 is the area per lattice site of the surface. If $s(\theta,T)$ is the coverage and temperature dependent fraction of impinging atoms or molecules that "stick" to the surface, then the adsorption rate will be

$$j_{\text{des}} = \frac{p\lambda^2 s(\theta,T)}{\sqrt{2\pi mkT}}. \tag{7.28}$$

At equilibrium, atoms or molecules must, by detailed balance, desorb exactly as fast as they adsorb. Since, at equilibrium, the coverage of a strictly regular solution surface phase is related to the pressure by Equation 7.26, the equilibrium desorption rate can also be expressed in terms of coverage as

$$j_{\text{des}} = \frac{p\lambda^2 s(\theta,T)}{\sqrt{2\pi mkT}} = \frac{p_o\lambda^2 s(\theta,T)}{\sqrt{2\pi mkT}} \left(\frac{\theta}{1-\theta}\right) e^{\Omega(1-\theta)/kT} e^{-\Delta j_{\text{des}}/kT}. \tag{7.29}$$

If we now assume that desorption depends directly on coverage, and only indirectly on the equilibrium pressure required to achieve that coverage, then Equation 7.29 holds even away from equilibrium. Hence, the net adsorption rate for a regular solution surface phase is

$$\begin{aligned} \dot{\theta} &= j_{\text{net}} \\ &= j_{\text{ads}} - j_{\text{des}} \\ &= \frac{\lambda^2 s(\theta,T)}{\sqrt{2\pi mkT}} \left[p - p_o \left(\frac{\theta}{1-\theta}\right) e^{\Omega(1-\theta)/kT} e^{-\Delta g_{\text{des}}/kT} \right], \end{aligned} \tag{7.30}$$

which is a first-order differential equation for the time evolution of the coverage.

Often, the sticking coefficient decreases linearly with coverage as $s(\theta, T) = s_o(1-\theta)$. Then,

$$\dot{\theta} = j_{\text{net}} = \frac{s_o\lambda^2}{\sqrt{2\pi mkT}}\left[p(1-\theta) - p_o\theta e^{\Omega(1-\theta)/kT}e^{-\Delta g_{\text{des}}/kT}\right]. \tag{7.31}$$

The net adsorption rate can be seen to be the difference between the rate at which atoms or molecules stick on uncovered portions of the substrate, and the rate at which atoms or molecules desorb from the covered portions of the substrate.

If the surface phase is an ideal solution, then $\Omega = 0$, and Equation 7.31 simplifies to

$$\dot{\theta} = j_{\text{net}} = \frac{s_o\lambda^2}{\sqrt{2\pi mkT}}\left[p - \theta(p+p_o)e^{-\Delta g_{\text{des}}/kT}\right]. \tag{7.32}$$

A surface having initially a coverage of θ_{ini} approaches exponentially the equilibrium coverage given by Equation 7.27 with a time constant τ given by

$$\frac{1}{\tau} = \frac{s_o\lambda^2(p+p_oe^{-\Delta g_{\text{des}}/kT})}{\sqrt{2\pi mkT}} = \frac{s_o\lambda^2 p_o e^{-\Delta g_{\text{des}}/kT}}{\sqrt{2\pi mkT}(1-\theta_{\text{equ}})}. \tag{7.33}$$

In other words,

$$\theta = \theta_{\text{equ}} + (\theta_{\text{ini}} - \theta_{\text{equ}})e^{-t/\tau}. \tag{7.34}$$

Note that for small deviations from the equilibrium coverage at pressure p_{equ}, the rate at which the surface will return to its equilibrium coverage is

$$\frac{d(\Delta\theta)}{dt} = j_{\text{net}}(\theta_{\text{equ}} + \Delta\theta) = j_{\text{net}}(\theta_{\text{equ}}) + \Delta\theta\left[\frac{\partial j_{\text{net}}}{\partial\theta}\right]_{\theta_{\text{equ}}}. \tag{7.35}$$

Since $j_{\text{net}}(\theta_{\text{equ}}) = 0$ at equilibrium,

$$\frac{1}{\tau} = -\frac{d(\Delta\theta)}{\Delta\theta dt} = -\left[\frac{j_{\text{net}}}{\partial\theta}\right]_{\text{equ}} \tag{7.36}$$

is the "small signal" approach rate back toward the equilibrium coverage.

For an ideal solution surface phase, Equations 7.32 and 7.36 give

$$\frac{1}{\tau} = \frac{s_o\lambda^2(p+p_oe^{-\Delta g_{\text{des}}/kT})}{\sqrt{2\pi mkT}} = \frac{s_o\lambda^2 p_o e^{-\Delta g_{\text{des}}/kT}}{\sqrt{2\pi mkT}(1-\theta_{\text{equ}})}, \tag{7.37}$$

which reproduces Equation 7.33. For a strictly regular solution surface phase, Equations 7.31 and 7.36 give

$$\frac{1}{\tau} = \frac{s_o\lambda^2}{\sqrt{2\pi mkT}}\left(\frac{1}{\theta_{\text{equ}}} - \frac{2\Omega\theta_{\text{equ}}}{kT}\right)e^{-\Delta g_{\text{des}}/kT}, \tag{7.38}$$

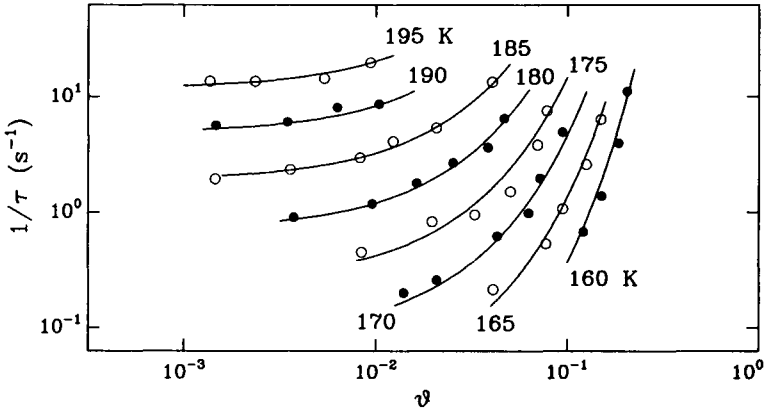

Figure 7.5: Coverage dependences of the small-signal vapor-adsorbate equilibration rate for CO on Cu(111). The open and filled circles are data measured[a] at the various indicated temperatures. The solid lines are the predictions of Equation 7.39, with a desorption molar Gibbs free energy of $\Delta g_{\rm des} = (0.67\ {\rm eV}) - (37.8kT)$, a mixing enthalpy of $\Omega_{\rm h} = 0.107$ eV, and a mixing entropy of $\Omega_{\rm s} = 20.7k$.

[a] B.J. Hinch and L.H. Dubois, "First-order corrections in modulated molecular beam desorption experiments," *Chem. Phys. Lett.* **171**, 131 (1990).

where $\theta_{\rm equ}$ is given by Equation 7.26. For a regular solution with both an enthalpy and entropy of mixing, $\Omega = \Omega_{\rm h} - T\Omega_{\rm s}$, and

$$\frac{1}{\tau} = \frac{s_o\lambda^2}{\sqrt{2\pi mkT}}\left(\frac{1}{\theta_{\rm equ}} - \frac{2\Omega_{\rm h}\theta_{\rm equ}}{kT} + \frac{2\Omega_{\rm s}\theta_{\rm equ}}{k}\right)e^{-\Delta g_{\rm des}/kT}. \qquad (7.39)$$

Examples of such coverage and temperature-dependent small-signal equilibration rates are illustrated in Figure 7.5 for CO on Cu(111). In this case there are both positive enthalpies and entropies of mixing. A positive enthalpy of mixing implies a repulsion between adatoms and missing adatoms, or, equivalently, an attraction between adatoms. Hence, the enthalpic barrier to desorption increases with increasing coverage. A positive entropy of mixing, however, implies an entropic barrier to desorption that decreases with increasing coverage. The two effects "compensate" each other to some extent, although, as illustrated in Figure 7.5, the balance tilts toward increasing the desorption rate with increasing coverage.

7.3 Surface Segregation and Trapping

In Section 7.1 we discussed the preferential segregation of one component from the bulk to the surface. In equilibrium, such segregation occurs when there are differences either between the surface tensions of the pure-component endpoint materials or between the free energies of mixing in the surface and bulk phases. Away from equilibrium, such segregation may or may not be significant, and will depend on the relative kinetics of crystal growth and interdiffusion between the surface and bulk phases. In this section, we discuss these dependences.

We will begin, in Subsection 7.3.1, by discussing the important simple case of segregation of a dilute solute under steady-state growth conditions.[10] This discussion will lead to an expression for the nonequilibrium partitition coefficient, κ, governing the ratio between the solute concentrations in the bulk and surface phases.

Then, in Subsection 7.3.2, we will make the assumption that, under non-steady-state conditions, this nonequilibrium partition coefficient still applies *locally* to the ratio between solute concentrations in the bulk phase just adjacent to the surface phase and in the surface phase itself. In this way, the nonequilibrium partition coefficient can be used to define a boundary condition connecting the non-steady-state evolution of solute concentrations in the bulk and surface phases.

7.3.1 Steady-State Compositional Partitioning

In this subsection, we consider steady-state segregation of a dilute solute b in a host solvent a. As illustrated in Figure 7.6, there are three phases to consider: the vapor, $(\mathrm{a}_{1-x^{\mathrm{v}}}\mathrm{b}_{x^{\mathrm{v}}})$, at composition x^{v}, the bulk solid, $\langle \mathrm{a}_{1-x^{\beta}}\mathrm{b}_{x^{\beta}} \rangle$, at composition x^{β}, and the surface monolayer dividing the two, $\rangle \mathrm{a}_{1-x^{\sigma}}\mathrm{b}_{x^{\sigma}} \langle$, at composition x^{σ}.

Between these three phases there are two basic kinetic processes that compete with each other.[11] First, vapor condenses, forming simultaneously a new surface layer (layer 1 in the right side of Figure 7.6), and transforming the previous surface layer into a new bulk solid layer (layer 2 in the right side of Figure 7.6). If condensation is "partitionless," in that the composition of the new surface layer mimics the composition of the vapor, then the system

[10] We do not treat the more complicated case of a nondilute solute; see, e.g., J.M. Moison, C. Guille, F. Houzay, F. Barthe, and M. Van Rompay, "Surface segregation of third-column atoms in group III-V arsenide compounds: ternary alloys and heterostructures," *Phys. Rev.* **B40**, 6149 (1989).

[11] J.J. Harris, D.E. Ashenford, C.T. Foxon, P.J. Dobson, and B.A. Joyce, "Kinetic limitations to surface segregation during MBE growth of III-V compounds: Sn in GaAs," *Appl. Phys.* **A33**, 87 (1984).

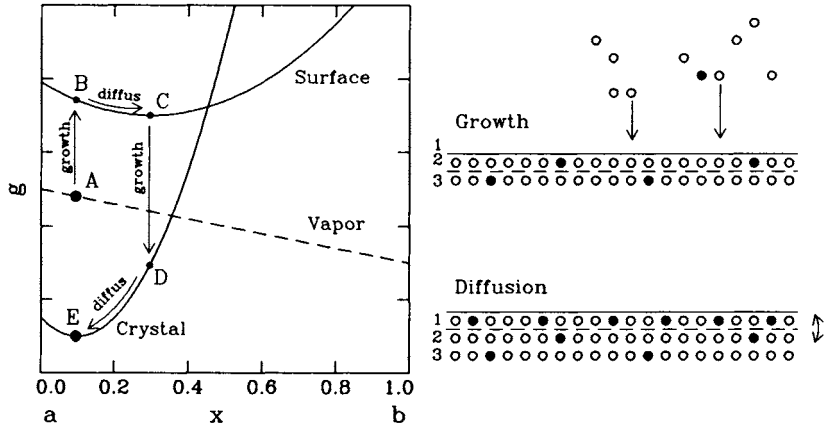

Figure 7.6: Left: Schematic molar Gibbs free energies of crystal $\langle a_{1-x^\beta} b_{x^\beta} \rangle$, vapor $(a_{1-x^v} b_{x^v})$ and surface $\rangle a_{1-x^\sigma} b_{x^\sigma} ($ phases. Right: Schematic of two competing kinetic processes: partitionless growth followed by solute partitioning via diffusion.

moves from point A to point B in the left side of Figure 7.6. At the same time, the previous surface layer, possibly enriched in solute, is transformed into a new bulk layer. Therefore, the system also moves from point C to point D in the left side of Figure 7.6.

Second, if the previous surface layer (layer 2 in the right side of Figure 7.6) were enriched in solute, then as it becomes a new bulk layer, it will also be enriched in solute. As a consequence, solute will tend to diffuse out into the new surface layer (layer 1 in the right side of Figure 7.6), moving the system from point D to point E and from B to C on the left side of Figure 7.6. In other words, partitionless condensation from vapor to surface to bulk solid is followed by partitioning by interdiffusion between the surface and the bulk solid. Note that, from start to finish, the system has moved *downward* from point A to point E in the left side of Figure 7.6, so that there is a net driving force for condensation.

Two extremes of behavior may be imagined, depending on the ratio between the rate of growth, j (in ML/s), and the rate of interdiffusion between bulk and surface layers, D_i/a^2. As in Section 6.3, this ratio, $a^2 j/D_i$, is a kind of Péclet number in that it is a dimensionless measure of the relative importance of convective over diffusional mass flow. Also as in Section 6.3, another way of understanding this Péclet number is to note that it is also the ratio between the time required for diffusion between the surface layer and its adjacent bulk layer, a^2/D_i, and the monolayer growth time, $\tau_{\mathrm{ML}} = 1/j$.

On the one hand, if $a^2 j/D_i \ll 1$, then interlayer diffusion is fast relative to growth. The surface layer will be in compositional equilibrium with its adjacent bulk layer, and the ratio between their compositions will be given by the equilibrium partition coefficient κ_{equ}. This extreme of behavior is therefore characterized by equilibrium solute segregation. On the other hand, if $a^2 j/D_i \gg 1$, then interlayer diffusion is slow relative to growth. The surface layer and its adjacent bulk layer will not have time during a monolayer growth cycle to reach composition equilibrium, and the ratio between their compositions, κ, will approach unity. This extreme of behavior is therefore characterized by nonequilibrium solute trapping.

Periodic and Aperiodic Step-Wise Growth

To quantify the dependence of κ on the Péclet number, consider a simple model in which growth proceeds by the passage of steps on a vicinal surface.[12] Suppose the composition of the surface layer just ahead of a moving step is x^σ. At time $t = 0$, just after the step has passed, that surface layer has become a bulk layer. If the new bulk layer has preserved its composition, then

$$\left[x^\beta\right]_{t=0} = x^\sigma. \tag{7.40}$$

During the subsequent time interval $\tau_{\text{ML}} = 1/j$ until yet another step passes, solute atoms in the bulk layer will diffuse to the surface layer, at a rate proportional to the deviation of the composition of the bulk layer from its equilibrium value, $\kappa_{\text{equ}} x^\sigma$. In other words,

$$\frac{\partial x^\beta}{\partial t} = \frac{-D_i}{a^2}(x^\beta - \kappa_{\text{equ}} x^\sigma). \tag{7.41}$$

From Equations 7.40 and 7.41, the solute concentration in the bulk decays exponentially with time according to

$$x^\beta = \kappa_{\text{equ}} x^\sigma + (x^\sigma - \kappa_{\text{equ}} x^\sigma) e^{-D_i t/a^2}. \tag{7.42}$$

Suppose now that once this bulk layer has been covered by yet another surface layer, further interdiffusion becomes negligible. There are two extreme possibilities for the ways in which the next layer may arrive.

On the one hand, if the steps on the surface are equispaced, then they pass over the surface *periodically*, at time intervals separated by $\tau_{\text{ML}} = 1/j$.

[12] M.J. Aziz, "Model for solute redistribution during rapid solidification," *J. Appl. Phys.* **53**, 1158 (1982).

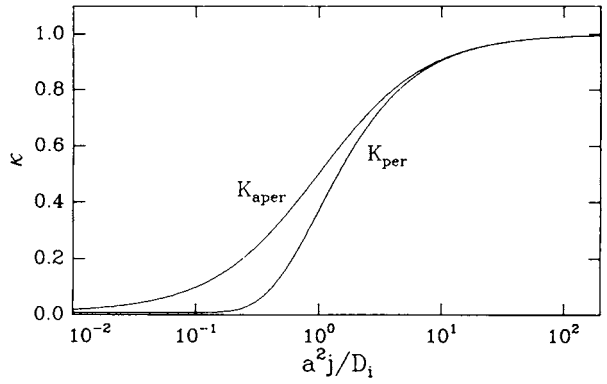

Figure 7.7: Dependence of nonequilibrium partition coefficients on the Péclet number, $a^2 j/D_i$, for periodic and aperiodic step flow. The equilibrium partition coefficient in both cases was taken to be 10^{-2}.

Then, the steady-state composition of the bulk layer will be that which it has reached at time $\tau_{\mathrm{ML}} = 1/j$, or

$$x^\beta = \kappa_{\mathrm{equ}} x^\sigma + (x^\sigma - \kappa_{\mathrm{equ}} x^\sigma) e^{-D_i/(a^2 j)}. \tag{7.43}$$

In other words, when segregation occurs by interdiffusion of solute punctuated by the periodic passage of steps, then the steady-state ratio between bulk and surface compositions is

$$\kappa_{\mathrm{per}} = \frac{x^\beta}{x^\sigma} = \kappa_{\mathrm{equ}} + (1 - \kappa_{\mathrm{equ}}) e^{-D_i/(a^2 j)}. \tag{7.44}$$

As illustrated in Figure 7.7, κ is κ_{equ} for $a^2 j/D_i$ much less than unity, but increases to unity as $a^2 j/D_i$ approaches and exceeds unity.

On the other hand, if the steps on the surface are distributed randomly, then they pass over the surface *aperiodically*.[13] If this aperiodic passage obeys a Poisson arrival distribution, then the probability that a step will pass in an interval dt after time t will be $e^{-t/\tau_{\mathrm{ML}}} dt/\tau_{\mathrm{ML}} = g e^{-gt} dt$. Hence, the average composition of the bulk layer will be its composition after time t, weighted by this probability, or

$$x^\beta = \int_0^\infty \left[\kappa_{\mathrm{equ}} x^\sigma + (x^\sigma - \kappa_{\mathrm{equ}} x^\sigma) e^{-D_i/(a^2 j)}\right] j e^{-jt} dt$$

[13] L.M. Goldman and M.J. Aziz, "Aperiodic stepwise growth model for the velocity and orientation dependence of solute trapping," *J. Mater. Res.* **2**, 524 (1987).

$$= \kappa_{\text{equ}} x^{\sigma} + (x^{\sigma} - \kappa_{\text{equ}} x^{\sigma}) \frac{j}{j + D_i/a^2}. \tag{7.45}$$

In other words, when segregation occurs by interdiffusion of solute punctuated by the aperiod passage of steps, then the steady-state ratio between bulk and surface composition is

$$\kappa_{\text{aper}} = \frac{x^{\beta}}{x^{\sigma}} = \frac{\kappa_{\text{equ}} + ja^2/D_i}{1 + ja^2/D_i}. \tag{7.46}$$

Again, as illustrated in Figure 7.7, κ is κ_{equ} for $a^2 j/D_i$ much less than unity, but increases to unity as $a^2 j/D_i$ approaches and exceeds unity. The increase is not as steep, however, as it is for κ_{per}.

A Segregating Dopant: Sb on Si (001)

To illustrate this behavior, consider the well-established[14] segregation of Sb impurities during MBE of Si on Si (001). Figure 7.8 shows measurements of the partition coefficient κ at various growth rates and temperatures. As temperature increases the partition coefficient initially decreases as Sb interdiffuses more and more quickly to the surface. At high temperatures, Sb diffusion is so fast that equilibrium is reached, and the partition coefficient approaches the equilibrium partition coefficient κ_{equ}. Finally, as temperature continues to increase, the surface and bulk phase compositions tend to equalize, and κ_{equ} itself approaches unity (see Equation 7.15). Therefore, as temperature continues to increase, ultimately κ begins to increase again, due to an increase in κ_{equ}.

Also shown in Figure 7.8 are the predictions of Equation 7.44 for segregation mediated by periodic step flow. As can be seen, the predictions agree reasonably well with the data, although there is some disagreement at the lower growth temperatures for the higher growth rates. The disagreement may be due to the onset of a 2D nucleation and growth mode, hence the onset of segregation mediated by aperiodic step flow.

7.3.2 Non-Steady-State Compositional Partitioning

In Subsection 7.3.1, we derived expressions for the nonequilibrium partition coefficient, κ. There, we assumed a steady-state solute concentration in the surface layer. In other words, we assumed that surface solute depletion due to incorporation into the bulk was just compensated for by adsorption from the vapor.

[14] J.C. Bean, "Arbitrary doping profiles produced by Sb-doped Si MBE," *Appl. Phys. Lett.* **33**, 654 (1978).

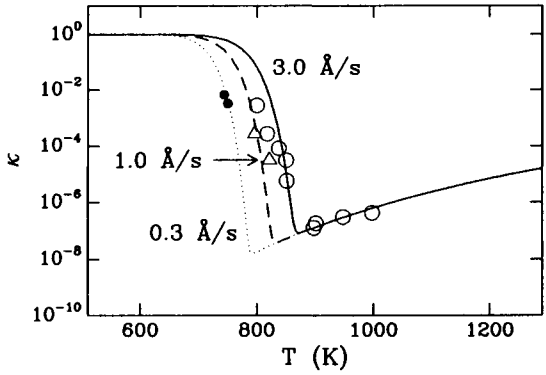

Figure 7.8: Temperature dependence of nonequilibrium partition coefficients for Sb during MBE of Si on Si (001). The data points[a] and predictions of Equation 7.44 are for growth rates of 3.0 Å/s (open circles and solid line), 1.0 Å/s (open triangles and dashed line), and 0.3 Å/s (filled circles and dotted line). The diffusivity was assumed to be Arrhenian, and given by $D_i/a^2 = 2\times10^{11}\exp(-1.67eV/kT)$, while the equilibrium partition coefficient was assumed to be $\kappa_{\text{equ}} = exp(-1.23eV/kT)$, consistent with the form given by Equation 7.15.

[a]H. Jorke, "Surface segregation of Sb on Si (100) during molecular beam epitaxy growth," *Surf. Sci.* **193**, 569 (1988).

In this subsection, we relax this assumption, and allow the solute concentration in the surface layer to evolve. To do so, recall that the nonequilibrium partition coefficient, κ, is the ratio between solute concentrations in a bulk layer just adjacent to the surface layer and in the surface layer itself. It can therefore be thought of as the fraction of solute in the surface layer that becomes "trapped" in the adjacent bulk layer during each monolayer growth cycle. If the overall growth velocity is v, then the rate of decrease of solute in the surface layer due to trapping will be $v\kappa x^\sigma/a$, where a is a monolayer step height.

At the same time, solute may also adsorb from the vapor onto the surface, or desorb back into the vapor from the surface. If $v_{\text{ads}} = j_{\text{ads}}^{\text{solute}} a$ is the adsorption "velocity" and $v_{\text{des}} = j_{\text{des}}^{\text{solute}} x^\sigma a$ is the desorption "velocity" of solute, then the overall rate of change of solute concentration in the surface layer will be[15]

$$\dot{x}^\sigma = \frac{v_{\text{ads}}}{a} - \frac{(v_{\text{des}} + v\kappa)x^\sigma}{a}. \tag{7.47}$$

[15]C.E.C. Wood and B.A. Joyce, "Tin-doping effects in GaAs films grown by molecular beam epitaxy," *J. Appl. Phys.* **49**, 4854 (1978).

This equation describes the time evolution of the solute concentration in the surface layer during growth. It increases due to adsorption from the vapor, and decreases due to a combination of desorption back into the vapor and trapping in the bulk.

Note, though, that even after the solute has become trapped in the bulk, it may still diffuse, albeit at rates determined by the bulk diffusivities, which may be much slower than the diffusivity for exchange between the surface layer and its adjacent bulk layer. Therefore, the bulk solute concentration will evolve, after trapping, according to

$$\frac{\partial x^\beta}{\partial t} = D_\beta \frac{\partial^2 x^\beta}{\partial z^2}, \tag{7.48}$$

where z is a distance scale perpendicular to the surface in a stationary reference frame.[16]

The boundary condition on this diffusion equation is the solute concentration most recently trapped in the bulk layer just adjacent to the surface, or

$$\left[x^\beta\right]_{z=z_\sigma(t)} = \kappa x^\sigma. \tag{7.49}$$

In this equation, $z_\sigma(t) = z_{\sigma,o} - \int_0^t v dt$ is the position of the interface between the surface layer and its adjacent bulk layer. Equations 7.47, 7.48 and 7.49 together completely describe the time evolution of the overall bulk solute concentration due to nonequilibrium segregation followed by bulk diffusion. They are complicated, however, by the boundary condition in Equation 7.49, which must be applied at a moving surface. It is convenient, therefore, to transform into a reference frame, $z' = z + \int v dt'$, that moves with the surface.[17] In this reference frame, Equation 7.48 becomes

$$\frac{\partial x^\beta}{\partial t} = D_\beta \frac{\partial^2 x^\beta}{\partial z'^2} - v \frac{\partial x^\beta}{\partial z'}, \tag{7.50}$$

and Equation 7.49 becomes

$$\left[x^\beta\right]_{z'=0} = \kappa x^\sigma. \tag{7.51}$$

To illustrate the use of these equations, Figure 7.9 shows time evolutions of the spatial distributions of solute during growth of a structure

[16] We neglect electrostatic effects near the surface, which may cause solute "drift" toward or away from the surface. See, e.g., E.F. Schubert,, J.M. Kuo, R.F. Kopf, A.S. Jordan, H.S. Luftman, and L.C. Hopkins,, "Fermi-level-pinning-induced impurity redistribution in semiconductors during epitaxial growth," *Phys. Rev.* **B42**, 1364 (1990).

[17] S.A. Barnett and J.E. Greene, "Si molecular beam epitaxy: a model for temperature dependent incorporation probabilities and depth distributions of dopants exhibiting strong surface segregation," *Surf. Sci.* **151**, 67 (1985).

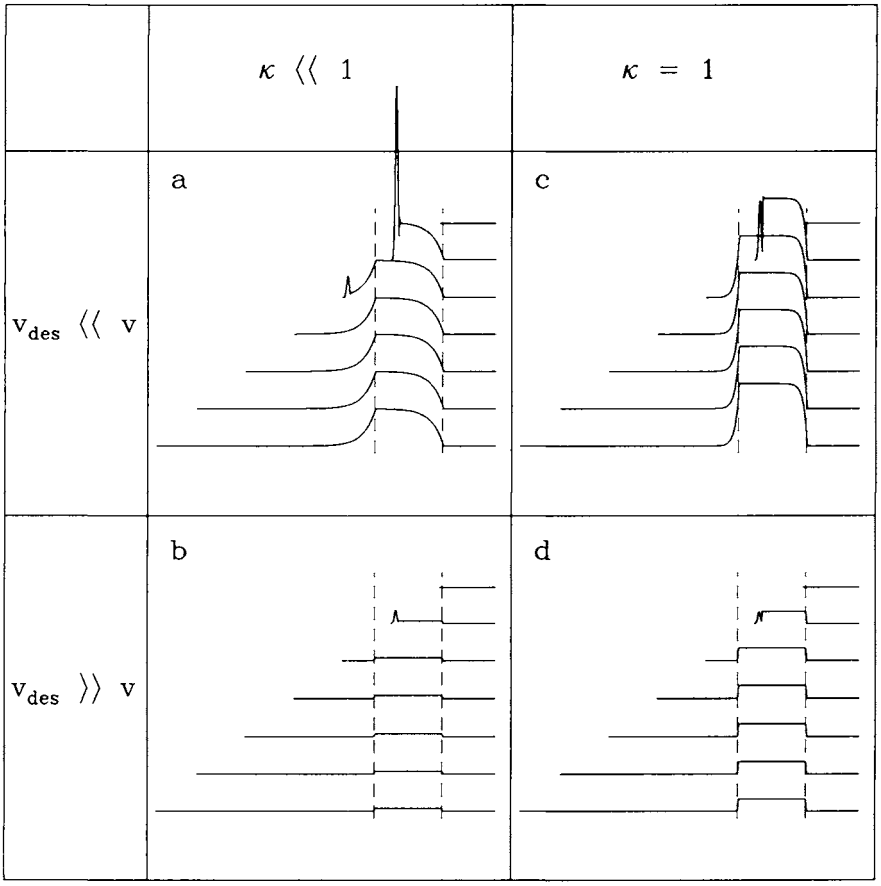

Figure 7.9: Four series of snapshots in time of solute composition profiles during MBE. All four series correspond to a square doping pulse indicated by the dashed lines, but differ according to whether v_{des} is much less than or greater than v and whether κ is much less than unity or equal to unity.

having a square pulse of solute. In the absence of bulk diffusion, there are four extremes of behavior, depending on (1) the relative rate between the growth velocity and the effective desorption velocity and (2) whether the nonequilibrium partition coefficient is near-unity or very different from unity.

Consider first the cases where the effective desorption velocity is much lower than the growth velocity. Then, a negligible fraction of the solute atoms that land on the surface leave, and virtually all ultimately incorpo-

rate into the growing crystal. On the one hand, if the partition coefficient is unity, as in panel (c), then all the solute atoms in the surface layer are incorporated into the bulk as growth proceeds. The depth profile of the final solute concentration mimics within one to two monolayers the square pulsed arrival rate of solute. On the other hand, if the partition coefficient is much less than unity, as in panel (a), then only a fraction of the solute atoms in the surface layer is incorporated into the bulk as growth proceeds. The depth profile of the final solute concentration now tails off gradually, as solute "rides" and gradually accumulates on the growing surface, and continues to be incorporated into the crystal even after the square pulse of solute has ended.

Consider second the cases where the effective desorption velocity is much higher than the growth velocity. Then, many of the solute atoms that land on the surface leave, and only a fraction ultimately incorporates into the growing crystal. That fraction is $\kappa v/(v_{\rm des} + \kappa v) \approx \kappa v/v_{\rm des}$, and increases linearly with the partition coefficient. The depth profile of the final solute concentration again mimics the square pulsed arrival rate of solute, because any solute in the surface layer that does not incorporate in the bulk desorbs from, rather than "rides" on, the surface.[18] Note that as growth proceeds, there is a competition between desorption and trapping of solute. On the one hand, if the partition coefficient is much less than unity, as in panel (b), then most of the solute atoms in the surface layer eventually desorb, and the absolute concentration of solute in the bulk is low. On the other hand, if the partition coefficient is unity, as in panel (d), then more of the solute atoms in the surface layer incorporate into the bulk, and the absolute concentration of solute in the bulk is higher.

Of the four extremes of behavior just discussed, only one results in a solute composition profile that is broadened beyond the square solute arrival pulse. Unfortunately, that extreme is a commonly observed one, in which appreciable solute segregates to and rides on the surface, rather than either incorporating or desorbing. It may be circumvented to some extent by reduced growth temperature, which reduces solute diffusion from the bulk to the surface.[19]

[18]S.S. Iyer, R.A. Metzger, and F.G. Allen, "Sharp profiles with high and low doping levels in silicon grown by molecular beam epitaxy," *J. Appl. Phys.* **52**, 5608 (1981).

[19]H.J. Gossman, E.F. Schubert, D.J. Eaglesham, and M. Cerullo, "Low-temperature Si molecular beam epitaxy: Solution to the doping problem," *Appl. Phys. Lett.* **57**, 2440 (1990).

Suggested Reading

1. A.W. Adamson, *Physical Chemistry of Surfaces*, 4th Ed. (John Wiley and Sons, New York, 1982).

2. J.M. Blakely, *Introduction to the Properties of Crystal Surfaces* (Pergamon Press, Oxford, 1973).

3. R. Defay, I. Prigogine, A. Bellemans and D.H. Everett, *Surface Tension and Adsorption* (John Wiley and Sons, New York, 1966).

Exercises

1. Verify that minimizing Equation 7.14 is equivalent to the parallel tangent construction.

2. Show that, for a given bulk composition, the surface work given by Equations 7.16 and 7.18 is minimum when the surface composition is such that the surface and bulk phases are in equilibrium with each other, i.e., when the parallel tangent construction is satisfied.

3. Show, beginning with Equation 7.16, that

$$\partial\gamma^{\langle \mathrm{Ag}_{1-x^\beta}\mathrm{Au}_{x^\beta}\rangle \mathrm{Ag}_{1-x^\sigma}\mathrm{Au}_{x^\sigma}(}/\partial x^\sigma = \mu_{\mathrm{Au}}^{\mathrm{exc}} - \mu_{\mathrm{Ag}}^{\mathrm{exc}}. \tag{7.52}$$

   Note that both $\mu_{\mathrm{Au}}^{\mathrm{exc}}$ and $\mu_{\mathrm{Ag}}^{\mathrm{exc}}$ depend on x^σ.

4. Derive Equation 7.15, the equilibrium partition coefficient between bulk and surface phases for strictly regular bulk and surface phases.

5. Derive Equation 7.26 for the dependence of the equilibrium coverage of a strictly regular adsorbate phase on pressure.

6. For a given Péclet number, the nonequilibrium partition coefficient, κ, is higher for aperiodic than for periodic passage of steps. Physically, why is this so?

7. In principle, solute segregation and trapping may occur at a number of stages in the growth cycle. Solute may ride ahead of the edges of steps sweeping laterally over terraces by horizontal diffusion following kink flow; they may also ride on the surface by vertical diffusion following step flow. Suppose the horizontal and vertical interdiffusivities at the step edges and at the surface are D_{hor} and D_{ver}, and that the average terrace width is L/a, in units of lattice spacings.

Assuming periodic *partitionless* kink flow followed by horizontal diffusive segregation, what is the nonequilibrium partition coefficient κ_{step} associated with segregation ahead of the moving step? Then, assuming periodic, *non*-partitionless step flow followed by vertical diffusive segregation, what is the nonequilibrium partition coefficient κ_{terr} associated with segregation on top of the growing terraces?